LEABHARLANN CHOLÁISTE NA TRÍONÓIDE, BAILE ÁTHA CLIATH | TRINITY COLLEGE LIBRARY DUBLIN
Ollscoil Átha Cliath | The University of Dublin

Terms and Conditions of Use of Digitised Theses from Trinity College Library Dublin

Copyright statement

All material supplied by Trinity College Library is protected by copyright (under the Copyright and Related Rights Act, 2000 as amended) and other relevant Intellectual Property Rights. By accessing and using a Digitised Thesis from Trinity College Library you acknowledge that all Intellectual Property Rights in any Works supplied are the sole and exclusive property of the copyright and/or other IPR holder. Specific copyright holders may not be explicitly identified. Use of materials from other sources within a thesis should not be construed as a claim over them.

A non-exclusive, non-transferable licence is hereby granted to those using or reproducing, in whole or in part, the material for valid purposes, providing the copyright owners are acknowledged using the normal conventions. Where specific permission to use material is required, this is identified and such permission must be sought from the copyright holder or agency cited.

Liability statement

By using a Digitised Thesis, I accept that Trinity College Dublin bears no legal responsibility for the accuracy, legality or comprehensiveness of materials contained within the thesis, and that Trinity College Dublin accepts no liability for indirect, consequential, or incidental, damages or losses arising from use of the thesis for whatever reason. Information located in a thesis may be subject to specific use constraints, details of which may not be explicitly described. It is the responsibility of potential and actual users to be aware of such constraints and to abide by them. By making use of material from a digitised thesis, you accept these copyright and disclaimer provisions. Where it is brought to the attention of Trinity College Library that there may be a breach of copyright or other restraint, it is the policy to withdraw or take down access to a thesis while the issue is being resolved.

Access Agreement

By using a Digitised Thesis from Trinity College Library you are bound by the following Terms & Conditions. Please read them carefully.

I have read and I understand the following statement: All material supplied via a Digitised Thesis from Trinity College Library is protected by copyright and other intellectual property rights, and duplication or sale of all or part of any of a thesis is not permitted, except that material may be duplicated by you for your research use or for educational purposes in electronic or print form providing the copyright owners are acknowledged using the normal conventions. You must obtain permission for any other use. Electronic or print copies may not be offered, whether for sale or otherwise to anyone. This copy has been supplied on the understanding that it is copyright material and that no quotation from the thesis may be published without proper acknowledgement.

Synthesis and characterisation of nanocrystalline ZnO for electronic applications

By

Suresh C. Pillai

A thesis submitted to the University of Dublin for the degree of Doctor of Philosophy

Department of Chemistry

University of Dublin

Trinity College

January 2002

TRINITY COLLEGE
14 MAR 2002
LIBRARY DUBLIN
THESIS 6659

Declaration

This thesis has not been submitted as an exercise for a degree at any other University. Except as otherwise indicated the author carried out the work described herein alone.

I give permission for the Library to lend or copy this thesis upon request.

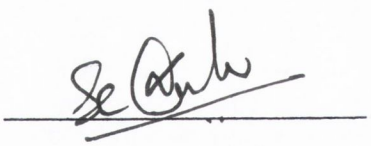

Suresh C. Pillai

Summary

The main focus of this work was to develop novel industrially viable procedures, based on sol gel technology, for the preparation of nano-size doped ZnO materials for varistor applications.

Initially three well-established synthetic routes for the preparation of nanocrystalline ZnO were selected. Further doping and sintering of these materials showed that none of these methods could be used to produce a varistor material. The poor electrical characteristics are attributed to the presence of impurity ions such as lithium and sodium. Thus it was decided to develop new processing routes to make nano-size ZnO and doped ZnO varistor materials.

A novel synthetic procedure based on a non-hydrolytic sol gel condensation reaction was conducted and subsequent calcination at 500°C was used to make ZnO nano materials. ZnO precursor gels were prepared by the reaction of ethanolic solutions of zinc acetate and oxalic acid. Further drying and calcination produced ZnO nanoparticles of size ca. 30 nm. In a similar experiment chemical modifiers (diethanolamine and ethylene glycol) were added to the ethanolic solution of zinc acetate before the addition of oxalic acid. The gel formed was dried, calcined and characterised by electron microscopy and X-ray powder diffraction. Scanning Electron Microscopy studies revealed that these materials were composed of nanowires of 2 to 4 μm in length. Further investigations by Transmission Electron Microscopy showed that these wires consisted of approximately spherical nanoparticles of average diameter 21 ± 3 nm. The morphology of the wires was found to be similar to that previously reported for gold, silver, palladium and CdSe nanoparticle arrays. The precursor morphologies and formation mechanism of these wires were studied in detail by various techniques. Conventional solid-state mixing and core shell type doped varistors were fabricated from these materials. Core shell type material showed considerably higher breakdown voltage values compared to that of the other materials. Even though the electrical properties were superior, nearly full density was not achieved even at 1050°C. Studies were directed to make a better material with good densification and better electrical properties.

A new procedure based on a mixed precursor route was performed to make nano-size doped ZnO materials. The synthesised powder had a particle size of 15 ± 3 nm and a surface area as high as 45 m^2/g. Dry ball milling for up to 30 minutes made less agglomerated nano powders. The milled powder was pelletised and sintered at various temperatures ranging from 700°C to 1050°C. 100% densification with a breakdown voltage of 941 ± 30 V/mm and a reasonably good α of 33 ± 3 were obtained for these materials conventionally sintered at 1050°C. A novel step sintering procedure was also tried for sintering these materials at lower temperature. Electrical measurements were carried out at various temperatures and a higher breakdown voltage (906 ± 30 V/mm) with considerably higher non-linear characteristics (α= 36 ± 3) compared to the commercial sample was obtained for step-sintered samples prepared from nano-size varistors. Phase analysis of the sintered samples was studied by powder X-ray Diffraction (XRD) and Energy Dispersive X-ray (EDX) analysis. Industrial pilot plant operations were successfully carried out in Littelfuse Ltd., Dundalk.

Acknowledgements

I would like to express my deep sense of gratitude and appreciation to my supervisors Professor John M. Kelly, Dr. Declan E. McCormack and Dr. Ramesh Raghavendra for their help, advice and encouragement during each and every stage of this programme.

The financial support given by Enterprise Ireland and Littelfuse Ireland Ltd. is greatly acknowledged.

I am grateful to Professor Paul O'Brien, Manchester Materials Science Centre, UMIST, Manchester, UK for allowing me to use HRTEM and for giving me such a warm welcome during my stay at Manchester.

It gives me a great pleasure to thank the Electron Microscope Unit, Trinity College Dublin, for a bursary and allowing me to use their instruments. Thanks are due to David John (Manager EM Unit), Neal Leddy and Colin G. Reid.

I wish to thank Professor John Corish, Head, Department of Chemistry for allowing me to use departmental facilities. In addition to **all** the academic staff members of the chemistry department, I would like to thank Dr. Yurii Gun'ko for his help and support during various stages of this work.

I would like to thank Dr. Neil McLoughlin (Littelfuse Ireland Ltd), Dr. Tim Prescott (Enterprise Ireland), and Dr. Robert Flood (Enterprise Ireland) for their comments and participation in various meetings of this project.

I wish to thank Dr. Sunil Kumar, Materials Ireland Research Centre, University of Limerick for all his support and friendship over the last five years.

Thanks are due to Michael Seery whose expertise I called up on many occasions during this work and for the extensive proof reading. I wish to give my appreciation to all past and present members of the Kelly group, Mark, Carlos, Ruth, Emmanuel, Sarah, Conor, Yvonne, Antonella, Aine, Karen, Aoife, and Isabelle.

I wish to express my sincere thanks to Littelfuse Ireland Ltd for allowing me to use Industrial facilities for my research. I wish to acknowledge Sheena Kelly for her help in electrical measurements and Kevin for his help during pilot plant operations. I would like to thank School of Chemistry, Dublin Institute of Technology, Kevin Street for allowing me to use their instrumental facilities. I am particularly grateful to Dr. John Fox, Dr. Irina Gun'ko and Dr. Tia Keyes for their help with mass spectroscopy, FTIR and Raman spectroscopy respectively.

I am grateful to Paul P. Lyons, Ceramic Technologist, Enterprise Ireland for giving me a training in BET surface area analysis and to Dr. David Doff for a training in X-ray diffractometry. Also thanks to Dr. Robbie Goodhue for his help.

Many thanks to Prof. J. M. D. Coey, Physics Department, and his research group for their help during various stages of the project. I am particularly thankful to Dr. M. Venkatesan for thermo gravimetric analysis.

I would like to thank Dr. K. G. K. Warrier, Deputy Director, RRL, CSIR, Trivandrum, India and his research group and in particular Dr. Hareesh Nair, Dr. Asha Vasudevan, Dr. G. M. Anil Kumar, K. M. Nair, P. Krishnapillai, P. Mukundan, S. K. Ghosh, S. Anantha Kumar, Dr. S. Siva Kumar, P. Perumal, Padamaja, and Rajesh.

I wish to thank my teachers, lecturers and professors, too numerous to mention, but all are remembered here. Many thanks to Professor M. Padmanabhan, Professor V. N. R. Pillai, Professor Sabu Thomas, Mr. E. K. Ravindranathan Nair and Professor P.R. Das for their encouragement during the past several years.

I wish to express my sincere appreciation to **all** technical and secretarial staff especially Dr. Martin Feeney, Dr. Tom McCabe, Brendan Mulvaney, Fred Cowzer, Eddy Tierney, Patsy Greene and Theresa Mc Donnell. I am grateful to Corrine Harrison, Teresa Lalor and Helen O'Halloran for all their help during various occasions.

Heart-felt thanks to Dr. Vera Thoss, Iskra Kelly and Bhama Ramesh for their support and encouragement during my first few months stay in Dublin which, I will never forget in my life.

I would like to thank **all** my friends and fellow post-graduates at Trinity College especially Thorri's and Yurii's groups. I very much appreciated the company of B. Sivakumar and special thanks to Mark Glynn for a warm welcome to Ireland.

I would like to thank **all** my friends in Ireland with whom I enjoyed my stay in Dublin. Special thanks to Andre, Geraldine, Juho, Ram, Manoj, Vandana, Jyothi, Ciaran, Miriam, Malini, Philip, Rexon, Lona, Rethi, Raman, Nia, Aran and Sudheer who were always willing to help me when necessary.

I am greatly indebted to my father for his dedication, my mother for all her love and prayers, my sister and brother in law for their love and support. Thanks also to my little niece Amrutha, cousins, friends, relatives and late grand parents.

Dedicated to my father who sacrificed so much for his children

TABLE OF CONTENTS

Chapter 1 Introduction 1

1.1 Nanostructured materials 2

1.2 Properties of nanomaterials compared to bulk materials 3

1.2.1 Mechanical properties 4

1.2.2 Optical properties 4

1.2.3 Magnetic properties 4

1.2.4 Electrical properties 5

1.3 Synthesis of nanostuctured materials 6

1.3.1 High energy milling 6

1.3.2 Hydrothermal Synthesis 7

1.3.3 Reactive electrode submerged arc (RESA) method 7

1.3.4 Gas condensation method 7

1.3.5 Emulsion synthesis 8

1.3.6 Sol gel synthesis 9

1.3.7 Advantages and disadvantages of different procedures 10

1.4 Nano ZnO –previous studies 11

1.5 Varistors 13

1.5.1 Mechanism of varistor action 16

1.6 Synthesis of metal oxide varistor powders – a review of recent advances 19

1.6.1 Historical developments 19

1.6.2 Conventional synthesis 18

1.6.3 Need for new processing routes 21

1.6.4 Different chemical procedures used to prepare varistors 21

1.6.4.1 Amine processing 21

1.6.4.2 Aqueous precipitation 21

1.6.4.3 Citrate gel synthesis 22

1.6.4.4 Combustion synthesis 23

1.6.4.5 Micro-emulsion synthesis 23

1.6.4.6 Plasma synthesis 24

1.6.4.7 Precipitation reaction 24
1.6.4.8 Sol gel processing 25
1.7 Objective of the thesis 29
1.8 An overview of the experiments performed 31
1.9 References 32

Chapter 2 Experimental, materials and methods 36

2.1 Introduction 37
2.2 Materials used 37
2.3 Synthesis 38
2.3.1 Synthesis of well defined ZnO nanoparticles 38
2.3.1.1 ZnO prepared using Spanhel's method 38
2.3.1.2 Meulenkamp method 39
2.3.1.3 ZnO nano powder synthesis 39
2.3.2 Novel synthesis of ZnO nanoparticles and nanowire arrays of ZnO 40
2.3.2.1 Synthesis of nanoparticular ZnO without chemical modifiers 40
2.3.2.2 Synthesis of nanoparticular ZnO with chemical modifiers 40
2.4 Varistor preparations 40
2.4.1 Varistor preparation from ZnO nanomaterials 40
2.4.2 Core shell synthesis ZnO varistor materials 41
2.5 Bulk synthesis of varistor materials by sol gel mixed precursor route 41
2.6 Methods 42
2.6.1 UV/Vis analysis 42
2.6.2 Infrared absorption spectroscopy 43
2.6.3 Thermal analysis 43
2.6.4 X-ray powder diffraction 43
2.6.5 Transmission electron microscopy 44
2.6.6 Scanning electron microscopy 46
2.6.7 BET Surface area analysis 47

2.6.8 Density determinations 48

2.7 Sintering studies 49
2.7.1 Conventional sintering studies 49
2.7.2 Novel sintering procedures 50
2.8 Electrical characterisation 51
2.9 References 52

Chapter 3 Synthesis of nanometer size ZnO by three different procedures and the study of varistor properties of these materials 53
3.1 Introduction 54
3.2 Results and discussions on ZnO nanoparticles 54
3.2.1 Nanocrystalline ZnO through Spanhel and Anderson procedure 54
3.2.1.1 UV/Vis absorption spectra of ZnO sol 55
3.2.1.2 X-ray Diffraction 57
3.2.1.3 Transmission Electron Micrographs 57

3.2.2 Nanocrystalline ZnO prepared through Meulenkamp's method 58
3.2.2.1 UV/Vis absorption spectra of ZnO sol 60
3.2.2.2 X-ray diffraction 60
3.2.2.3 Transmission electron micrographs 62
3.2.3 Comparison of the Spanhel and Anderson and the Meulenkamp procedures 63
3.3 Synthesis of nanocrystalline solid ZnO by weller method 63
3.4 Comparison of the three procedures 65
3.5 Aging studies 68
3.6 Calcination and sintering of nano-size ZnO prepared by the above methods 72
3.7 Sintering and electrical properties of varistors prepared by above three method 75
3.8 Conclusions 77
3.9 References 78

Chapter 4 Synthesis of novel ZnO nanoparticles and self assembled nanowire arrays 79

4.1 Introduction 80
4.2 Synthesis of ZnO nanoparticles 82
4.3. Synthesis of nanowire arrays of ZnO 85
4.4 A detailed microstructural study of the two precursors 90
4.4.1 Gel structure of the precursor of ZnO nanoparticles prepared without using modifiers 90
4.4.2 FTIR analysis of the dried and calcined powder prepared without chemical modifiers 91
4.4.3 Thermal analysis of the xerogel 93
4.4.4 Gel Structure of the precursor of ZnO nanowires 94
4.4.5 FTIR Analysis of the fresh gel, xerogel and nanowire 98
4.4.6 Thermal analysis of the nanowire xerogel 100
4.5 Variation in modifier concentration 104
4.6 Coating of dopants on ZnO materials 108
4.7 Varistor properties of the doped ZnO materials 111
4.8 Conclusions 114
4.9 References 116

Chapter 5 Varistors prepared from nano-size precursors 120

5.1 Introduction 120
5.2 Results and discussion on the synthesis of varistor nanopowder 121
5.2.1 Phase analysis of the nanopowder calcined at 500°C 121
5.2.2 Characterisation of the precursor xerogel 124
5.2.3 Phase analysis of the nanopowder calcined at 500°C 126
5.2.4 Surface area and morphology of the nanopowder calcined at 500°C 128
5.2.5 Nanopowder de-agglomeration 132
5.3 Sintering, grain growth and electrical studies of varistors

prepared from nano-size precursors 133
5.3.1 Grain growth studies 135
5.3.2 Electrical studies of varistors prepared from nano-size precursors 137
5.3.2.1 Electrical characteristics of samples sintered at 950°C/ 2h 137
5.3.2.2 Electrical characteristics of samples sintered at 1000°C/ 2h 140
5.3.2.3 Electrical characteristics of samples sintered at 1050°C/ 2h 141
5.3.2.4 Step sintering 142

5.4 Discussion on varistor action and phase analysis of sintered samples 144
5.5 Conclusions 149
5.6 References 150

Chapter 6 Conclusions and summary for the present work and suggestions for future work 152

6.1 Conclusions and summary 153
6.2 Suggestions for future work 156
6.3 References 157

Appendix I
Brus equation for particle size from absorption spectra 158

Appendix II
List of author's publications 159

Chapter 1

Introduction

" What I want to talk about is the problem of manipulating and controlling things on a small scale. What I have demonstrated is that there is room - that you can decrease the size of things in a practical way. I now want to show that there is plenty of room."

Richard Feynman

December 29th 1959 at the annual meeting of the American Physical Society at the California Institute of Technology.

1.1 Nanostructured materials

Albert Einstein calculated the size of a single sugar molecule as about a nanometer (a billionth of a meter) in diameter and nearly 100 years after Einstein's predictions, the nanometer size, looms large in scientific research.[1] The term 'nano' came into frequent use in early 1990 in scientific and industrial research. Until then the more general terms 'submicron' and 'ultrafine' were used to define the smaller particles.[2] Nanoparticles are materials possessing microstructural dimensions less than 100 nm. The increased importance of nanomaterials is a result of the unique properties that can be obtained and the applications that result from such nanostructuring.[1-12]

The small size of nanoparticles, which is responsible for different properties (optical, magnetic, structural, electrical and electronic), with respect to the bulk materials makes them suitable for new applications. They manifest fascinating and useful properties which can be exploited for a variety of applications such as electronic devices (sensors, varistors and next generation computer chips) and hard ceramics (SiC and zirconia).[1-4,13-15] In a nanophase material with an average size of 5 nm, about 50% of the atoms lie in the two nearest planes of a grain boundary. In such a spatial environment significant atomic displacement from normal lattice positions is exhibited. Therefore the properties are dominated by their ultra fine grain size, high surface area and the larger number of interfaces associated with their smaller grains.[16] Since the grain size is reduced to a few nanometers there is a change in the average bulk density and the formation of more grain boundaries. These will lead to differences in the mechanical and electrical properties from those of a single crystal.[15]

Nanomaterials research literally exploded during the early 1980's in the US and Japan. Currently 50 US companies are active in the research and development of various nanostructured materials and out of these more than 10 industries are involved in the production of nanomaterials on a commercial scale. According to BCC (Business Communication Co Inc) the world market for nano materials in electronic, magnetic and optoelectronic applications reached $333 million in 2000. BCC also estimates that the world market for nano materials will reach

$667 million, which corresponding to an average growth rate of 14.9% from 2000 to 2005.[17]

1.2 Properties of nanomaterials compared to bulk materials

The properties of nanocrystalline materials are strongly related to their unique structures. As discussed above, the physical and chemical properties of nanomaterials are different from the bulk materials of the same molecular structure. One of the basic concepts of the science of solids is the insight that most properties of solids depend on the microstructure *i.e.* chemical composition, the arrangement of atoms and the size of the solid. If there is change in one or any of these parameters, the properties of the solid vary.[2,4] Nanoparticles can be considered as a state of matter in the transition region between bulk solids and molecular structures.[18] Their physical and chemical properties gradually change from molecular to bulk with increasing particle size. The band structure (Fig.1.1) of the bulk solids gradually develops with increasing particle size (*i.e.* molecular orbitals convert into delocalised band states). This transition is seen in the absorption spectra of semiconductor nanoparticles.

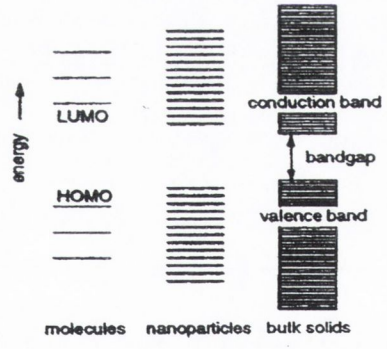

Fig. 1.1 Transition from molecules to bulk semiconductor. Discrete molecular electronic levels convert into the energy bands with increasing particle size.[18]

Sharp and discrete molecular (excitonic) absorption bands of the small particles (nanoclusters) gradually convert into the typical edge-like absorption of bulk materials with increasing particle size, whereby the onset of the absorption is shifted from short wavelengths towards the band edge.[2,8,9,18]

1.2.1 Mechanical properties

Because of the large number of interfaces the mechanical properties of nanomaterials such as their strength and toughness are significantly modified.[3,16] The hardness and strength of sintered nanophase ceramics are considerably higher than those observed in coarser grained materials.[4,19-21] Interfaces in crystalline solids play a role in high temperature creep since one of the predominant mechanisms of creep (grain boundary sliding) results from migration of grains along the grain boundary.[12] A material which is largely made up of grain boundaries will exhibit a greater creep rate leading to superplasticity. Ceramic nanostructures are found to be superplastic.[19-21]

1.2.2 Optical properties

When a quantum of light is absorbed in CdS or ZnO an electron is transferred from the valence band into the conduction band, leaving a net positive charge in the valence band. In small particles, the wave functions of the electron and the hole are confined to the particle volume. Hence if the particle size become comparable or smaller than the de-Broglie wavelength of the charge carriers, the confinement increases the energy required for creating an electron/hole pair. This increase shifts the absorption spectra towards shorter wavelengths.[2,8,9] Quantum dots can be used to provide light emitters of various colours by 'band gap tuning' using particle size effects. Another important advantage of nanoparticles is the long life time of electrons in the excited states which is an important requirement in laser optical applications.[2] Alivisatos[22] reported light emitting diodes with high conversion efficiencies (10%) by using quantum dots embedded in a polymer matrix.

1.2.3 Magnetic properties

In the area of magnetic storage media future progress will rely on the ability to control the microstructure at smaller size scales so as to impact on storage densities. The approach that will use magnetic nanoparticles of the size of a single magnetic domain is very important for development of high density magnetic recording materials. IBM researchers in New York and California[23] have made a new class of magnetic particles of iron and platinum each uniformly

containing only a few hundreds of atoms self-assembled into ordered arrays. This scientific discovery could lead to new solutions for storing a huge volume of data in much smaller devices.[23]

1.2.4 Electrical properties

Trapping of charge at the grain boundaries has a decisive influence on the electrical transport properties in polycrystalline semiconductors and the electrical properties can be altered by varying the microstructure at the grain boundary regions.[24] It is reported that the charge at the grain boundaries is related to the presence of impurity or dopant atoms.[24] As the nanostructured material contains numerous grain boundaries, more additive atoms can be accommodated at the boundary regions in order to tailor the material's properties. (More details on nanomaterials for varistor applications will be discussed in section 1.5)

1.3 Synthesis of nanostuctured materials

In order to obtain nanomaterials in a specific predefined size and morphology, much attention has to be paid to the processing route. There are many known methods to produce nanomaterials[2,3] some of them include high energy milling, reactive electrode submerged arc (RESA) method, emulsion synthesis hydrothermal synthesis, gas condensation method and sol gel synthesis. Important issues facing nanopowder processing includes cost, broad grain size distribution and agglomeration.[2,17]

1.3.1 High energy milling

By high-energy ball milling the grain size of powder particles can be reduced to the nanometer scale.[25] For longer duration of ballmilling extremely fine-grained microstructure with randomly oriented grains (5-13 nm.) are formed. The basic process can be represented as (Fig. 1.2):

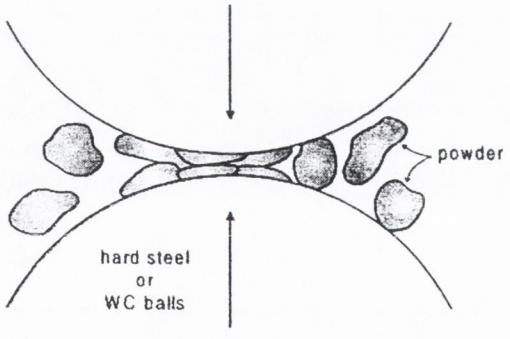

Fig. 1.2 Process of Mechanical attrition.[25]

Agglomeration of primary particles, high cost of production and a wide range of particle size distribution are the main disadvantages of this process.

1.3.2 Hydrothermal Synthesis

Hydrothermal synthesis involve heating reactants often metal salts, hydroxide or metal powders as a solution or suspension in a liquid usually water at elevated temperature and pressure. Nucleation and particle growth that occurs under these conditions can result in particles with well defined shape and size.[26]

Hirano and Kato[26] recently produced nanocrystalline CeO_2 powders by heating cerium (IV) salts in the presence of urea under controlled conditions at 120°C to 180°C. The synthesised particles were cubic in structure and 10 to 20 nm in size. The particle size of the synthesised ceria decreased with an increase in urea concentration.[26]

1.3.3 Reactive electrode submerged arc (RESA) method

This method utilises two metal or conducting electrodes, which are subjected to an arc submerged in a suitable dielectric fluid, typically water, that reacts with the metal. [27]

The spark provides an extremely high temperature for a short duration resulting in vaporisation of the electrode and the surrounding dielectric fluid and reaction within the bubble which forms. The reaction between various vapour species or between solids and vapour occurs and the reaction products in the form of a fine smoke are quenched in the surrounding liquid phase dielectric yielding a colloidal sol of spherically shaped particles. This method has been used to produce metal oxides, metal carbides and metal nitrides. [27]

1.3.4 Gas condensation method

This was the first attempt to generate nanomaterials in large scale.[3] The apparatus used in this technique is shown in Fig.1.3. The reaction involves a two step process. A solid compound with high vapour pressure (1-5 GPa) is evaporated by high temperature heating in a crucible. The evaporated atoms transfer their thermal energy to the inert gas and condense in the form of small crystals. There is a connective flow of the inert gas between the warm region near the vapour source and the cold surface where they are collected. Then the inert gas is

removed and the particles are scraped from the cold finger and funnelled into a piston and anvil like device where they are compacted. Composite materials can also be produced by mixing two or more evaporation sources.

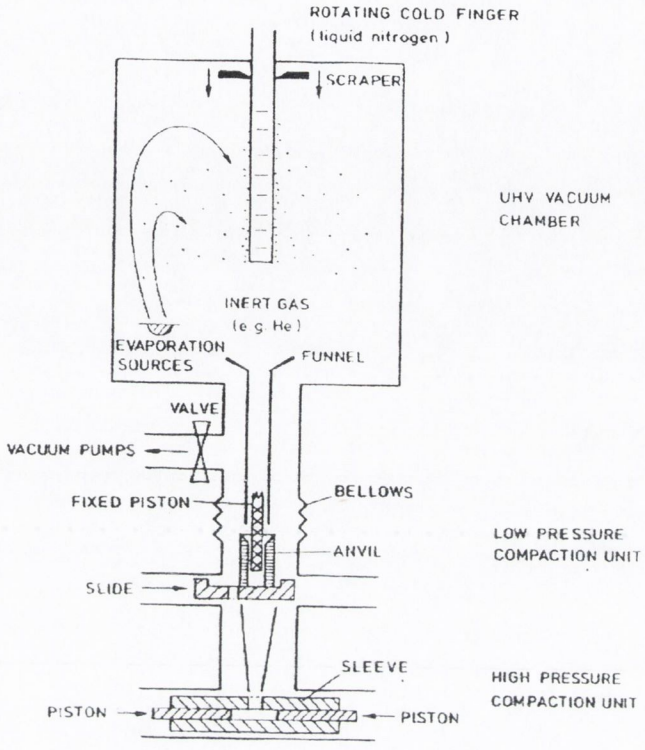

Fig. 1.3 Schematic drawing of a gas condensation chamber [3]

1.3.5 Emulsion synthesis

This is an effective method for the synthesis of nanopowders by using a liquid core of water or alcohol encapsulated in a microemulsion as nanoreactors for the synthesis of precursor particles. [28-30] Microemulsions are transparent dispersions containing two immiscible liquids (*e.g.* oil and water) stabilised by a surfactant. The aqueous core of microemulsions containing soluble metal salts is used as nanoreactors for the synthesis of finely divided ZnO particles. This solution was mixed with another microemulsion containing the precipitating agent as the aqueous phase. The microemulsions of reactant molecules continuously collide, coalesce and break again. During this process inter-droplet exchange and nuclei aggregation takes place and consequently the product precursor is formed. This method has been successfully used to prepare ZnO varistor nanoparticles and which will be discussed in section 1.7.4.5.

1.3.6 Sol gel synthesis

Several chemical routes have been reported for the synthesis of nanoparticles.[9,10, 25-30] Sol gel processing is one way of producing nanoparticles and is also a way of manipulating precursors to form bulk oxide materials.[31-37] Controlled hydrolysis and condensation reaction of metal alkoxides or acetates will give a sol and the particles will join together to give a gel, which is a highly viscous network of metal oxide bonds containing trapped solvent molecules. The gel can then be heated to remove the solvent and other organic groups to produce the crystalline oxide powder or dense ceramic (Scheme 1.1).

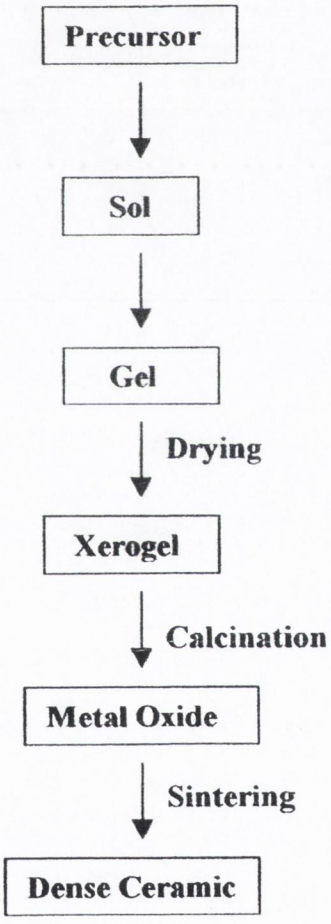

Scheme 1. 1 Schematic representation of sol gel process

The sol gel process can generally be divided into two classes depending on the nature of the precursors; inorganic precursors (acetates, nitrates and chlorides) and alkoxide precursors. The latter is very expensive compared to the former.

The hydrolysis and condensation processes are chemical reactions, which depend on various parameters such as pH, temperature, and concentration of metal ions and solvents. It is interesting to note that although the gel formed has the appearance of an amorphous solid, its pores contain a gelation medium and hydrolysis and condensation continue to occur until the solid is perfectly dried. Thus the aging, drying and calcination conditions such as the rate of heating, temperature and the atmosphere inside the furnace also affect the extent of branching and crosslinking and thereby influence the final properties of the oxides produced. If the gel contains extensive polymeric chains with significant branching and crosslinking, it will be structurally rigid and the resulting oxide after calcination will possess a high surface area. In other words the gel with weaker crosslinking is structurally weak and thus collapses rapidly on calcination to give a powder with lower surface area.[34,37]

1.3.7 Advantages and disadvantages of different procedures

A critical analysis of the advantages and disadvantages of various procedures for the production of nanomaterials are listed in Table 1.1

Table 1.1 Advantages and disadvantages different procedures for the production of nanomaterials

Method	Advantages	Disadvantages
High energy milling	Simple, bulk production is possible and particle size can be controlled by changing milling time	High cost of production and wide range of particle size distribution
Hydrothermal	Simple to reproduce, particle growth can be controlled by changing experimental conditions	Agglomeration during synthesis
RESA	Colloid particles of metal and metal oxides can be easily produced	Expensive and special set up required to perform the process
Gas condensation	Bulk production is possible and composite materials can be produced	Wide range of particle distribution and agglomeration
Emulsion	Simple to reproduce and composite nanoparticles can be produced	Large volume of solvents required and comparatively expensive
Sol gel	Synthesis of mixed oxide systems possible, offer low tmperature sintering, produce large quantities of materials and control the microstructure of the final product	High purity chemicals are relatively expensive raw materials and multi step processing adds time and expenses

1.4. Nano ZnO – previous studies

Nanocrystalline ZnO has achieved considerable significance recently because of its wide technological applications as solar cells,[39] photovoltic devices,[40] varistors,[41] and sensors.[42] Various preparation techniques (Scheme 1.2) have been attempted to synthesise nanosize ZnO.[5,6,8,9,43-55]

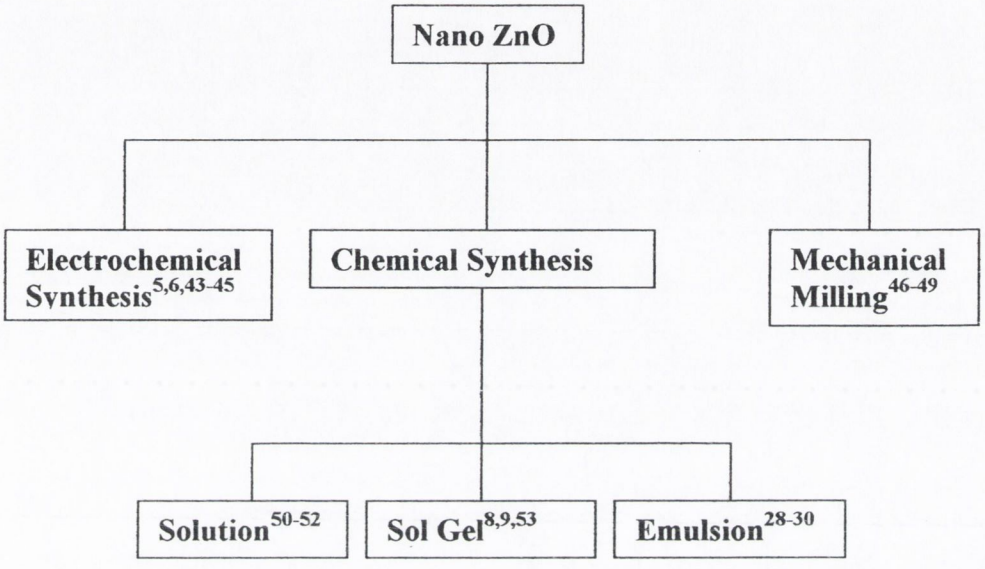

Scheme 1.2 Different synthetic procedures reported to produce nanosize ZnO.

ZnO nanowire arrays were fabricated by generating alumina templates with nanochannels or Au-coated silicon substrates by electrodepositing Zn in them and then oxidising the Zn particles.[5,6,43-45] Alamdari[46] synthesised ZnO nanoparticles by high energy milling for different times ranging from 0.5 to 20 h. The crystalline size obtained was below 100 nm. Recently mechanochemical processing has been applied to the synthesis of ZnO nanoparticles.[47-49] Milling of precursor powders leads to the formation of a nanoscale composite structure of the starting material which react during milling or subsequent heat treatment to form separated nanocrystals. The particle size produced by such methods was found to be 15-30 nm. Shah and co-workers[28-30] reported the micro-emulsion mediated synthesis of ZnO nanoparticles in the range of 10-20 nm. ZnO nanoparticles with different particle sizes have been reported[50-52] by controlling different parameters of the precipitation process such as solution concentration,

pH and washing medium. The ZnO nanoparticles (~50 nm) obtained are agglomerated into spherical structures of 1 μm. ZnO nanoparticles of size of 15 nm and ZnO fibre length/diameter = 16:1 were prepared from zinc acetate solution under hydrothermal conditions.[50] Spherical well defined particles were obtained in the range of 2 to 7 nm either by the reaction of zinc salt with alkali metal hydroxides or alkoxide based sol gel synthesis. [7,8,52,53]. Advantages and disadvantages of electrochemical, chemical and mechanical milling procedures are given in Table 1.2

Table 1.2 Advantages and disadvantages of various procedures for the synthesis of ZnO nanoparticles

Method	Advantages	Disadvantages
Electrochemical	Different morphologies like rods and wires can be produced	Expensive. A template (*e.g.* alumina) is usually required for the uni-directional organisation of these materials.
Chemical	Narrow particle size distribution and composite materials can be produced	Multi step processing required and a large amount of agglomeration occurred during synthesis
Mechanical milling	Bulk production is possible and simple to reproduce	Wide range of particle size distribution

1.5 Varistors

Varistors are electronic ceramic devices whose primary function is to sense and limit transient voltage surges and to do so without being destroyed.[54-64] The ZnO varistor was initially developed by Matsuoka in Japan[54] and has been available on the market since 1972. Zinc oxide varistors are known by various names such as voltage arrestors, non-linear resistors, surge suppressers and voltage regulators (Fig.1.4). They are electroceramic devices, which have voltage dependent

switching capabilities. In other words varistors are ceramic based semiconductors with highly non-linear current voltage characteristics. This device can be regarded as insulating up to a certain field, (the breakdown field Vc). Above that it becomes highly conducting.

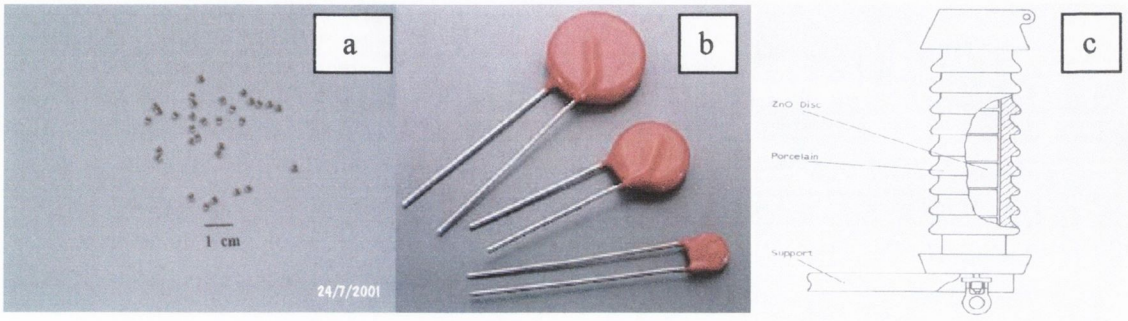

Fig. 1.4 Various types of ZnO varistors fabricated for different uses a) varistors used in electronic circuits for overvoltage protection b) varistors used in common electronic equipments c) surge arrester [60] for electric power distribution applications.

The varistor is usually connected across the power line in parallel with the instrument to be protected. The resistivity of a ZnO varistor is very high (more than 10^{10} Ω. cm) below a threshold voltage and is very low (less than several Ω. cm) above the threshold voltage.[55-56] When the voltage exceeds the switch voltage, the varistor becomes conducting and draws the current through it and when the voltage returns normal the varistor returns to its highly resistive state and pass only leakage current.[59] The relationship between current and voltage in a varistor device is often described as

$$I=C(V)^{\alpha} \qquad [1.1]$$

where **I** = current; **V** = voltage ; α = coefficient of nonlinearity; C = material constant

If α= 1 we would have an ohmic device *i.e.* current is proportional to the applied voltage. As the α approaches ∞ we have a perfect varistor *i.e.* the current varies

infinitely for a small changes in the applied field (α can be calculated as the inverse of the slope in the non-linear region of the I-V curve). Typical α values for ZnO varistors are from 30 to 100. Previously varistors were made from SiC and TiO_2 and did not show α values above 10.[56,61] In contrast, a ZnO varistor has a high value of α which make it a highly effective transient voltage protection devices. Today ZnO varistors are used in all areas of electronics and communication technology. Varistor behaviour can be illustrated as shown in Fig.1.5.

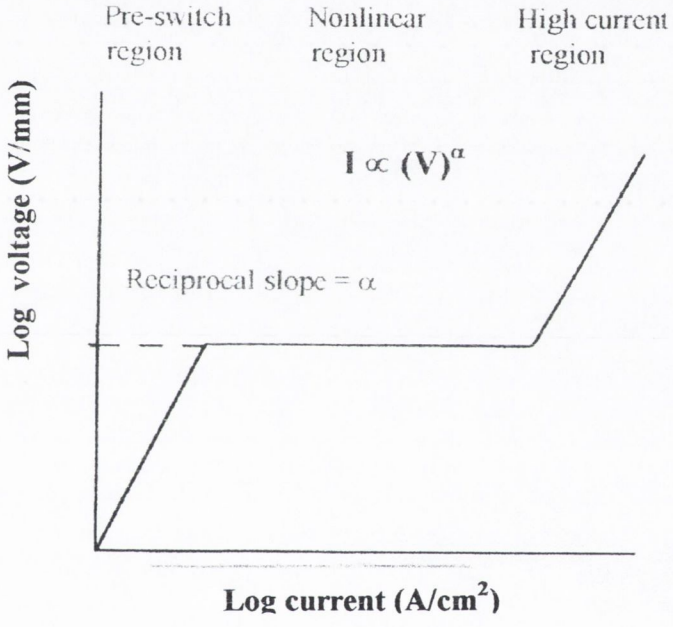

Fig. 1.5 Diagrammatic representation of a varistor material.

In regions I (pre-switch region) and III (high current region) the electrical behaviour is ohmic and α is approximately 1. In region II (nonlinear region) after the voltage reaches a critical value, the material becomes highly conducting and α reaches maximum value.

The most desirable device should have a high value of nonlinear coefficient, an acceptable rating of nonlinear voltage (breakdown field), a low value of leakage current, a long varistor life and a high-energy absorption capability.

1. Nonlinear Coefficient (α)

Nonlinear Coefficient (α) is the reciprocal of the slope of the I-V curve (Fig.1.5) in the nonlinear region.[59,65] The higher the value of α, the better the device. The nonlinear coefficient α is a very important parameter for instrument protection.

2. Nonlinear voltage/ break down field

ZnO varistors are characterised by the threshold voltage (nonlinear voltage), which marks the transition from linear to nonlinear mode. The voltage at the onset of this nonlinearity, just above the knee of the I-V curve, is the nonlinear voltage. Because of the lack of sharpness of the transition in the I-V curve the exact location of this voltage is difficult to determine in most varistors, the varistor voltage in the literature has often been described as the voltage (nonlinear voltage) observed at 1 mA.[56]

3. Leakage current

Leakage current determines the amount of watt loss (as heat ~I^2R) that a varistor is expected to generate upon application of a steady state operating voltage.[59] For an AC application, the total leakage current (I_L) in the pre-breakdown region is composed of a resistive current (I_R) and a capacitive current (I_C). In the design of a surge suppresser from a ZnO varistor, it is the resistive current (I_R), which is of importance since this is responsible for joule heating within the elements. The parameters, which are known to influence the leakage current, are (a) formulation of the ZnO varistor, (b) applied voltage and (c) time duration of the applied voltage. [58-62]

1.5.1 Mechanism of varistor action

ZnO without any additives is a nonstoichiometric n-type semiconductor with a linear I-V behaviour. To make it nonlinear various metal oxides have to be incorporated in the ZnO. [54,56,58,59] Chief among these oxides is Bi_2O_3, which can be considered as a varistor former, without which it is difficult to make a varistor. The first highly nonlinear composition with α = 50 was reported by Matsuoka.[54] In addition to 97 mol % ZnO he added 0.5 mol % each of Bi_2O_3, CoO, MnO, Cr_2O_3 and 1 mol% Sb_2O_3. Inada in 1980[62] reported the formation of

chemical phases during the heat treatment in the range 950-1050°C. The ZnO-Bi_2O_3-Sb_2O_3 system forms a pyrochlore phase $Zn_2Bi_3Sb_3O_{14}$ above 650°C. Together with ZnO, pyrochlore further reacts to form spinel ($Zn_7Sb_2O_{12}$).

$$2\ Zn_2Bi_3Sb_3O_{14} + 17\ ZnO \xrightarrow{950\text{-}1050\ ^\circ C} 3\ Zn_7Sb_2O_{12} + 3\ Bi_2O_3\ [L] \quad [1.2]$$

(Pyrochlore) (Spinel)

Thus the basic components can be seen in a typical varistor microstructure are ZnO, Spinel, pyrochlore and several bismuth rich phases (Fig 1.6). Spinel and pyrochlore are found in intergranular phases and Bi-rich phases are seen at the triple points.[56,58,61]

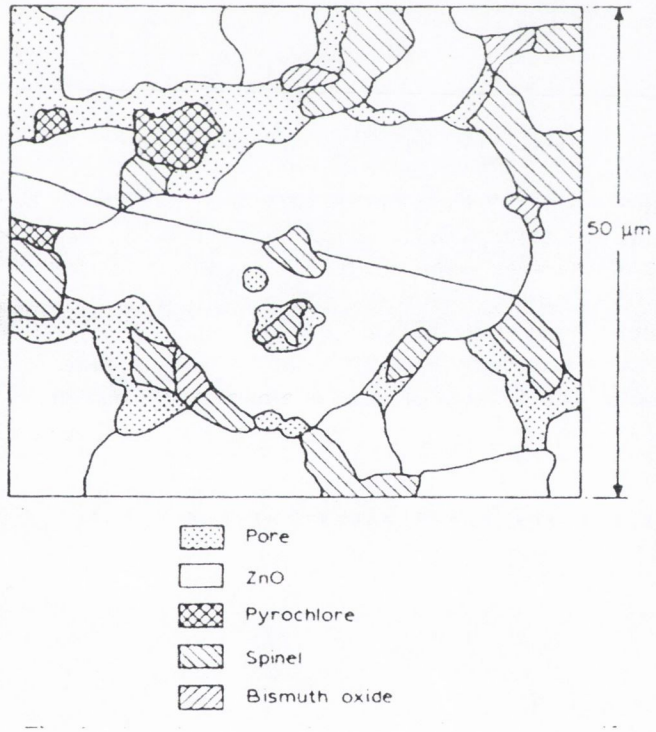

Fig. 1.6 Schematic diagram of the microstructure of a sintered ZnO varistor material.[60]

During sintering various phases are distributed in such a way that the grain boundary region becomes highly resistive and ($\rho_{gb} \sim 10^{12}\ \Omega$ cm) and the grain interior becomes highly conductive (ρ_{gb} 1 ~ 10 Ω cm) (Fig.1. 7).

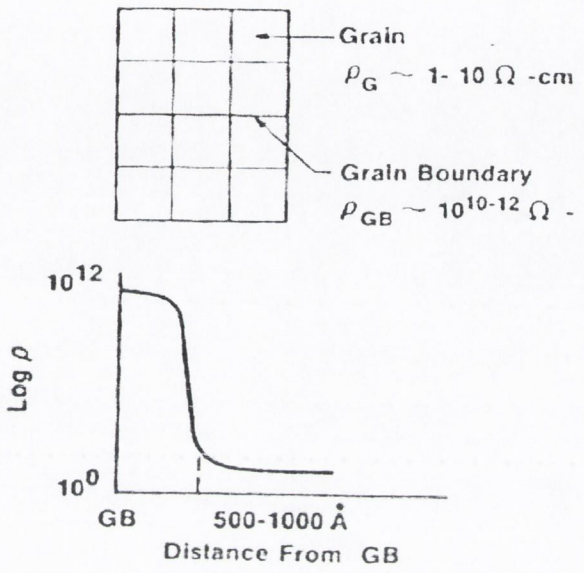

Fig. 1.7 Diagrammatic representation of the mechanism of electrical characteristics at the grain and grain boundary and the formation of a depletion layer at the grain boundaries. [56]

A sharp drop in resistivity (Fig.1.7) from grain boundary to grain occurs within a distance of ~ 50 to 100 nm. This is known as the depletion layer. Thus at each grain boundary there exists a depletion layer extending into the adjacent grains. The varistor action arises as a result of the presence of this depletion layer. The conduction mechanism in varistors can further be explained by Fig. 1.8. Path (1) through the region of closest grain-grain contact represents conduction over the Schottky barrier and path (2) is through the grain boundaries and inter-granular materials.

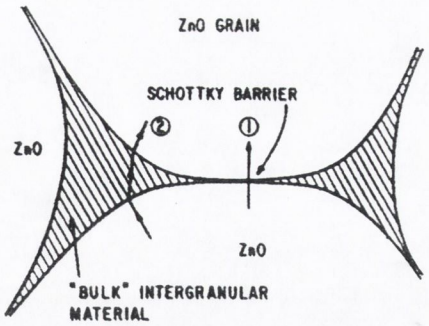

Fig. 1.8 Conduction mechanism of varistors.[64]

1.6 Synthesis of metal oxide varistor powders – a review of recent advances

1.6.1 Historical developments

ZnO varistors were first developed by Matsuoka at Matsushita Electric, Japan, in 1968 and commercialised under the trade name ZNR.[56,59-61] Commercial varistors are usually fabricated from ZnO particles with small amount of dopant oxides such as Bi_2O_3, Sb_2O_3, CoO, MnO, NiO and Cr_2O_3.[54-57] The mixed powder is then pressed to desired shapes and sintered at higher temperatures. The final grain size after sintering is on the order of 8 μm and the corresponding breakdown voltage is around 2-4 kV/cm which is equivalent to a voltage drop of ~1.5-3.0 volts per intergranular barrier.[64] Thus the breakdown voltage of the sintered body is proportional to the number of grain boundaries.

1. 6.2 Conventional synthesis

ZnO varistors are conventionally prepared by weighing, mixing, plastification and sintering. The powders are usually mixed using an agate mortar in dry form or a ball mill in wet form. After adding organic binders the above mixture is pressed into discs of desired dimensions. The pressed discs are sintered at 1200-1400°C. The sintered pellets are further electroded, leads are attached and finally it may be encapsulated in a polymeric material and electrically tested. A simplified flow diagram is given in Scheme 1.3.

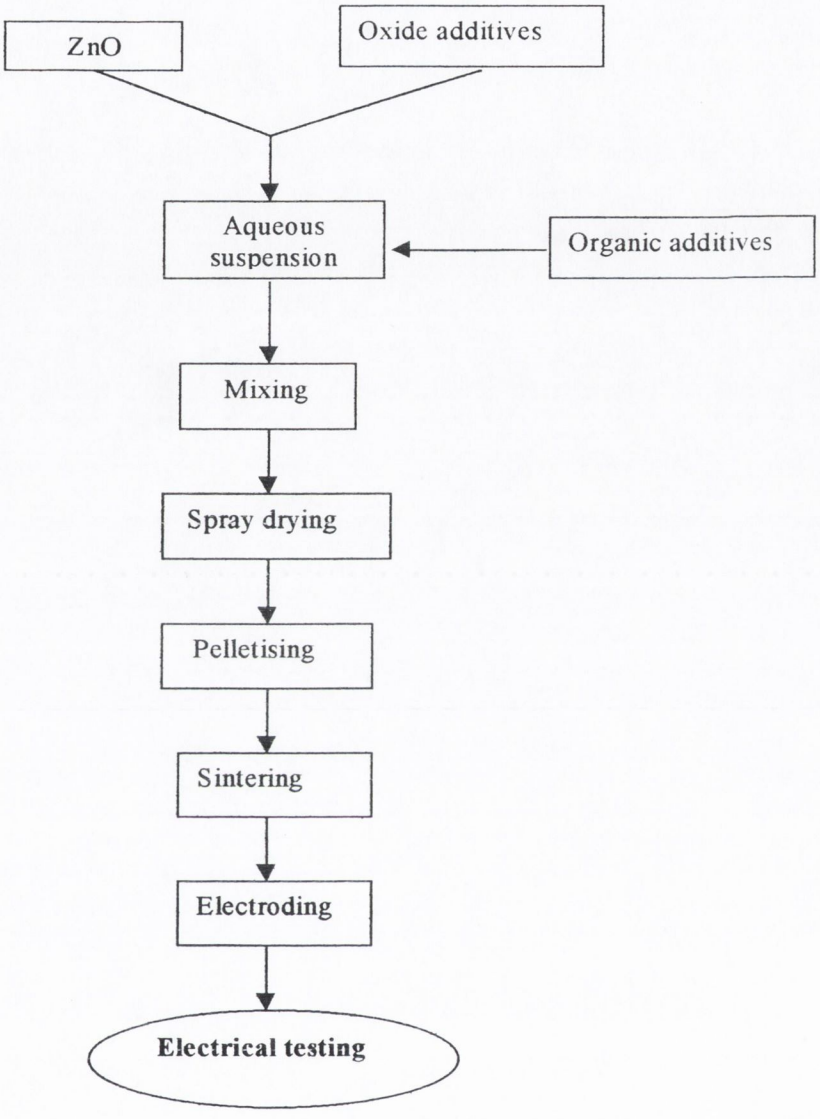

Scheme 1.3 Different steps in conventional industrial processing of varistor ceramics.

The conventional varistor processing route is the preferred method in the industry at present. The ease by which the powder methods can be utilised on an industrial scale and the low cost associated with the use of inexpensive oxide powders are the two main attractions of this route.

1.6.3 Need for new processing routes

Microstructural homogeneity is a key parameter to control the ohmic and non-ohmic behaviour of varistors. An ideal varistor has a crystalline microstructure of uniform grain size, shape and composition. Compositional homogeneity is difficult to achieve by conventional ceramic routes. By wet chemical methods homogeneity of the dopant ions among the ZnO grains can be achieved at the molecular level. The temperature required for sintering also depends on the particle size and homogeneous distribution of dopants among the individual grains.

There are a few disadvantages of the solution processing route; these include a) large processing time b) comparatively higher cost of precursors c) large amount of solvents required for synthesis and d) the shrinkage in volume during processing.

1.6.4 Different chemical procedures used to prepare varistors

1.6.4.1 Amine processing

Hishita *et al*[65] developed a powder preparation method involving amines as precipitants. The mixed acidic solution of ZnO, Bi_2O_3, $SbCl_3$, $CoCl_2$ was added to diethylamine solution to coprecipitate all components. The resulting mixture was washed, dried and calcined to produce active and uniform composition powders (200 nm). High nonlinearity coefficients (α = 50) were achieved in varistors fabricated from these powders by sintering in the range 1100°C to 1250°C. Large breakdown voltage (711 V/mm) was also achieved with lower sintering temperature compared to the conventional methods(1200-1300°C).

1.6.4.2 Aqueous precipitation

Haile *et al*[66] used the aqueous precipitation technique for the synthesis of spherical ZnO particles (Scheme 1. 4).

$$ZnSO_4.\ 7H_2O + NH_4OH \longrightarrow xZnSO_4.yZn(OH)_2.\ 2H_2O$$

$$\xrightarrow{H_2O/pH=9/\ heat} Zn(OH)_2 + (NH_4)_2\ SO_4 + NH_3 \xrightarrow{55°C} ZnO$$

Scheme 1.4 Aqueous precipitation technique to synthesise ZnO particles.[66]

Chemical coating of these powders has been achieved by precipitation, which allowed the fabrication of varistors with improved properties over the conventionally fabricated varistors. They reported a high coefficient of nonlinearity of 44 and a breakdown voltage of 180 V/mm.

1.6.4.3 Citrate gel synthesis

The citrate gel process has been employed successfully to prepare varistors.[68-69] The process consists of the production of solid amorphous precursors by the dehydration of gels, which are produced by the addition of citric acid to a nitrate solution containing salts of zinc and dopant metals. The solid precursors are subsequently decomposed and oxidised in air to yield the oxide materials. The technical advantage of this method is high chemical homogeneity in the resulting powder and the simplicity of the procedure. Therefore it is potentially a promising method for the preparation of ZnO varistor powder.[67-69]

Fan and Sale[67] prepared ZnO varistors through a citrate gel route. The dried precursor has been thermally decomposed to give an oxide powder of submicron particle size. They reported a high breakdown voltage of 400 V/mm and nonlinear exponent α of 20. The differences in electrical properties has been explained by the chemically more homogeneous microstructures obtained in the gel processed material.

Sinha and Sharma[68] presented a modified citrate gel technique for preparation of ZnO varistors, which involved the preparation of mixed oxides by adding citric acid to a nitrate solution. The powder (37 nm) sinters to a high density (98%) in one hour at 1150°C. These pellets also exhibited a reasonably high non-linear coefficient (35) low leakage current (11.1 μA) and a reasonably high breakdown field of 515 V/mm.

Recently Duran *et al*[69] successfully synthesised nano-sized (~28 nm) ZnO based ceramic powders by citric acid route. A dense ceramic was fabricated by normal liquid phase sintering at 850°C and 940°C for 1 to 5 hours. Electrical studies

showed a high non-linear coefficient (70) and a high breakdown voltage (1500 V/mm)

1.6.4.4 Combustion synthesis

The basis of the combustion synthesis technique comes from the thermochemical concepts used in the field of propellants and explosives.[70] The combustion synthesis technique begins with the reactants that oxidise easily (such as nitrates) and a stable organic fuel (*e.g.* urea, $CO(NH_2)_2$) that acts as a reducing agent. The mixture is brought to boil until it ignites and a self-sustaining and rather fast combustion reaction takes off, resulting in a dry unagglomerated fine oxide powder. Sousa *et al*[70] synthesised pure and doped ZnO powders from mixtures of relevant water soluble metal nitrates as cation precursors and urea as fuel. The mixtures were ignited at 500°C resulting in the varistor precursor with particle sizes ranging from 52 to 158 nm. No electrical results were reported.

1.6.4.5 Micro-emulsion synthesis

A micro-emulsion is generally defined as a thermodynamically stable dispersion of two immisible liquids (usually water and a hydrocarbon). The aqueous cores of micro-emulsion containing soluble zinc salt are used for the synthesis of nanoparticles by adding ethanol and a precipitating agent.[28,29]

Shah and co-workers[28-30] reported the micro-emulsion mediated synthesis of ZnO nanoparticles for varistor studies. The optimised micro-emulsion system consisted of surfactant CTAB, 1-butanol as co-surfactant, *n*-butane as continuous oil phase and aqueous solution as the dispersed phase. They have obtained a value of nonlinear exponent α, as high as 83, with a breakdown voltage of 450 V/mm.

1.6.4.6 Plasma synthesis

Plasma pyrolysis technology was used to synthesise nanometer size precursor powders of ZnO.[41] The ZnO and additive composite powders are composed of spherical particles whose size is about 10-50 nm. Varistors were fabricated by sintering the material at 1050°C. The combination of the powder's nanoparticle effect, high reactivity and narrow grain size distribution were the reasons found to decrease the sintering temperature. Electrical results revealed a breakdown voltage of 500 V/mm, nonlinear coefficient of 54 and a leakage current of 1 μA.

1.6.4.7 Precipitation reaction

Viswanath *et al* [71] prepared varistors from ultra fine zinc oxide powders with the crystallites in the range between 3 and 10 nm. Synthesis of nanosize ZnO involved chemical reaction between zinc perchlorate ($Zn(ClO_4)_2$) and sodium hydroxide in methanol medium under nitrogen atmosphere. Precipitation and centrifugation methods were used to collect the resultant powders. The nano powder thus obtained was doped with Bi, Sb, Co, B, Sn and Cu oxides. The material produced has an extremely high breakdown voltage of 3000 V/mm with a nonlinear exponent α of 50. Suguwara *et al*[72,73] produced ZnO varistors by a precipitation method using zinc acetate as a starting material with praseodymium oxide and cobalt chloride as additives. The additives were dissolved in ethanol by evaporation and drying after being dissolved in hydrochloric acid solution. Precipitation has been conducted by adding oxalic acid dihydrates. No systematic electrical studies were reported on these materials.

1.6.4.8 Sol gel processing

Varying the microstructure at the grain boundary regions can alter varistor properties. Sol gel processing provides a method for homogeneous doping at the molecular level[31-33] which is very important in the varistor since inhomogeneous distribution of dopants in a varistor results in the formation of hot spots as the current follows the path of least resistance. This causes the failure of the varistor at a lower current density than the expected value. There are a few reports available in the literature where ZnO prepared through sol gel technique have been used for varistor applications.

Westin *et al*[74-76] reported the sol gel preparation of varistor powders. They have tried different sol gel methods to obtain the varistor precursors. The microstructural and electrical properties have been determined. Higher breakdown voltages (249 V/mm) are obtained for the ZnO coated with additive oxides. In 1998 Ya *et al*[77,78] reported the fabrication of varistors by doped ZnO powders (20 nm). This materials displayed superior electrical properties with a high value of the nonlinear coefficient (α = 45) and lower leakage current (I_L<1 μA). Puyane *et al*[79,80] reported the production of ZnO varistor by various solution routes and studied their sintering behaviour. The aqueous solution route has given a ZnO powder, which sinters at higher temperatures than those observed in conventional mixed oxide powders, whereas the metal organic route produces ZnO powders, which sinter at lower temperatures than conventional mixed oxide powders. Hohenberger and Tomandl[81] adopted a new sol gel based technique for the synthesis of ZnO varistor powders. They showed that the varistor ceramics made from the sol gel powders can be sintered at lower temperatures and show improved electrical behaviour (α= 55, leakage current 0.9 μA, breakdown 375 V/mm).

Kong and co-workers[82] presented a novel method to prepare ZnO varistors. ZnO powders were prepared by chemical precipitation and a B-Si-Pb coating synthesised following a sol gel process. The phases crystallised from the glass formed a layer with higher resistivity at the grain boundaries of ZnO, which acted as a potential barrier in the varistors. Lauf and Bond[83] fabricated varistor

precursor powders by sol gel processing and further hot pressing the powders below 800°C in a reducing environment achieved a high green density (pre-sintered density). Subsequently they were heat treated in air up to 1000°C, which developed the non-ohmic electrical properties (α= 30). Espinola *et al*[84] prepared ZnO varistors by a colloidal gel route using water soluble salts. Sintering at 1100°C produced a varistor with α of 26-40 and breakdown voltage 800- 1000 V/mm.

Recently Chu *et al*[85] reported a novel sol gel processing method for the preparation of ZnO varistor powder using zinc acetate dihydrate, ethylene glycol, *n*-propyl alcohol and glycerol. The varistor material thus obtained could be sintered at 1000°C.

The electrical properties and sintering temperatures are discussed in Table 1.1

Table 1.3 Various chemical synthesis procedures for ZnO varistors and comparison of the electrical characteristics.

Synthetic route	Reference	Sintering temperature (°C)	Electrical results	
			V_C (V/mm)	α
Amine Processing	*Hishita*[65]	1050	711	50
		1200	339	52
		1300	256	36
Aqueous Precipitation	*Haile*[66]	1200	180	44
Citrate gel	*Fan*[67]	1200	400	20
	Sinha[68]	1150	515	35
	Duran[69]	850	1500	70
Combustion	*Sousa*[70]	-	-	-
Micro-emulsion	*Shah*[28-30]	1200	105	76
		1200	450	83
Plasma pyrolysis	*Lin*[41]	1050	500	54
Precipitation	*Viswanath*[71]	750	3000	50
	Suguwara[72,73]	1200	-	-

Table 1.3 Continued……

Synthetic route	Reference	Sintering temperature (°C)	Electrical results	
			V_C (V/mm)	α
Sol gel				
	Westin[74-76]	1100	249	37
	Puyane[79]	1100	-	12
	Puyane[80]	-	259	-
	Tomandl[81]	1100	375	60
	Ya[77,78]	950	1000	45
	Kong[82]	-	-	-
	Lauf[83]	1000	980	30
	Espinola[84]	1100	800-1000	26-40
	Chu[85]	1000	-	50

1.7 Objective of the thesis

Controlling a material's properties at the molecular level is one of the challenges of advanced materials science. Sol gel processing is one way of producing nanoparticles and also is a way of manipulating precursors to form bulk oxide materials. The advantages of sol gel processing are primarily the higher purity and homogeneity and the lower processing temperature. Multi-component dopant oxides can also be developed by mixing relevant salt solutions of metal salts by these methods.

Recently the production of personal computers, mobile phones and electronic devices has been experiencing phenomenal growth with rapidly increasing performance and miniaturisation. As a result there has been an increase in demand for miniaturisation of protective devices such as zinc oxide based varistors which find their use as voltage surge absorbers. The aim of this project is to study the varistor properties of materials prepared from doped nanoparticular ZnO.

The breakdown voltage of the sintered body is proportional to the number of grain boundaries between the electrodes. The breakdown voltage per grain boundary is calculated as ~3V.[58,59] This indicates that the breakdown voltage is proportional to the inverse of the ZnO grain size. As the nanocrystalline material contains large grain boundary volumes, more varistor active grain boundaries per unit volume can be produced in order to develop a better device in a smaller dimension. The threshold voltage is about 4 kV/cm for a conventional highly (5-6%) doped ZnO varistor material.[86] It is reported that pure nanophase ZnO can also exhibit varistor behaviour with a small but usable threshold voltage of 100V/mm of material for a 60 nm diameter grain size prepared through gas condensation technique.[86] Work on doped nanophase ZnO with 3-10 nm grains show a varistor behaviour for voltages up to 3000 V/mm.[71] Therefore it is possible through nanostructuring to produce ZnO varistors with threshold voltage up to 30 kV/cm by controlling the grain size and hence the number of grain boundaries in the material.

Sintering temperature can also be reduced by nanostructuring. The smaller the particle size the lower the temperature required because the increased surface force cause the particles to flow together at lower temperatures. This has been one of the driving forces behind the formation of nanoscale particles in which the sintering temperature is greatly reduced.[87] It is also important that the dopant distribution in the microstructure is highly homogeneous, which can be achieved through sol gel processing. Chemical homogeneity is nearly impossible to guarantee by mechanical milling or grinding processes. Two approaches are tried here. In one way by nanostructuring of the precursors, much smaller grain sizes will be produced compared to the conventional processing and secondly by sol gel processing a molecular level mixing of dopants can be achieved in order to get a homogeneous microstructure.

The objectives of this project can be summarised as follows.

1. To synthesise nanoparticulate ZnO based on reported procedures and investigate methods to characterise these particles including Transmission Electron Microscopy (TEM), X-ray powder diffraction (XRD), UV/Visible spectroscopy, thermal analysis and FESEM.
2. To compare the electrical properties of nanoparticulate ZnO prepared through previously reported procedures.
3. To develop novel procedures based on sol gel technology for preparation of nanocrystalline ZnO suitable for varistor applications.
4. To develop suitable methods to add dopants to ZnO nanoparticles at the molecular level for a better homogeneity.
5. To develop inexpensive routes for the synthesis of more efficient varistors by nanostructuring and study the varistor properties in collaboration with Littelfuse, Ireland Ltd.
6. To develop new mixed oxide varistor materials with higher breakdown voltage, low leakage and reasonably higher α for a better varistor by optimising the processing and sintering conditions.

1.8 An overview of the experiments performed

Three types of synthetic procedures were tried to make varistor discs;

a) Nano-size ZnO prepared from well established synthetic procedures (Spanhel and Anderson,[8] Meulenkamp[9] and Weller[51]) were mixed with additives;

b) Nanosize ZnO prepared from a novel sol gel route was mixed with additives

c) Varistor precursor nano-powders were prepared by a novel mixed precursor oxide method.

The methods[8,9,51] used for the preparation of well defined nanoparticular ZnO are based on the reaction of zinc salts with alkali metal hydroxides under controlled conditions. A novel and simple procedure to fabricate ZnO nanoparticles and ZnO nanowire arrays using a non-hydrolytic sol gel condensation reaction and subsequent calcinations was also tried. The nano ZnO materials produced as described above were treated with additives, pressed into discs and sintered to get a varistor material. A mixed precursor method using inexpensive inorganic salts was employed to fabricate better varistors with considerably higher breakdown voltage and nonlinear coefficient. The varistor properties of the sintered samples were compared with the commercial samples (Littelfuse Ireland Ltd.) sintered under similar experimental conditions.

1.9 References

1. G. Stix, *Scientific American,* 2001, **285**, 26.
2. F. E. Kruis, H. Fissan and A. Peled, *J. Aerosol Sci.*, 1998, **29**, 511.
3. H. Gleiter, *Prog. Mater. Sci.*, 1989, **33**, 223.
4. H. Gleiter, *Nanostruct. Mater.*, 1995, **6**, 3.
5. M. H. Huang, S. Mao, H. Feick, H. Yan, Y. Wu, H. Kind, E. Weber, R. Russo and P. Yang, *Science,* 2001, **292,** 1897.
6. M. H. Huang, Y. Wu, H. Feick, N. Tran, E. Weber and P. Yang, *Adv. Mater.,* 2001, **13**, 113.
7. B. Nikoobakht, Z. L. Wang and M. A. El-Sayed, *J. Phys. Chem. B*, 2000, **104**, 8635.
8. L. Spanhel and M. A. Anderson, *J. Am. Chem. Soc.*, 1991, **113,** 2826.
9. E. A. Meulenkamp, *J. Phys. Chem. B.,* 1998, **102**, 5566; E. A. Meulenkamp, *J. Phys. Chem. B.,* 1998, **102**, 7764.
10. S. Fullam, D. Cottel, H. Rensmo and D. Fitzmaurice, *Adv. Mater.,* 2000, **12,** 1430.
11. Y. Chen, D. Bagnall and T. Yao, *Mater. Sci. Eng. B,* 2000, **75**, 190.
12. W. Seigel, S. Ramaswamy, H. Hahn, L. Zongquan, L. Ting and R. Gronsky, *J. Mater. Res.,* 1988, **3**, 1367.
13. S. Edelstein, J.S. Murday and B. B. Rath, *Prog. Mater. Sci.,* 1997, **42**, 5.
14. R. Z. Ma, J. Wu, B. Q. Wei, J. Liang and D. H. Wu, *J. Mater. Sci.,* 1998, **33,** 5243.
15. U. S. Hareesh, A. D. Damodaran, K. G. K. Warrier, *Brit. Ceram. Trans.,* 1997, **96**, 99.
16. R. W. Seigel, *J. Phys. Chem. Solids.,* 1994, **10**, 1097.
17. M. Rajan, *High Tech Ceramics News*, 2001, **13**, 1.
18. H. Weller and A. Eychmuller, *Semiconductor Nanoclusters- Studies in Surface Science and Catalysis,* Elsevier Science, Amsterdam, 1996.
19. A. H. Chokshi, A. Rosen, J. Karch and H. Gleiter, *Scripta Metallurgica.*, 1989, **23**, 1679.
20. D. M. Owen and A. H. Chokshi, *Acta Mater.,* 1998, **46**, 667.
21. D. M. Owen and A. H. Chokshi, *Acta Mater.,* 1998, **46**, 719.
22. P. Alivisatos, *Science*, 1996, **271**, 933.

23. R. F. Service, *Science*, 2000, **287**, 1902.

24. F. Greuter and G. Blatter, *Semicond. Sci. Technol.*, 1990, **5**, 111.

25. U. Schubert, N. Husing, *Inorganic Materials: A Chemical Approach* Wiley-VCH, London, 2000.

26. M. Hirano and E. Kato, *J. Am. Ceram. Soc.*, 1999, **82**, 786.

27. A. Kumar and R. Roy, *J. Mater. Res.*, 1998, **3,** 1373.

28. M. Singhal, V. Chhabra, P. Kang and D. O. Shah, *Mater. Res. Bull.*, 1997, **32**, 239.

29. S. Hingorani, V. Pillai, P. Kumar, M. S. Multani and D. O. Shah *Mat. Res. Bull.*, 1993, **28**, 1303.

30. S. Hingorani, D. O. Shah and M. S. Multani, *J. Mat. Res.*, 1995, **10,** 461.

31. C. J. Brinker, and G. W. Scherer, *Sol-Gel Science.*, Academic Press Inc., New York, 1990.

32. S. Doeuff, M. Henry, C. Sanchez, and J. Livage, *J. Non. Cryst. Solids.*, 1987, **89**, 206.

33. L. L. Hench and J. K. West, *Chem. Rev.*, 1990, **90**, 33.

34. C. Suresh, V. Biju, P. Mukundan and K. G. K. Warrier, *Polyhedron.*, 1998, **17**, 3131

35. T. V. Mani, H. K. Varma, A. D. Damodaran, K. G. K. Warrier and U. Balachandran, *J. Am. Ceram. Soc.*, 1994, **77**, 1597.

36. J. Yang, and J. M. F. Ferreira, *Mater. Res. Bull.*, 1998, **33,** 389.

37. H. H. Kung, and E. I. Ko, *Chem. Eng. Journal.*, 1996, **64,** 203.

38. S.R. Kumar, S. C. Pillai, U.S. Hareesh, P. Mukundan and K. G. K. Warrier, *Materials Letters,* 2000, **43**, 286.

39. B. O'Regan , D. T. Schwartz, S. M. Zakeeruddin and M. Grätzel, *Adv. Mater.*, 2000, **12,** 1263.

40. Y. Chen, D. Bagnall and T. Yao, *Mater. Sci. Eng. B,* 2000, **75,** 190.

41. Y. Lin, Z. Zhang, Z. Tang, F. Yuan and J. Li, *Adv. Mater. Opt. Electro.*, 1999, **9**, 205.

42. H-M. Lin, S-J. Tzeng, P-J. Hsiau and W-L. Tsai, *Nanostruct. Mater.*, 1998, **10,** 465.

43. Y. Li, G. W. Meng, L. D. Zhang and F. Phillipp, *App. Phys. Lett.*, 2000, **76**, 2011.

44. Y. Li, G. S. Cheng and L. D. Zhang, *J. Mater. Res.*, 2000, **15**, 2305.

45. Y. C. Kong, D. P. Yu, B. Zhang, W. Fang and S. Q. Feng, *App. Phys. Lett.*, 2001, **78**, 407.

46. H. D. Alamdari, S. Boily, M. Blouin, A. V. Neste and R. Schulz, *Mater. Sci. Forum.*, 2000, **343**, 909.

47. H. M. Deng, J. Ding, Y. Shi, X. Y. Liu and J. Wang, *J. Mater. Sci.*, 2001, **36**, 3273.

48. T. Tsuzuki and P. G. McCormick, *Scripta Mater.*, 2001, **44,** 1731.

49. P. G. McCormick, T. Tsuzuki J. S. Robinson and J. Ding, *Adv. Mater.*, 2001, **13,** 1008.

50. L. Wenjum, S. Erwei, T. Mingyuan and Z. Weizhuo, *Science in China*, 1998, **5**, 449.

51. U. Koch, A. Fojtik, H. Weller and A. Henglein, *Chem. Phys. Lett.*, 1985, **122**, 507.

52. D. F. Bahnemann, C. Kormann and M. R. Hoffmann, *J. Phys. Chem. B*, 1987, **91**, 3789.

53. C. L. Carnes and K. J. Klabunde, *Langmuir*, 2000, **16**, 3764.

54. M. Matsuoka, *Jpn. J. Appl. Phys.*, 1971, **10**, 736.

55. K. Eda, *IEE Electrical Institution Magazine, 1989,* **5**, 28.

56. T. K. Gupta, *J. Am. Ceram. Soc.*, 1990, **73**, 1817.

57. J. Fan and R. Freer *British Ceramic Transactions,* 1993, **96**, 221.

58. T. Asokan and R. Freer, *J. Mater. Sci.*1990, **25**, 2447.

59. D. R. Clarke, *J. Am. Ceram. Soc.*, 1999, **82,** 485.

60. B. C. H. Steele, *Electronics ceramics*, Elsevier Applied Science London and New York, 1991, p 17.

61. R. Einzinger, *Ann. Rev. Mater. Sci.*, 1987, **17**, 299.

62. M. Inada, *Jpn. J. Appl. Phys.*, 1980, **19**, 409.

63. E. Olsson, L. K. L. Falk and G. L. Dunlop, *J. Mater. Res.*, 1985, **20**, 4091.

64. L. M. Levinson and H. R. Philip, *Ceramic Bulletin.*, 1986, **65**, 639.

65. S. Hishita, Y. Yao and S-I. Shirasaki, *J. Am. Ceram. Soc.*, 1989, **72**, 338.

66. S. M. Haile, D.W. Johnson, Jr. G. H. Wiseman and H. K. Bowen, *J. Am. Ceram. Soc.*, 1989, **72,** 2004.

67. J. Fan and F. R. Sale, *Electroceramics Production, Properties and*

Microstructure Ed by W.E. Lee and A. Bell The Institute of Materials London, p. 151.

68. A. Sinha and B. P. Sharma, *Mat. Res. Bull.*, 1997, **32**, 1571.
69. P. Duran, F. Capel, J. Tartaj, and C. Moure *J. Am. Ceram. Soc.*, 2001, **84**,1661.
70. V. C. Sousa, A. M. Segadaes, M. R. Morelli, R. H. G. A. Kiminami, *Int. J. Inorg. Mater.*, 1999, **1**, 235.
71. R. N. Viswanath, S. Ramasamy, R. Ramamoorthy, P. Jayavel and T. Nagarajan, *Nanostruct. Mater.*, 1995, **6**, 993.
72. M. Takehana, T. Nishino, K. Sugawara and T. Sugawara, *Mater. Sci. Eng. B,* 1996, **41,** 186.
73. M. Takehana, T. Nishino, K. Sugawara and T. Sugawara, *Korean J. of Chem. Eng.*, 1996, **13,** 538.
74. G. Westin and M. Nagren, *J. Mater. Chem.*, 1993, **3**, 367.
75. G. Westin, A. Ekstrand, M. Nagren, R. Osterlund and P. Merkelbach, *J. Mater. Chem.*, 1994, **4,** 615.
76. A. Ekstrand, M. Nagren and G. Westin, *J. Sol Gel Sci. Tech.*, 1997, **8**, 697.
77. K. X. Ya, H. Yin, T. M. De and T. M. Jing, *Mater. Res. Bull.*, 1998, **33,** 1703.
78. K. X. Ya, W. T. Diao, H. Yin, T. M. De and T. M. Jing, *Mater. Res. Bull.*, 1998, **32,** 1165.
79. R. Puyane, F.Toal and S. Hampshire, *J. Sol Gel Sci. Tech.*, 1996, **6**, 219.
80. R. Puyane, I. Guy and R. Metz, *J. Sol Gel Sci. Tech.*, 1998, **13**, 575.
81. G. Hohenberger and G. Tomandl *J. Mat. Res.*, 1992, **7,** 546.
82. L. Kong, F. Li, L. Zhang and X. Yao, *J. Mater. Sci. Lett.*, 1998, **17**, 769.
83. R. T. Lauf and W. D. Bond, *Ceramic Bulletin,*1984, **2**, 278.
84. M. C. S. Nobrega, M. S. Zolotar, W. A. Mannheimer and A. Espinola, *J. Non Cryst. Solids,* 1992, **147&148,** 803.
85. S. Y. Chu, T-M. Yan, S-L. Chen, *J. Mat. Sci. Lett.*, 2000, **19**, 349; S. Y. Chu, T-M. Yan and S-L. Chen, *Ceram. Int.*, 2000, **26**, 733.
86. J. T. Lee, J-H. Hawang J. J.Mashek, T. O. Mason, A. E. Miller and R. W. Siegel, *J. Mater. Res.*, 1995, **10**, 2295.
87. C. D. Chandler, C. Roger and J. Hampden-Smith, *Chem. Rev.*, 993,**93**,1205.

Chapter 2

Experimental, materials and methods

2.1 Introduction

Investigation required for the characterisation of the fresh gels and the xerogels (fresh gel dried at 80°C) by various techniques including Transmission Electron Microscopy (TEM), Differential Scanning Calorimetry (DSC), Thermo-Gravimetric Analysis (TGA) and Powder X-ray Diffraction (XRD) techniques. The xerogel was further calcined to 500°C and analysed by FESEM or TEM and surface area measurements. The calcined powder was plastified, pelletised and sintered at various temperatures to study the varistor properties. The sintered samples were subjected to density measurements and electrical characterisation. The microstructural and phase analysis were carried out using Scanning Electron Microscopy (SEM) and Energy Dispersive X-ray Analysis (EDX).

2.2 Materials Used*

Table 2.1 Chemicals used for the preparation of ZnO and varistor materials

Chemical	Manufacturer	Purity (%)
Zinc acetate dihydrate	Riedel-de Haen	99.5
Lithium hydroxide monohydrate	Sigma	99
Bismuth (III) nitrate pentahydrate	Aldrich	98
Antimony (III) acetate	Alfa	97
Cobalt (II) acetate tetrahydrate	Aldrich	98
Bismuth (III) chloride	Aldrich	98
Antimony (III) chloride	Aldrich	99
Cobalt (III) chloride hexahydrate	Aldrich	98
Manganese (II) acetate tetrahydrate	Aldrich	99
Nickel (II) acetate tetrahydrate	Aldrich	98
Chromium (III) nitrate nonahydrate	Aldrich	99

Aluminium nitrate nonahydrate	Aldrich	98
Sodium hexametaphosphate	Aldrich	96
Zinc perchlorate hexahydrate	Aldrich	-
Oxalic acid	Aldrich	99
Diethanolamine	Aldrich	99
Ethylene glycol	Aldrich	99

* ZnO, additive oxides and commercial varistor powder (Control, 26 E) were supplied by Littelfuse Ltd., Dundalk. All chemicals were reagent grade. ZnO (Grillo) Bi_2O_3 (Ferro corporation), Sb_2O_3 (Cookson), CoO (Outokumpu), MnO (Campbell Chemicals), NiO(Campbell Chemicals), Cr_2O_3(Merck) Al_2O_3 (Merck).

2.3 Synthesis

Five different experimental procedures for the production of nanocrystalline ZnO have been investigated.

2.3.1 Synthesis of well defined ZnO nanoparticles

2.3.1.1 ZnO prepared using Spanhel's method [1]

Zinc acetate dihydrate ($C_4H_6O_4Zn.\ 2H_2O$) and absolute ethanol were used as received. An ethanolic (0.1 M, 0.5 L) solution of zinc acetate (10.98g, 50mmol) was prepared in a 1 L round bottom flask, and rotary evaporation (65-70°C) was carried out over a period of about 3 hours. The condensate was collected continuously. At the end of this procedure about 300 mL of condensate and 200 mL of reaction mixture were obtained. The reaction mixture was again diluted with ethanol to 500 mL. Next, $LiOH.H_2O$ (2.93g, 70mmol) was added directly to the ethanol solution to produce a 0.14M LiOH solution. The suspension was then placed into an ultrasonic bath in order to dissolve the weakly soluble LiOH. At the end of this procedure a transparent ZnO sol was obtained. UV/Vis and

TEM measurements have been recorded for this sample. The sample was dried in an oven set at 70°C and the dried powder was calcined at 500°C.

2.3.1.2 Meulenkamp Method [2]

Zinc acetate dihydrate and absolute ethanol were used without further purification. Zinc acetate (0.1 M) solution was prepared by dissolving zinc acetate (10.98g, 50 mmol) in 500 mL ethanol in 1 L round bottom flask. The ethanol solution was boiled in order to dissolve the zinc acetate, the solution was then directly cooled to 0°C. A white powder precipitated after a period of 30 minutes. LiOH. H_2O (2.9 g, 70mmol) was dissolved in ethanol (500 mL) and was added dropwise to the ethanol solution, with vigorous stirring at 0°C. At the end of the procedure a transparent sol was obtained. A UV/Vis spectrum was recorded.

The following procedure was used to remove the reaction product, lithium acetate. A sol, which had been prepared one week previously was condensed to 50-100 mL by rotary evaporation and to this solution hexane (500 mL) was added. The resultant solution was allowed to stand in an ice bath for a week to ensure full precipitation. The supernatant liquid was decanted and the precipitate was again dispersed in ethanol (500 mL) and the same washing procedure repeated 5 times. This powder was dispersed in ethanol and Transmission Electron Microscopy was recorded. The washed sol was dried in an oven set at 70°C and the dried powder was calcined at 500°C.

2.3.1.3 ZnO nano powder synthesis[3]

Zinc perchlorate ($Zn(ClO_4)_2$) and methanol were used without further purification. $Zn(ClO_4)_2$ (0.8 g 2.2 mmol) was dissolved in methanol (1.2 L) and was bubbled with nitrogen gas for 10 minutes. Sodium hexametaphosphate ($(NaPO_3)_6$, 0.2 mL of 0.1M) was added to obtain an opalescent solution. On further bubbling for another 10 min the opalescence became weaker. NaOH (3 mL of 10 M) was added to this solution, which was left for another 30 minutes. It was then concentrated to 150 mL in a rotary evaporator and the solid was separated by centrifugation. Washing was carried out successively with a mixture

of a) 70% methanol + 30% water; b) methanol; c) acetone; d) diethyl ether. The washing was carried out twice with each solvent and the solid was dried in an evaporating dish in an oven set at 70°C. The dried powder was calcined at 500°C.

2.3.2 Novel synthesis of ZnO nanoparticles and nanowire arrays of ZnO

2.3.2.1 Synthesis of nanoparticular ZnO without chemical modifiers

In a typical experiment, zinc acetate (10.98g, 50 mmol) was treated with ethanol (300 mL) in a rotary evaporator at 60°C. The salt was completely dissolved in 20 - 40 minutes. Oxalic acid (12.6g, 100 mmol) in ethanol (200 mL) was simultaneously prepared by stirring for 10 minutes at 50°C. The oxalic acid solution was slowly added with stirring to the warm ethanolic solution containing Zn^{2+}. The thick white gel obtained was dried in an oven set at 80°C for 20 hours. Samples were collected at each step for analysis. This xerogel was calcined at 500°C for 2 hours in a chamber furnace at a constant heating rate of 3°C/ min.

2.3.2.2 Synthesis of nanoparticular ZnO with chemical modifiers (Nanowire formation)

Ethanolic solutions containing Zn^{2+} and oxalic acid were prepared separately in a similar way as explained previously (section 2.3.2.1). This time ethylene glycol (5.57 mL, 100 mmol) and diethanolamine (0.5mL, 5 mmol) were added to the ethanolic solution containing Zn^{2+} and stirring was carried out for 10 minutes. Oxalic acid solution was further added with stirring. The thick white gel obtained was dried in an oven set at 80°C for 20 hours. Samples were collected at each step for microstructure analysis. This xerogel was calcined at 250, 500 or 1000°C for 2 hours at a rate of 3°C/min.

2.4 Varistor preparations

2.4.1 Varistor preparation from ZnO nanomaterials

ZnO nanomaterials prepared by the above routes were mixed with commercial oxide additives by a 'solid-state mixing technique' with the following mole percentages. ZnO 94.2, Bi_2O_3 0.5, Sb_2O_3 1.2, CoO 1.0, MnO_2 1.0, NiO 0.6, Cr_2O_3 0.5 Al_2O_3 0.018 % and two other Littelfuse proprietary materials in small

amounts. These dopants were selected according to the Littelfuse Ltd varistor formulation. In a typical experiment ZnO nanomaterial (2g, 24.5 mmol) calcined at 500°C was added to bismuth trioxide (0.06 g, 0.13 mmol), antimony trioxide (0.094 g, 0.32 mmol), manganese dioxide (0.022 g, 0.25 mmol), nickel oxide (0.012 g, 0.16 mmol), chromium oxide (0.0196 g, 0.13 mmol), aluminium oxide (0.00048 g, 0.0047 mmol) and two other Littelfuse (Littelfuse Ireland Ltd, Co. Louth, Dundalk) proprietary materials in small amounts. The above powders were mixed by 'solid-state mixing technique'. In a typical experiment about 2g of ZnO powder and other dopant oxides were mixed in an agate mortar for 5 minutes. This mixture was then plastified with 1 drop each of 10% aqueous solution of poly(vinyl alcohol) and poly(ethylene glycol) and 0.015 gram of gum arabic. This was further dried in an oven for 5 minutes and pelletised into 7mm (d) x 0.7 mm (t) discs for further sintering and electrical studies. The pellets were sintered at 950, 1000 and 1050°C for 2 hours in a furnace.

2.4.2 Core shell synthesis of ZnO varistor materials

The nanoparticular ZnO (2 g, 4.5 mmol) prepared by the method, described in the section 2.3.2.1, was dispersed in ethanol (200mL) in a conical flask and ultrasonicated for 40 minutes. Antimony chloride (0.1471 g, 0.64 mmol) and cobalt chloride (0.066 g, 0.27 mmol) were dissolved in ethanol (20mL) in beaker. Bismuth chloride (0.081 g, 0.25mmol) was dissolved in acetone (10 mL). Solutions of the above antimony, cobalt and bismuth chlorides were added to the ethanolic suspension of zinc oxide and stirred for 5 minutes. Ammonium carbonate (4mL, 0.1 M) was added to the above solution and stirred for 10 minutes. Samples were collected for TEM. Nickel acetate (0.042g, 0.17mmol), manganese acetate (0.062 g, 0.25 mmol), chromium nitrate (0.1032g, 0.25 mmol) and aluminium nitrate (0.0017g, 0.0046 mmol) were dissolved in ethanol (20 mL). The above two solutions with two other Littelfuse proprietary materials in small amounts, were mixed and stirred for 20 minutes. The material thus obtained was dried in an oven set at 80°C and further calcined at 300°C. The calcined powder was plastified (using poly(vinyl alcohol), poly(ethylene glycol) and gum arabic as before and pressed into pellets for electrical measurements.

2.5 Bulk synthesis of varistor materials by sol gel mixed precursor route

Zinc acetate (274.50g, 1.25 mol), cobalt acetate (3.60g, 14 mmol), manganese acetate (3.20 g, 13 mmol) nickel acetate (1.85g, 7.4 mmol), aluminium nitrate (0.090 g, 0.24 mmol) and two other Littelfuse (Littelfuse Ireland Ltd, Co. Louth, Dundalk) proprietary materials in small amounts were mixed with ethanol (2.5 L) and diethanolamine (60.5 mL, 625 mmol) and dissolved by boiling in a 5 L flask. A pink solution was obtained after 20 minutes. Simultaneously the second solution containing bismuth nitrate (6.30g, 13.9 mmol), antimony acetate (9.80 g, 32 mmol) chromium nitrate (5.25g, 13 mmol) in ethylene glycol (250 mL, 4.55 mmol) was prepared in a 500 mL conical flask by warming (60°C) and stirring. A homogeneous green solution was obtained after 20 minutes. The first solution was allowed to cool for 15 minutes and then transferred to a 5 L beaker. The second solution was added to the first and stirred for 15 minutes with an overhead stirrer. To this solution oxalic acid (315 g, 2.50 mmol) dissolved in ethanol (1L) was added with vigorous stirring. A thick gel was obtained. Stirring was continued for another 15 minutes. The gel was poured into an evaporating dish and put it into an oven set at 80°C for 12 hours. The dried powder was calcined at 500°C. In order to reduce the amount of strong agglomerates, the nanopowder was milled for a maximum of 30 minutes in a conventional ball mill using zirconia balls in a sealed air atmosphere. The weight ratio of ball to powder was 30:1. 2g of the above material was plastified with 1 drop each of 10% aqueous solution of poly(vinyl alcohol) and poly(ethylene glycol) and 0.015 gram of gum arabic. This was further dried in an oven for 5 minutes and pelletised into 7mm x 0.7 mm discs for further sintering and electrical studies. The pellets were sintered at various temperatures from 700 to1050°C.

2.6. Methods

2.6.1 UV/Vis analysis

Optical absorption spectra were recorded using 1cm quartz cell on a UNICAM 5625 UV/Vis spectrometer with deuterium and tungsten lamps as light sources. Spectra were recorded in the range 250 to 400 nm.

2.6.2 Infrared absorption Spectroscopy

Infrared spectra were recorded on a Genesis II FTIR Spectrometer. Samples were prepared as gel or powder dispersed in KBr. Measurements were carried out in the wavenumber range 400- 4000 cm^{-1}.

2.6.3 Thermal analysis

Differential Scanning Calorimetric (DSC) measurements were performed with a Rheometric Scientific DSC QC. A small amount of sample (less than 3mg) was heated from room temperature to 500°C at a constant heating rate of 10°C/minute under nitrogen atmosphere. Thermo-Gravimetric Analysis (TGA) was carried out using a Thorn Scientific TG-750 instrument operated at a constant heat flow of 1°C/min. Dr. M. Venkatesan from the Magnetic Materials Laboratory in the Physics Department kindly obtained the thermo-gravimetric analysis curves of the xerogel. Dilatometric measurements were carried out with Netzsch 402 PC at a constant heat flow of 5°C/min. To study the sintering behaviour of varistor pellets made from nano-size samples, measurements were made in a high temperature, horizontal, single push rod dilatometer having a transducer with 5 mm linear range and a temperature range of 25-1100°C. The sample holder system used for these measurements was dense sintered alumina of high purity.

2.6.4 X-ray powder diffraction (XRD)[4-6]

The sample for analysis was prepared by making a thin film of the powder with acetone on a glass plate and the measurement has been performed with a Siemens D 500 or Philips PW 1540 X-ray diffractometer. The particle sizes were calculated by the Debye - Scherrer equation.[4]

$$\text{Crystalline size} = \frac{0.9\lambda}{B\cos\theta} \qquad [2.1]$$

where λ= X-ray wavelength, θ = Bragg angle B= Line broadening. The line broadening B is measured from the increased peak width at half the peak height and is obtained from Warren formula $B^2 = B_M^2 - B_S^2$ where B_M is the measured

peak width and B_S is the corresponding width of a peak of a standard material (commercial ZnO) whose particle size is greater than 200 nm.

2.6.5 Transmission Electron Microscopy

Transmission electron microscopy was performed with a Hitachi 7000 TEM or Philips CM 20 HRTEM (High Resolution Transmission Electron Microscopy). HRTEM measurements were carried out at Manchester Materials Science Centre, UMIST, Manchester. 400 mesh copper grids coated with formvar were used to prepare the samples. Fig. 2.1 illustrates the principle of a transmission electron microscope.

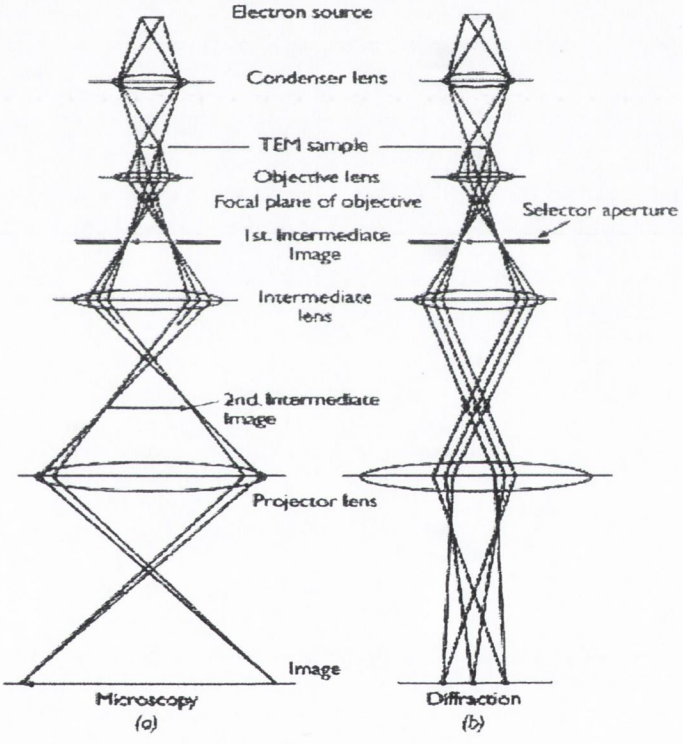

Fig. 2.1 Ray diagram for the generation of a) images and b) diffraction patterns in a transmission electron microscope.[7]

Using a high magnification instrument, it is possible to select individual crystallites from a powder sample and produce single crystal diffraction patterns.[4-6,8] This technique is known as selected area electron diffraction (SAED). Knowing the camera length L [mm] and the incident wavelength λ [nm] and by measuring R [mm] from the diffraction pattern, it is possible to

calculate the lattice spacing d_{hkl}.[8] A schematic representation of the set up is given in Fig. 2.2

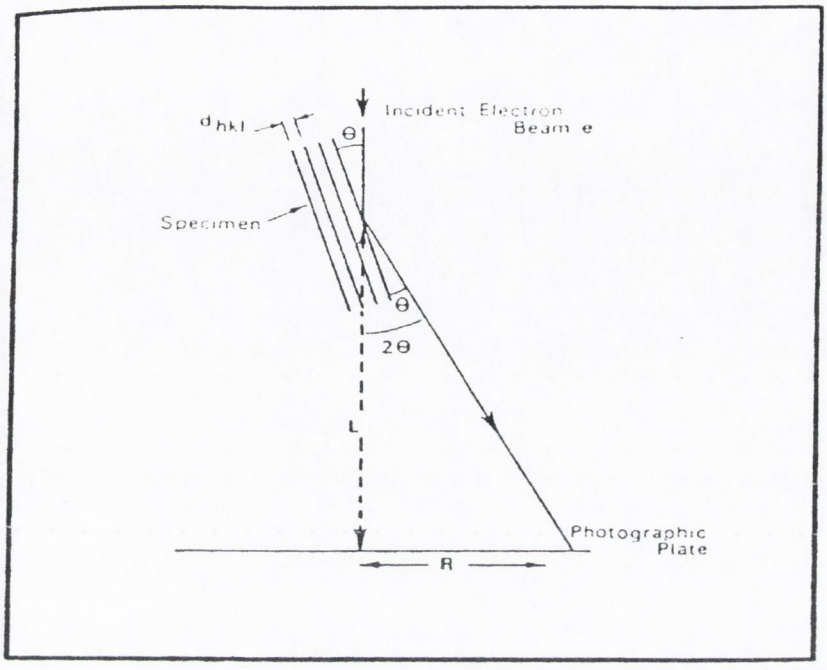

Fig. 2.2 Schematic representation of the electron diffraction set up.[8]

According to Bragg's law

$$\lambda = 2d \sin\theta \qquad [2.2]$$

Assuming the absence of lenses, then

$$R = L \tan 2\theta \qquad [2.3]$$

And since the θ, incident angle is very small (< 3°)

$$\tan 2\theta = 2 \sin \theta \qquad [2.4]$$

Therefore,

$$\frac{R}{L} = \frac{\lambda}{d} \qquad [2.5]$$

On rearrangement

$$d = \frac{\lambda L}{R} \qquad [2.6]$$

where d= distance between the adjacent crystalline planes, λ= X-ray wavelength, θ = Bragg angle, L = camera length, R = radius of the diffraction pattern.

2.6.6 Scanning Electron Microscopy (SEM)

Scanning Electron Microscopic studies were carried out by FESEM (Hitachi S-4300), which was operated at 5.0 kV or 20 kV. Samples for analysis were mounted on aluminium stubs and coated with graphite. A scanning electron microscope functions by scanning a focused beam of high energy electrons across the surface of a sample.[4-6] As the beam scans the sample electrons are ejected out and are collected by the collecting anode. The beam sample interaction produces many signals including back scattered electrons (BE), secondary electrons (SE) and X-rays. When an electron from the beam encounters a nucleus in the sample, the resultant coulombic attraction results in the deflection of electron's path. A few of these electrons will be completely backscattered from the incident surface of the sample. The high-energy back scattered electrons provide an image with good atomic number contrast (since the scattering angle is strongly dependent on the atomic number of nucleus involved). The beam of electrons interact with the loosely bound conduction band electrons in the sample. These low energy electrons are collected to yield SEM images with high resolution.

When the electron beam interacts with an atom, ionisation occurs in the inner shell and the energy is emitted by X-ray. These X-rays produced are characteristic of the elements in the sample and they may be separated out into an energy spectrum to allow the identification of the elemental composition of the sample. These X-rays can be detected by an additional detector attached to SEM. By scanning the energy of the emitted X-rays, it is possible to identify the elements present. This method is called Energy Dispersive X-ray analysis (EDX).

2.6.7 BET Surface area analysis

The BET Surface area analysis were carried out at Enterprise Ireland using a Micromeritics Gemini 2370 instrument under the supervision of Dr. Tim Prescott and Dr. Paul P. Lyons. The measurements were carried out at liquid nitrogen temperature after degassing for 2 hours at 200°C. The BET method developed by Brunauer, Emmett and Teller in 1938 is widely used for the surface area determination of solid powders. The basis of the BET procedure is gas adsorption (physisorption). The powdered sample is evacuated of all gases and cooled to the temperature of liquid nitrogen (77K). At this temperature inert gases such as nitrogen or argon will adsorb on the surface of the sample. The two gas reservoirs are filled with the inert gas (Fig. 2.3). From these reservoirs, gas is dosed into the sample and balance tubes. A transducer on the sample side monitors the target pressure. As the sample adsorbs gas the pressure would tend to decrease and it is detected by the transducer located between the sample and balance tube. A third transducer monitors the pressure between the two reservoirs to determine the amount of gas adsorbed on the sample. An adsorption isotherm is usually recorded as volume of gas adsorbed versus relative pressure. The BET equation is used to give the specific surface area from this data. BET equation gives the volume of gas needed to form a monolayer on the surface of the sample.

$$\frac{P}{V_{ads}(P_0 - P)} = \frac{1}{V_m C} + \frac{(C-1)(P-P_0)}{V_m C} \qquad [2.7]$$

where, P the pressure, P_0 the saturation pressure at measurement temperature, V_{ads} the volume of gas adsorbed at pressure P, V_m the monolayer volume and the parameter C is related to the heat of adsorption. The BET surface area of the sample is expressed in m^2/g.

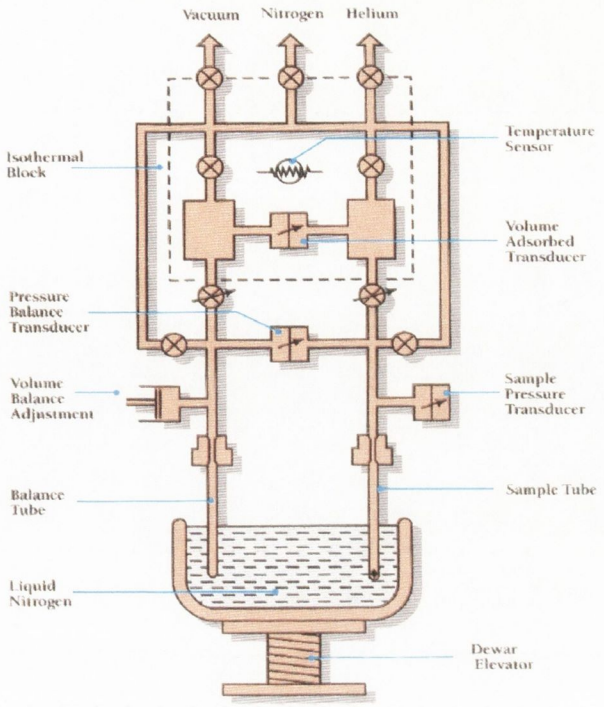

Fig. 2.3 Diagrammatic representation of a surface area analyser

2.6.8 Density Determinations

Density determinations of the sintered samples were performed using the *Archimedes principle*. This principle states that every solid body immersed in a fluid loses weight by an amount equal to that of the fluid it displaces. The density of the sintered samples usually determined with the aid of a liquid whose density is known (usually water). If the sample does not have any open porosity it can just be weighed in air (W_1) and water (W_2) to calculate the density (D) according to the equation.

$$D = \frac{W_1.d}{W_1 - W_2} \qquad [2.8]$$

where d= density of water

The measurements were carried out using Ohaus P/N 470007-010 (Fig. 2.4)

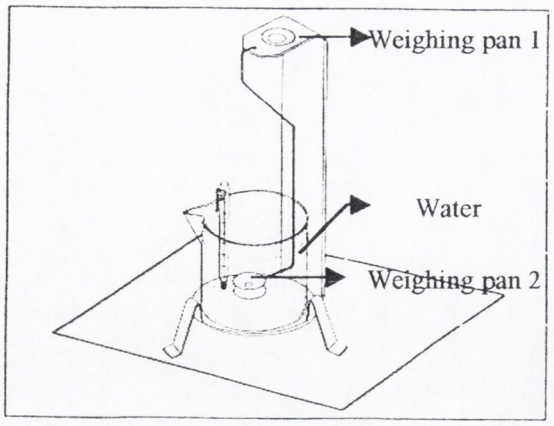

Fig. 2.4 Experimental set up for the determination of density by Archimedes principle.

2.7. Sintering studies

Sintering is a process of densification, which reduces the solid-vapour interfacial area and porosity.[9-10] This is the preferred manufacturing method for industrial ceramics. ZnO varistors are normally sintered at 950-1400°C.[11-18] Two different types of sintering procedures were tried for varistors to study the densification and electrical characteristics.

2.7.1 Conventional sintering

The conventional sintering was performed in a chamber furnace (Nabertherm-S 27) with the following rate of heating (Scheme 1).

$$\text{Room Temperature} \xrightarrow{1.5^\circ\text{C/min}} 300^\circ\text{C/1hr} \xrightarrow{3^\circ\text{C/min}} \text{Final Temperature}$$

Scheme 1 Sintering schedule used for conventional sintering

ZnO varistor discs were sintered in air at various temperatures ranging from 700-1050°C for 2hrs and then left cool under room temperature. Fig. 2.5 show a typical sintering profile used for the sintering at 1050°C for 2 hours.

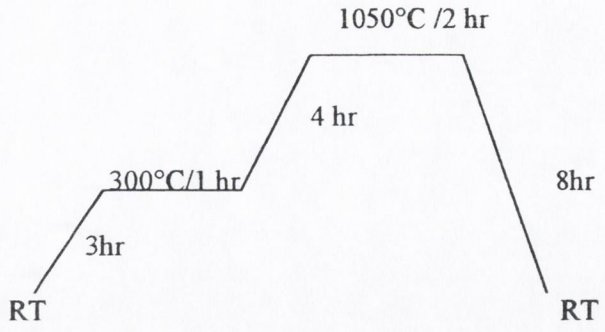

Fig. 2.5 Example of a profile used for conventional sintering

2.7.2 Novel sintering procedures

A novel sintering technique was also tried for varistors based on a similar report on the sintering of Y_2O_3 ceramics.[19] The method is based on a two step sintering schedule. The material is first heated to a higher temperature to achieve an intermediate density, then cooled down and held at a lower temperature to get full sintered density. The sintering experiments were performed in a chamber furnace (Nabertherm-S 27). A typical sintering profile based on this method is given in Fig. 2.6

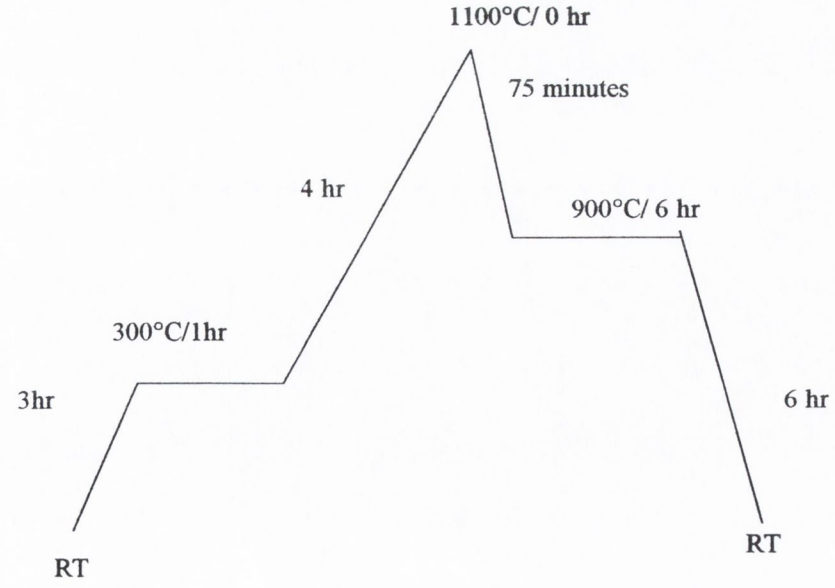

Fig. 2.6 Example of a sintering profile used for novel sintering

2.8 Electrical characterisation

I-V characteristics from 0.1μA to 0.01A was measured by using Keithley Instrument (Model 2410) and 0.1 A to 100A were measured by Keytek Model 711 surge generator. I-V plot obtained from the Keithley Instrument will be used in the following chapters. The nonlinear constant α was calculated from the I-V measurements between current densities 0.1 A and 1 mA using the relationship.

$$\alpha = \frac{\log I_2 - \log I_1}{\log V_2 - \log V_1} \qquad [2.9]$$

where V_2 and V_1 are the electric fields at current densities I_2 and I_1 respectively. The breakdown voltage, V_c was measured as the voltage at a current density of 1 mA.

2.9 References

1. L. Spanhel and M. A. Anderson, *J. Am. Chem. Soc.*, 1991, **113,** 2826.
2. E. A. Meulenkamp, *J. Phys. Chem. B.*, 1998, **102**, 5566; E. A. Meulenkamp, *J. Phys. Chem. B.*, 1998, **102**, 7764.
3. U. Koch, A. Fojtik, H. Weller and A. Henglein, *Chem. Phys. Lett.*, 1985, **122**, 507.
4. A. R. West, *Solid State Chemistry and Its Applications*; John Wiley & Sons London, 1984 p 174.
5. A. K. Cheetham and P. Day, *Solid State Chemistry Techniques,* Clarendon Press, Oxford, 1987.
6. C. N. R. Rao and J. Gopalakrishnan, *New Directions in Solid State Chemistry*, Cambridge University Press, 1997.
7. http://www.research.philips.com/generalinfo/special/rt-tem/temprin.html
8. D. E. McCormack, PhD. (1990), The University of Dublin, p 86.
9. W. D. Kingery, H. K. Bowen and D. R. Uhlmann, *Introduction to Ceramics*, John Wiley & Sons, New York,1975.
10. C. J. Brinker and G. W. Scherer, *Sol-Gel Science.*, Academic Press Inc., New York, 1990.
11. M. Matsuoka, *Jpn. J. Appl. Phys.*, 1971, **10**, 736.
12. K. Eda, *IEE Electrical Institution Magazine,* 1989, **5**, 28.
13. T. K. Gupta, *J. Am. Ceram. Soc.*, 1990, **73**, 1817.
14. D. R. Clarke, *J. Am. Ceram. Soc.*, 1999, **82,** 485.
15. B. C. H. Steele, *Electronics ceramics*, Elsevier Applied Science, London and New York, 1991, Page 17.
16. R. Einzinger, *Ann. Rev. Mater. Sci.*, 1987, **17**, 299.
17. M. Inada, *Jpn. J. Appl. Phys.*, 1980, **19**, 409.
18. L. M. Levinson and H. R. Philip, *Ceramic Bulletin.*, 1986, **65**, 639.
19. I. Wei and X.-H. Wang, *Nature*, 2000, **404**, 168.

Chapter 3

Synthesis of nanometer size ZnO by three different procedures and the study of the varistor properties of these materials

3.1 Introduction

As described in chapter 1, several techniques have been reported for the synthesis of varistor materials by chemical routes.[1-6] Here we report the synthesis of varistor materials from nanocrystalline ZnO prepared by three different techniques and subsequently doped with metal oxides by the conventional solid state mixing technique. The methods used for the preparation of nanoparticular ZnO was based on the reaction of zinc salt with alkali metal hydroxide under controlled conditions.

The following procedures were attempted to produce nano-size ZnO

a) Spanhel and Anderson procedure[7] (section 3.2.1)
b) Meulenkamp[8] procedure (section 3.2.2) and
c) Weller[9] procedure (section 3.3).

Experimental details of these methods are given in section 2.3.1.

The aim of this study was to find a suitable procedure to make varistor materials and to compare the electrical properties and grain growth of nanocrystalline ZnO prepared through these methods.

3.2 Results and discussions on ZnO nanoparticles

3.2.1 Nanocrystalline ZnO through Spanhel and Anderson procedure[7]

This procedure (scheme 3.1) affords nanocrystalline ZnO colloids within a few hours. The organometallic zinc oxide precursor[7,8] was made by refluxing an ethanolic solution of zinc acetate. This solution was further diluted and LiOH powder added. Finally, the suspension was placed into an ultrasonic bath in order to dissolve the weakly soluble LiOH powder. Ultrasonication accelerates the release of hydroxide ions, resulting in an immediate reaction to form a stable ZnO sol.

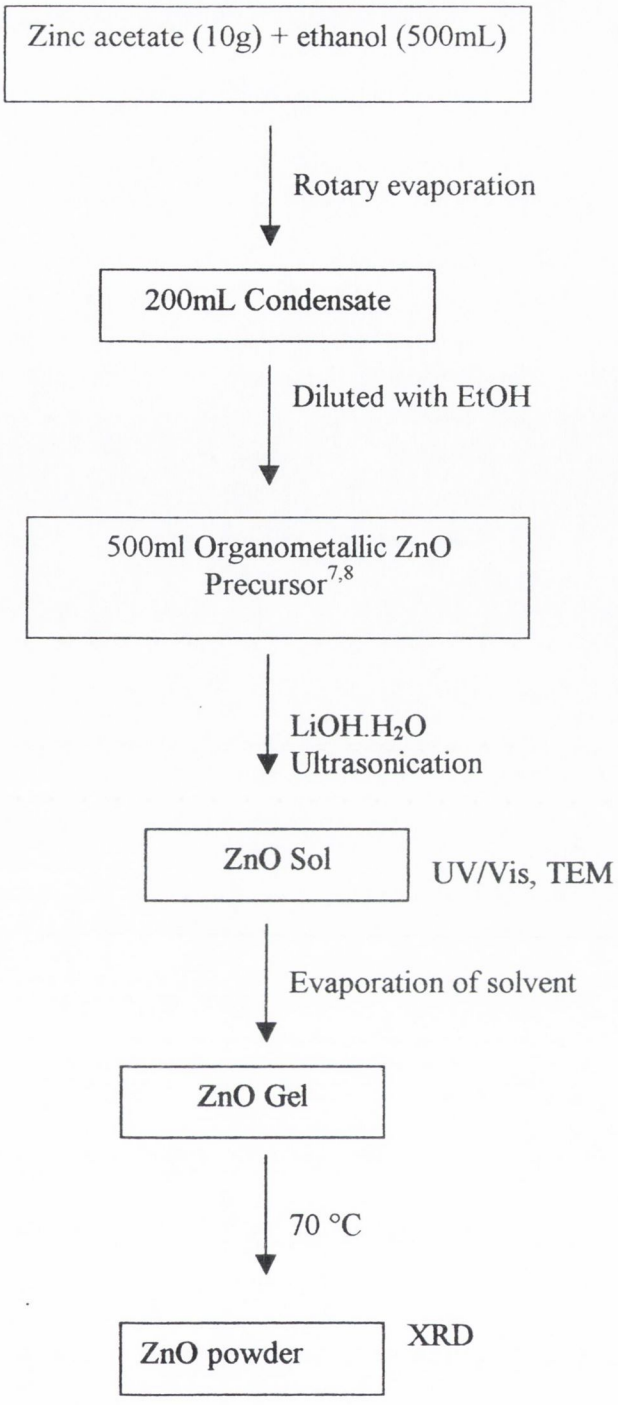

Scheme 3.1 Flowchart for the synthesis of ZnO through Spanhel and Anderson Procedure.

3.2.1.1. UV/Vis absorption spectra of ZnO sol

Fig.3.1 shows the UV/Vis absorption spectrum observed just after the synthesis of the ethanolic sol of ZnO nanoparticles. The spectrum shows a main peak at 330 nm and a shoulder at 280 nm attributed to the exciton transition in small

ZnO clusters.[7,8] $\lambda_{1/2}$ (wavelength at which the absorption is 50% of the excitonic peak) is found to be 347 ± 5 nm.

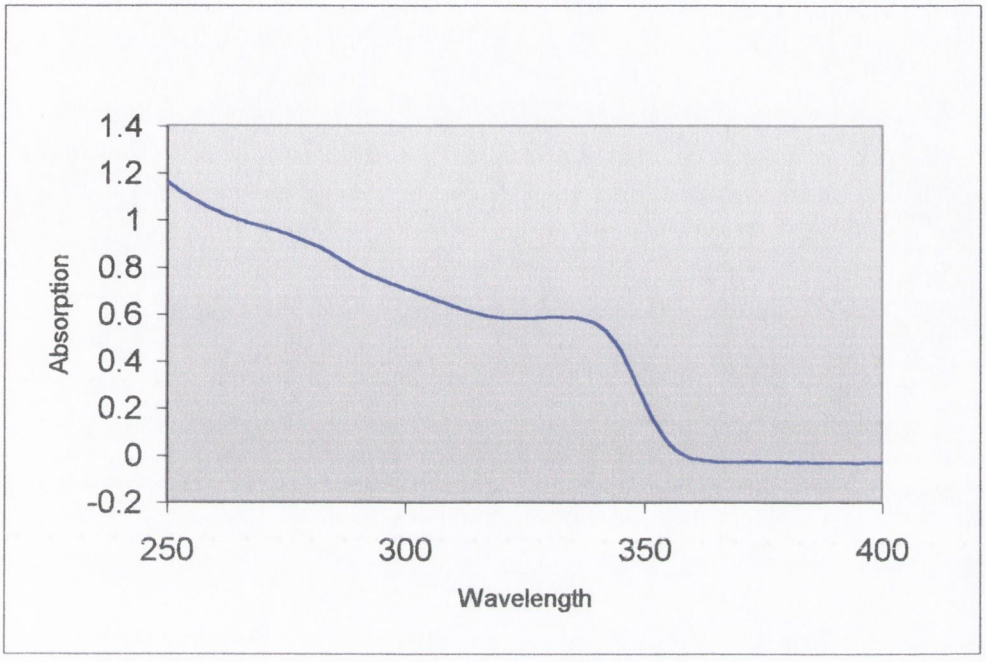

Fig. 3.1 UV/Vis absorption spectra of fresh ZnO sol (~0.001 M) prepared by Spanhel and Anderson procedure.

The blue shift observed for the quantum size ZnO (E_g= 3.57 ev) compared to the bulk material (E_g = 3.44 ev) can be explained by a molecular orbital model (*e.g.* see Fig. 1.1 in Chapter 1). It is clear from the figure how the splitting of energy levels into a filled and an empty region proceeds as the number of contributing MO's increases. As the HOMO–LUMO gap increases, more energy is required for creating an electron/hole pair. This increase shifts the absorption spectra to shorter wavelengths.

Meulenkamp[7] has established a simple relationship between the particle diameter (D) in Å and $\lambda_{1/2}$ (wavelength at which the absorption is 50% of the excitonic peak) similar to Brus equation (Appendix 1).

$$\frac{1240}{\lambda_{1/2}} = 3.556 + \frac{799.9}{D^2} - \frac{22.64}{D} \qquad [3.1]$$

The spectrum (Fig.3.1) indicated a $\lambda_{1/2}$ at 347 ± 5 nm giving a particle size of 3.4± 0.5 nm.

3.2.1.2 X-ray Diffraction

The XRD pattern (2 θ from 5°-60°) for ZnO produced by the Spanhel and Anderson route is given in Fig.3.2. The X-ray powder diffraction pattern of the powder dried in an oven set 70°C shows d spacing values and relative intensities of the peaks coincident with JCPDS data of Zincite.

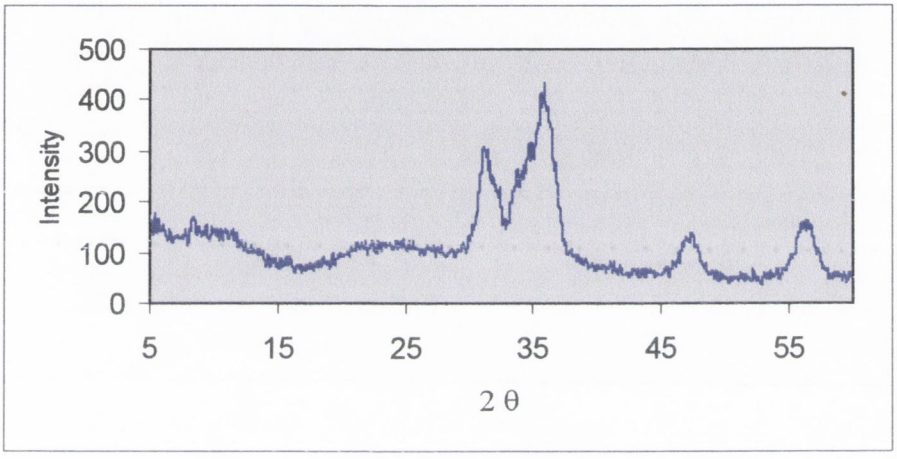

Fig. 3.2 X-ray powder diffraction plot of ZnO powder produced by Spanhel and Anderson route

The particle sizes were calculated by the Debye -Scherrer equation.[10] The particle size was found to be 4.5 ± 0.5 nm for a sample prepared through Spanhel and Anderson procedure which is higher than that obtained in either TEM or UV/Vis spectroscopy. This may be due to the fact that XRD pattern is recorded after drying the sample (sol) in an oven at 70°C for two days.

3.2.1.3 Transmission Electron Micrographs

Transmission Electron Micrograph (TEM) provides comparatively good measurement of particle sizes for colloids and powders. The TEM pictures obtained for a 5 days aged ZnO is given in Fig.3.3. Particle sizes were determined by plotting a histogram from the TEM figures and indicated an average size of 3.3 ± 0.5 nm (Fig.3.4).

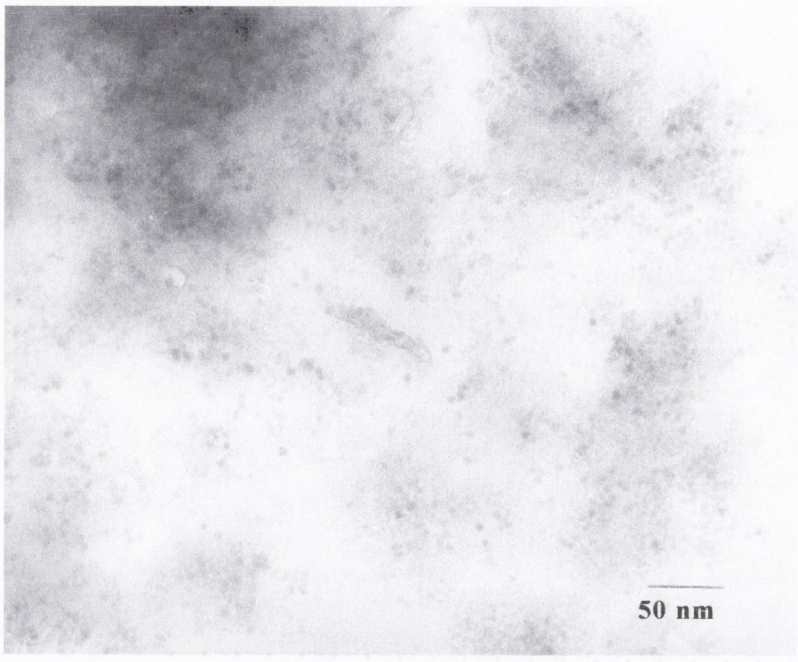

Fig. 3.3 TEM picture of ZnO nanoparticles Spanhel and Anderson route

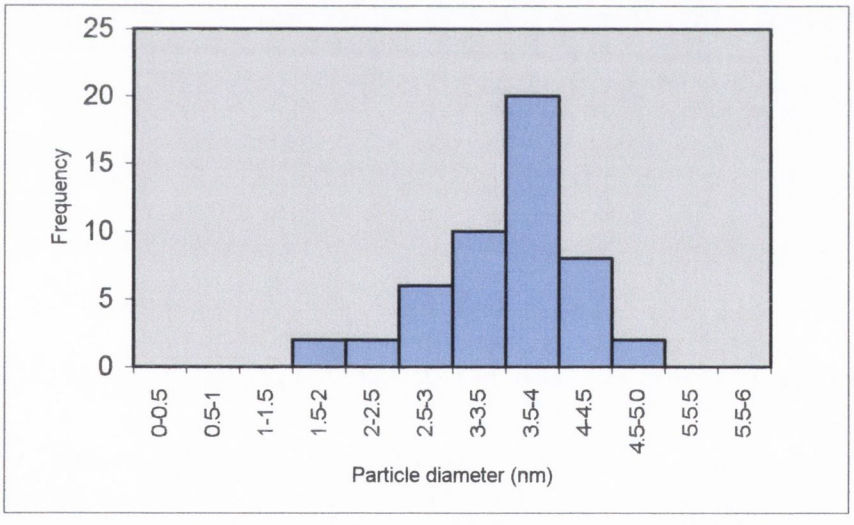

Fig. 3.4 Size histogram (TEM) of the ZnO particles prepared through Spanhel and Anderson route.[7]

3.2.2 ZnO nanocrystals prepared through Meulenkamp's method

The procedure employed was slightly different from Spanhel's[7] procedure. In this case the ethanolic solution is only refluxed for 30 minutes and then directly cooled to 0°C. Zn^{2+} ions are reacted with LiOH in alcohol solution making use of

the dehydrating properties of the solvent to prevent the formation of zinc hydroxide.

$$Zn(C_2H_3O_2)_2.2H_2O \xrightarrow{\text{Ethanol/- } H_2O} Zn_{10}O_4(Ac)_{12} \xrightarrow{\text{LiOH}} ZnO$$

Scheme 3.2 Synthesis of ZnO through Meulenkamp's Procedure.[8]

A detailed experimental flowchart is given in Scheme 3.3

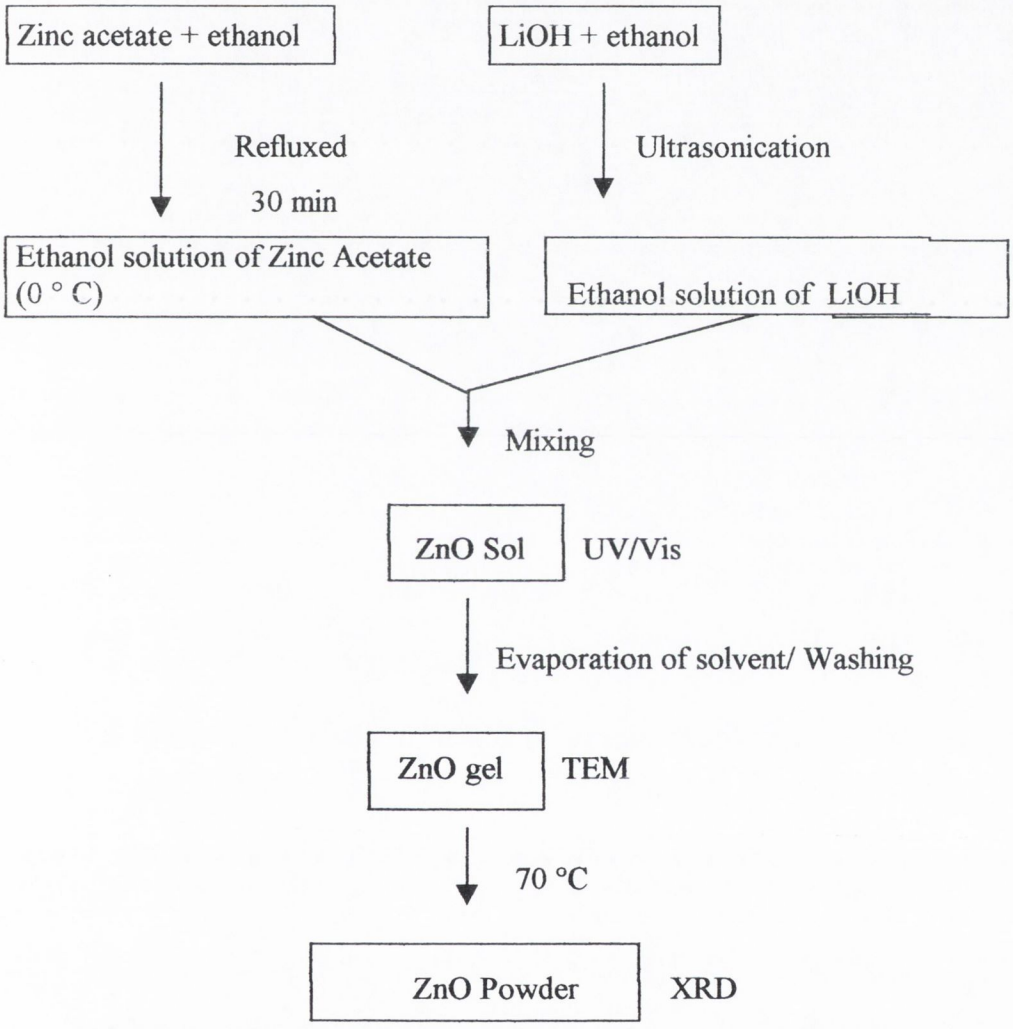

Scheme 3.3 Flowchart for the synthesis of ZnO through Meulenkamp's Procedure.[8]

The mechanism of ZnO formation is rather complex and poorly understood, although Meulenkamp[8] provides a possible explanation involving the formation of anhydrous zinc acetate and its reaction with LiOH to produce ZnO.

3.2.2.1 UV/Vis absorption spectra of ZnO sol

The UV/Vis spectrum (Fig. 3.5) obtained is that for a typical ZnO nanocolloid and similar to the earlier presented one (Fig. 3.1). The spectrum indicated a peak at 320 nm with a $\lambda_{1/2}$ value of 334 nm giving a particle size of 2.9 nm (Fig. 3.5).

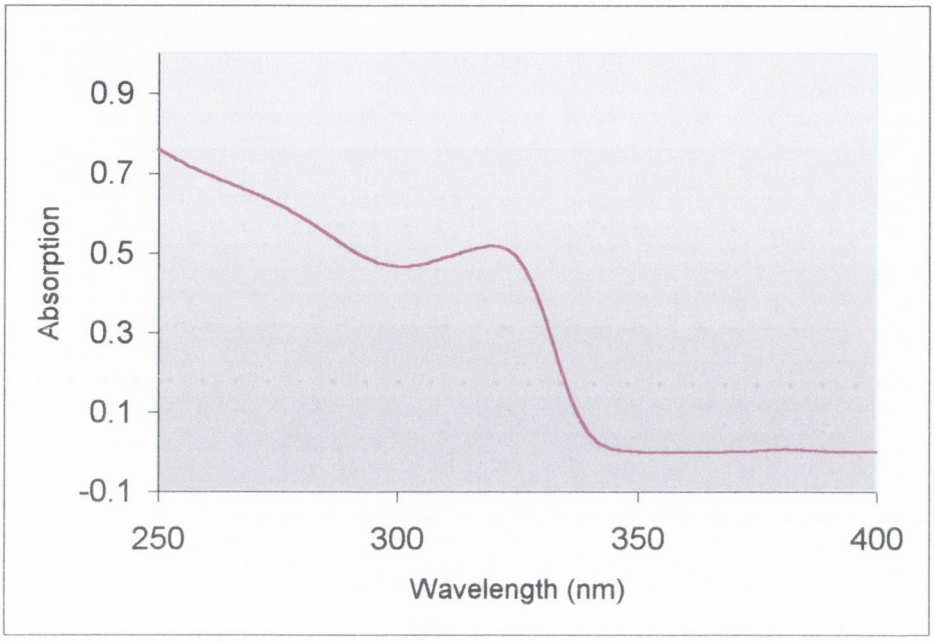

Fig. 3.5 UV/Vis absorption spectra of fresh ZnO sol (0.001 M)

3.2.2.2 X-ray Diffraction

Fig. 3.6 & 3.7 are the XRD patterns recorded for the ZnO sample before and after washing. The X-ray powder diffraction pattern (2θ from 5°-60°) showed d spacing value and relative intensities of the peaks coincident with JCPDS data for zincite. However it is observed that there are also a lot of impurity peaks with 2θ values below 30°. The peaks were identified as a complex of zinc –lithium-acetate.[8] The intensity of the peaks are reduced on washing and after washing several times impurity free ZnO is obtained.

These are obvious in the Figs. 3.6 & 3.7. The particle sizes were calculated by the Scherrer method.[10] The particle size was found to be 6.2 ±0.5 nm for sample prepared through Meulenkamp's procedure.

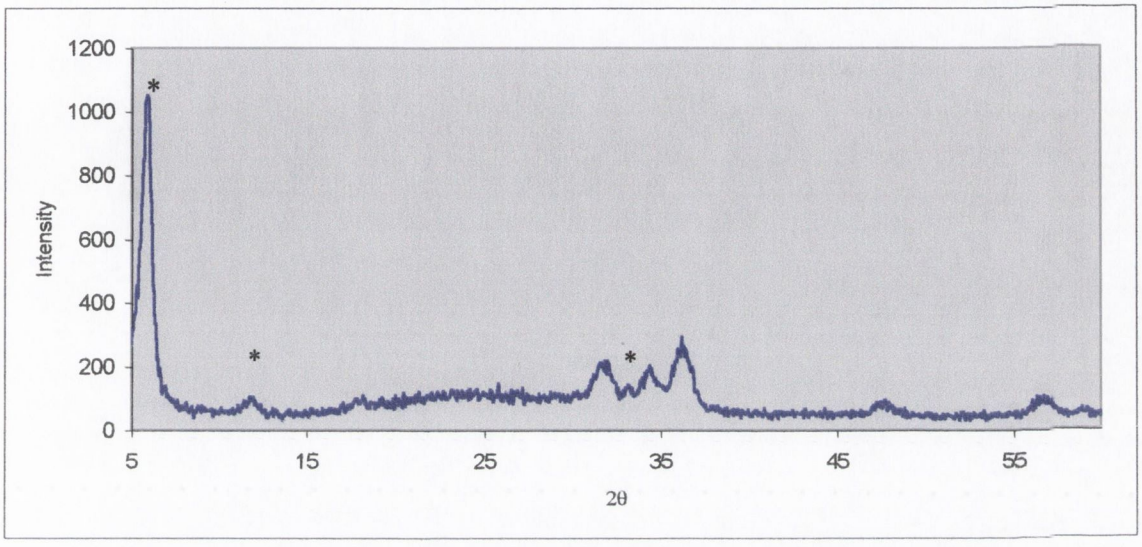

Fig. 3.6 X-ray powder diffraction plot of ZnO powder, prepared by Meulenkamp's[8] procedure, before washing (* = impurity peaks)

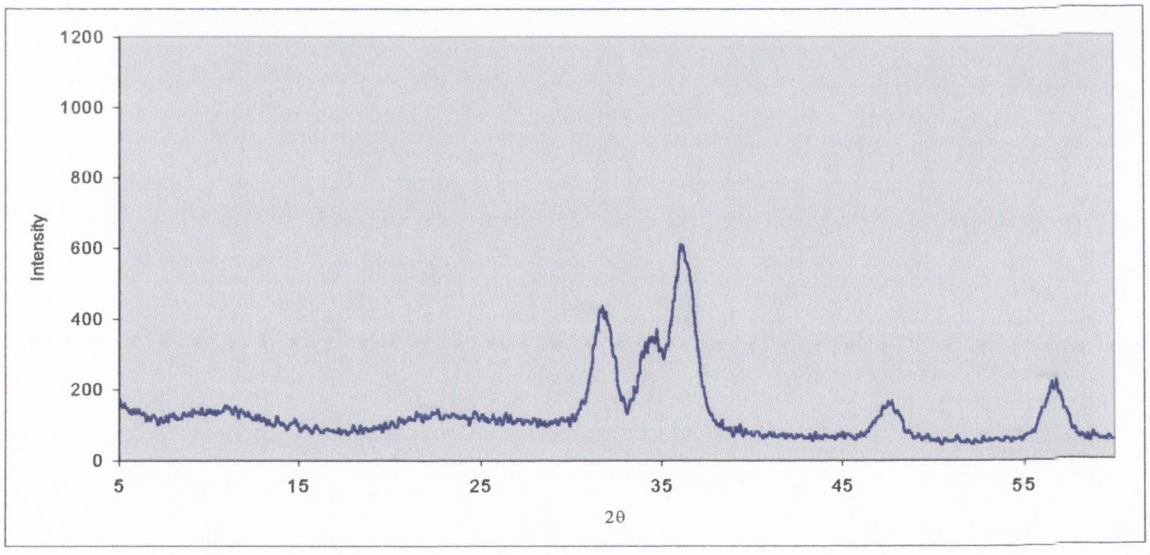

Fig. 3.7 X-ray powder diffraction plot of ZnO powder, prepared through Meulenkamp's[8] procedure, after washing

3.2.2.3 Transmission Electron Micrographs

The TEM obtained for a five days aged ZnO is given in Fig.3.8. The particle size histogram of the TEM indicated an average size of 4. 40 $\pm$ 0.5nm. (Fig.3.9)

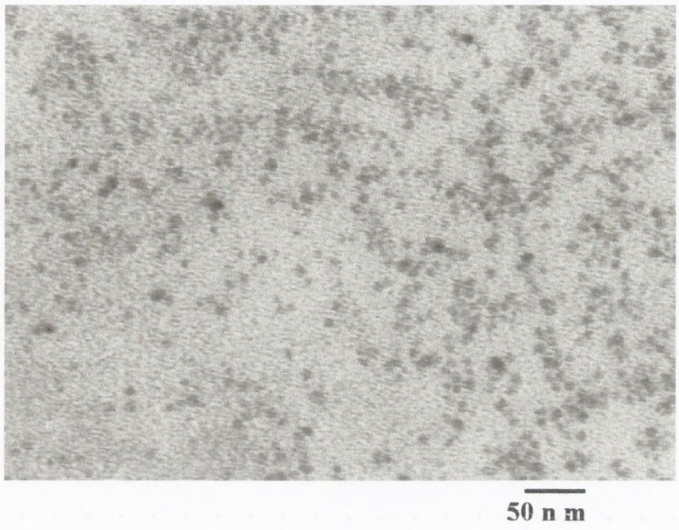

Fig. 3.8 TEM picture of ZnO nanoparticles

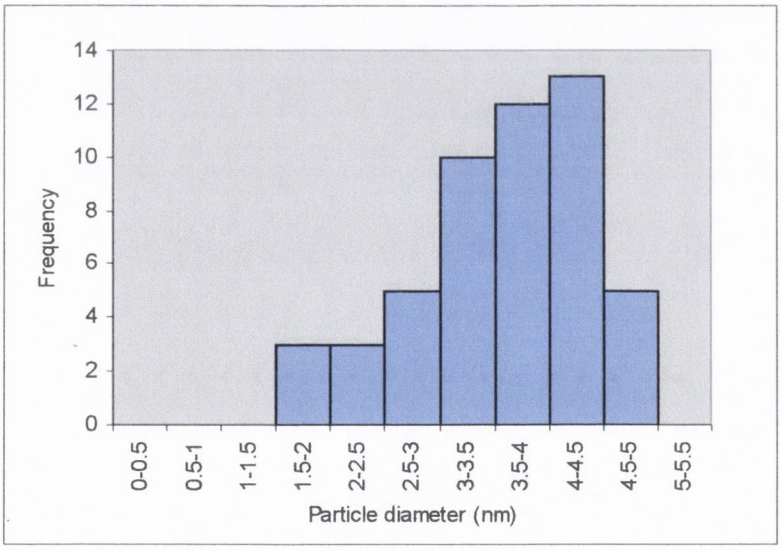

Fig. 3.9 Size histogram (TEM) of the ZnO particles prepared by Meulenkamp's route.

3.2.3 Comparison of the Spanhel and Anderson[7] and Meulenkamp's[8] procedures

ZnO synthesised by two different routes (*ie* Spanhel and Anderson[7] and Meulenkamp's[8]) have resulted in formation of ZnO nanoparticles of a similar particle size. However, the synthesis of ZnO by the Meulenkamp route is found to be easier to reproduce. For example, in the case of Spanhel and Anderson's route, it was found that a precipitate sometimes formed during refluxing. On these occasions, ZnO was not formed. It was always very difficult to set the reaction conditions in such a way to get 0.3 L condensate within three hours (if reaction times were less than three hours a precipitate was noted. On the other hand a turbid reaction product was produced for reaction times longer than four hours!). A transparent and stable precursor was only obtained after three hours reaction time. In our hands, out of seven experiments only four were successful. The total time taken for the complete reaction was five hours. On the other hand the Meulenkamp procedure is very simple, experiments were successful each and every time, and the complete reaction occurs in one hour thirty minutes.

3.3 Synthesis of Nanocrystalline Solid ZnO by Weller method[9]

When zinc ions are precipitated by using hydroxide ions in an aqueous medium, the formation of $Zn(OH)_2$ is favoured over ZnO.[9] Weller has shown that the precipitation can also be carried out in methanolic solution and by making use of the dehydrating properties of alcohols, ZnO nanoparticles can be obtained. Particle stabilisation is achieved by the addition of a small amount of polyphosphate.[9] A detailed experimental flowchart is given in Scheme 3.4

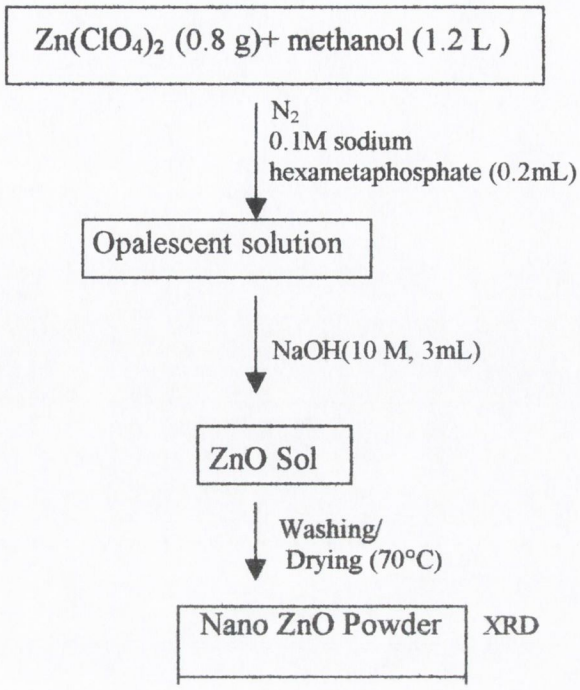

Scheme 3.4 Flowchart for the synthesis of ZnO through Weller's procedure.

The UV/Vis spectrum obtained is typical of that for a ZnO nano colloid and is similar to those recorded earlier. The spectrum indicates a value of $\lambda_{1/2}$ of 350 nm, which corresponds to a particle size of 3.6 ±0.5nm. The X-ray powder diffraction pattern (Fig. 3.10) (2θ from 5°-60°) shows d spacing value and relative intensities of the peaks coincident with JCPDS data of Zincite.

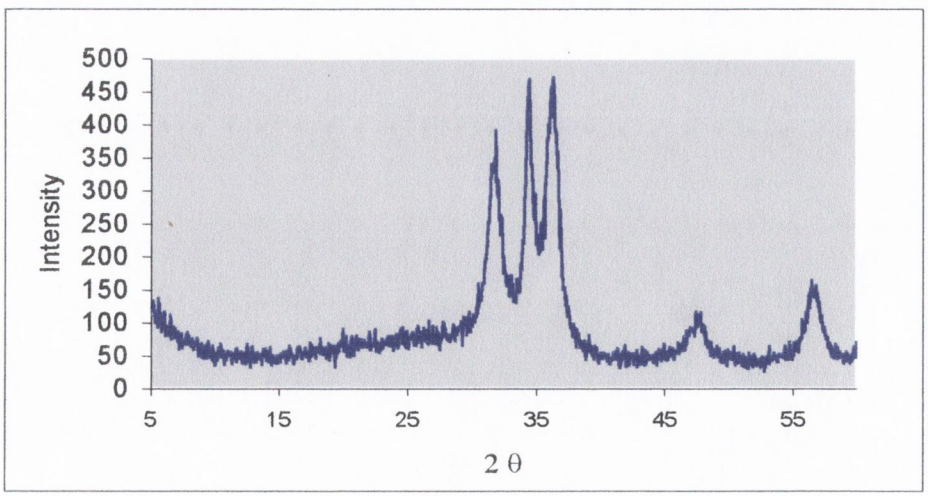

Fig. 3.10 X-ray powder diffraction plot of ZnO powder after washing (Weller method[9])

The particle size histogram of TEM (Fig. 3.11) indicated an average size of 3.58 ±0.5nm.

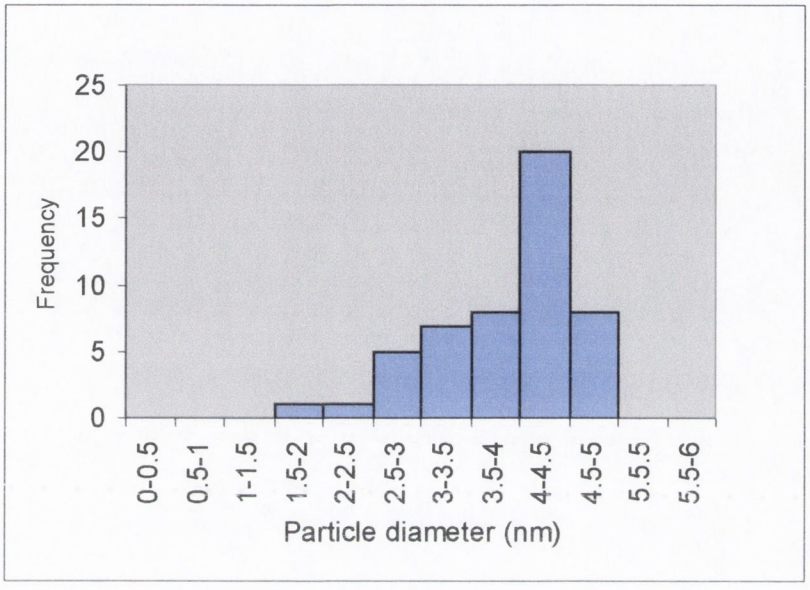

Fig. 3.11 Size histogram (TEM) obtained for ZnO nanopowder (Weller method[9])

3.4 Comparison of the three procedures.[7,8,9]

- ZnO synthesised by three different routes[7,8,9] produce similar particle sizes (Table 3.2). However, the synthesis of ZnO by the Weller route is found to be easier to reproduce, as the other two methods depend strongly on the reaction conditions such as temperature, concentration and time.

- The Weller procedure is very simple to carry out as unlike the other two methods does not involve various steps like rotary evaporation and ultrasonication.[7,8] The total time taken by the Weller method was around 3 hours including washing while the other two methods took around 24 hours for the synthesis and washing.

- After washing the solid ZnO obtained by the Weller method is in very high yield (80%).

- As far as varistors and other electronic materials are concerned the Weller method is more suitable as it does not require any Li^+ based reactants. A small amount of Li^+ can destroy the varistor properties of ZnO.[12] A comparison of the various methods for the synthesis of nanocrystalline ZnO is given in Table 3.1.

Table 3.1 Comparison of the three different procedures used in the synthesis of Nanocrystalline ZnO

Procedure	Chemicals Used	Method	% of success rate	Advantages	Limitations
Spanhel and Anderson[7]	$Zn(C_2H_3O_2)_2.2H_2O$ LiOH. H_2O, Ethanol	Condensation, Dilution, LiOH addition Ultra sonication and Drying	Out of seven, only four were successful (yield 70%)	Transparent thin films can be prepared from the sol	Some precipitation occurred during condensation and in this case no ZnO is formed. A transparent and stable precursor was only obtained after 3h reaction time. Out of seven experiments only four were successful. Total time taken for the complete reaction was 5 hrs. Li can affect varistor properties.
Meulenkamp[8]	$Zn(C_2H_3O_2)_2.2H_2O$ LiOH. H_2O Ethanol	Cooling, Precipitation LiOH addition Stirring and drying	Experiments were successful each and every time (yield 45%)	A method for washing the bi-products is described in the paper. More simple and reproducible compared to Spanhel[7]. Only 90 min taken to complete the reaction	Washing will take several hours, and a large amount of hexane is needed to precipitate the ZnO from the sol. Time taken for washing is several days (12 days)
Weller [9]	$Zn(ClO_4)_2$ NaOH $(Na(PO)_3)_6$ Methanol	N_2 Bubbling $(Na(PO_3))_6$ addition NaOH addition Washing	Experiments were successful each and every time (yield 80%)	Simple and reproducible compared to the above two procedures.[7,8] Pure ZnO is obtained after Washing. Time required for washing is 60 min	Dilute solutions need for the synthesis and large volume of solvent required for the synthesis compared to the above[7,8] two methods.

Table 3.2 Particle sizes obtained for ZnO prepared through various procedures

Procedure employed	Particle size (nm, ± 0.5)			
	UV/Vis		TEM	XRD
	Fresh	Aged (2 days)		
Spanhel and Anderson[7]	3.4	3.7	3.3	4. 5
Meulenkamp[8]	2.9	3.2	4.4	6.2
Weller[12]	3.6	-	3.6	5.7

Particle sizes of the ZnO nanopartcles obtained by various techniques (UV/Vis, XRD and TEM) are given in Table 3.2. The difference in particle size may be due to the fact that XRD pattern is recorded after drying the sample (sol) in an oven at 70°C for two days. It is also noted that the Debye–Scherrer equation is unreliable for particles of different size distributions since the mean given by this method depends strongly on the shape of the crystal size distribution.[11] Generally for the Debye–Scherrer method, it is assumed that all of the crystals have the same size, which is not true in this case. If there is a difference in distribution of sizes, then the Scherrer constant (K=0.9) changes.[11]

3.5 Aging studies

Aging studies have been carried out using UV/Vis spectroscopy. As discussed earlier ZnO shows a quantum size effect for very small particles[7,8] (<7nm) so UV/Vis absorption spectra provides a method to investigate the particle growth. It is seen that ZnO particles continue to grow after synthesis even at low temperature (0°C). In this way it is possible to obtain particle sizes of various range. The results of aging of a 0.001 M ZnO sol for periods up to 10 and 100 days at room temperature are given in Figs. 3.12 and 3.13. The absorption

spectra recorded for fresh ZnO colloid (0.001 M) is shown in the Fig. 3.5. After aging for one day at room temperature the absorption edge progressively red-shifted to 340nm. It is obvious from the spectral plots that the particle growth is time dependent and the rate of spectral shift is retarded towards the end of aging (Figs. 3.12 & 3.13) as observed by Wong *et al.*[13]

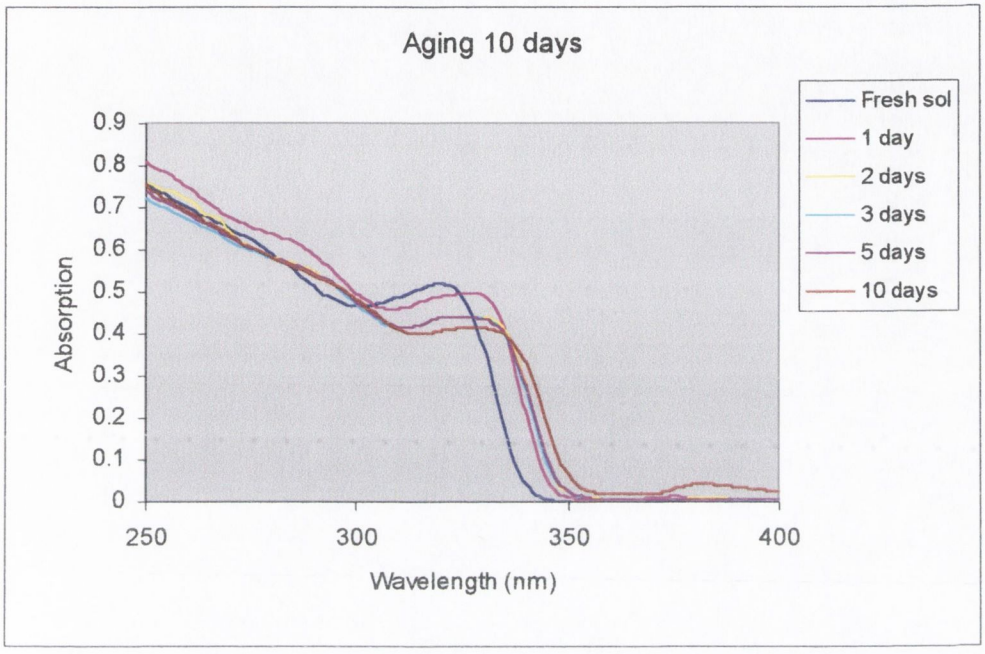

Fig. 3.12 UV/ Vis spectra showing the aging of the ZnO sol (prepared by Meulenkamp method) in ethanol up to 10 days

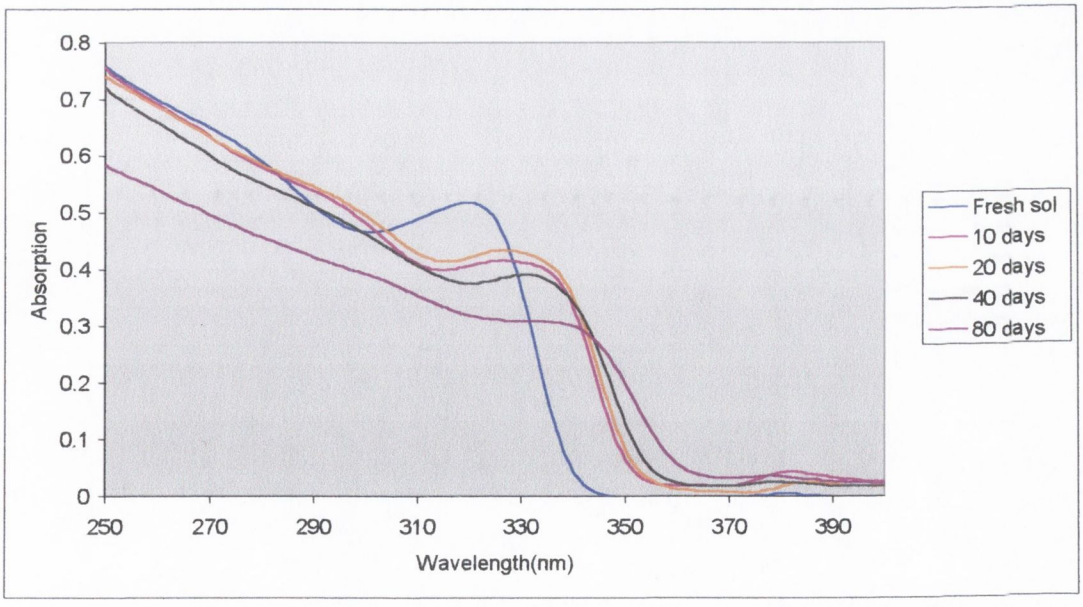

Fig. 3.13 UV/ Vis spectra showing the aging of ZnO sol (prepared by Meulenkamp method) in ethanol up to 80 days.

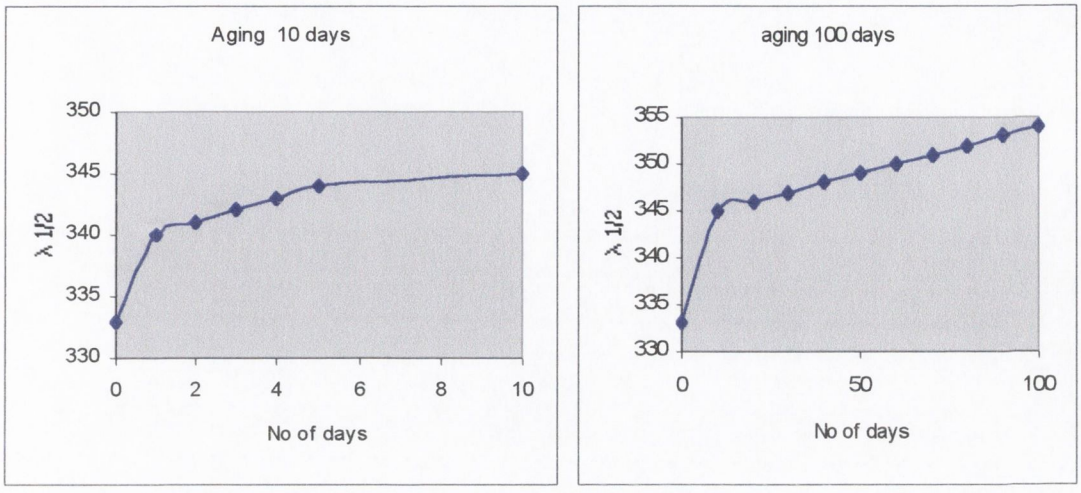

Fig. 3.14 Evolution of $\lambda_{1/2}$ as a result of aging of the Meulenkamp ZnO sol in ethanol a) 10 days of aging b)100 days of aging

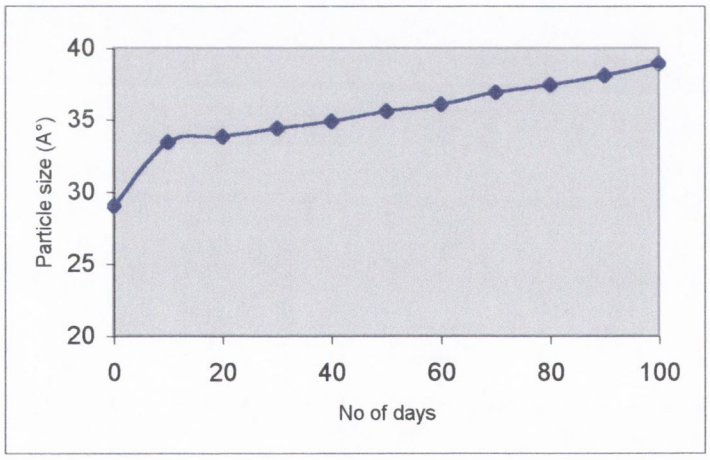

Fig. 3.15 Evolution of particle size as a result of aging of the Meulenkamp ZnO sol in ethanol for 100 days of aging

Possible explanations for the particle growth in colloidal systems are Ostwald ripening (Fig. 3.16) and aggregation.[7,8] If the particles are slightly soluble in the dispersion medium then, by the phenomenon of surface tension, the solubility of the very small particles is greater than that of the larger particles. Consequently if particles of different sizes are present, there will be a tendency for molecules to

dissolve from smaller particles and to precipitate on to larger ones. Smaller particles tend to be eliminated and the average particle size increases.[14] In an aggregation process, when the smallest stable clusters are formed, they rapidly combine together to give the next most stable aggregate.[7] In a simple way large particles are growing further making use of small particles as "seeds". After a particular time a stage is reached where particles will not grow further and this is obvious as the spectral shifts retard at the end of aging process (Fig. 3.12).

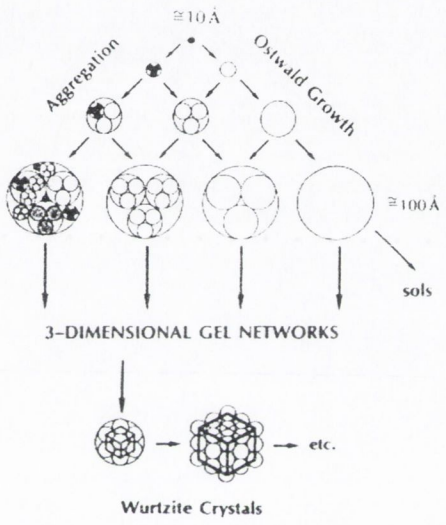

Fig. 3.16 Ostwald ripening and aggregation.[7]

3.6 Calcination of Nano-size ZnO prepared by the above methods

Nano-size ZnO powders prepared by the above three different routes were calcined at 500°C (3°C/min) and characterised by TEM and X-ray powder diffraction methods.

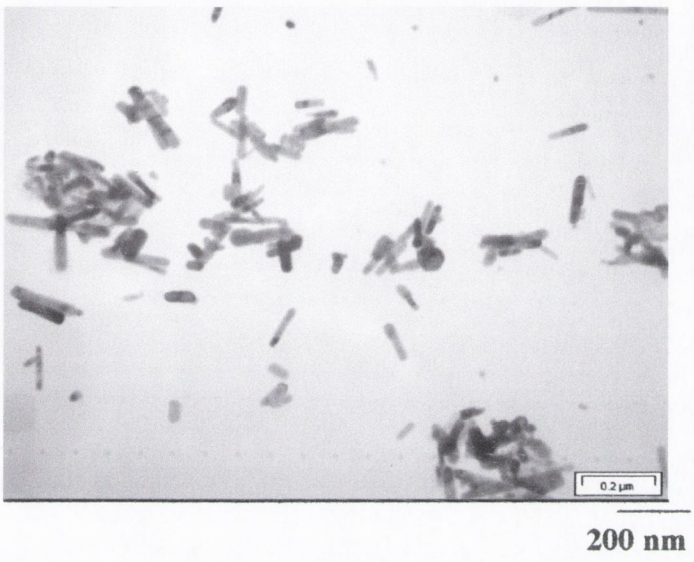

Fig 3. 17 TEM image of the nano ZnO calcined at 500°C (Spanhel and Anderson route)

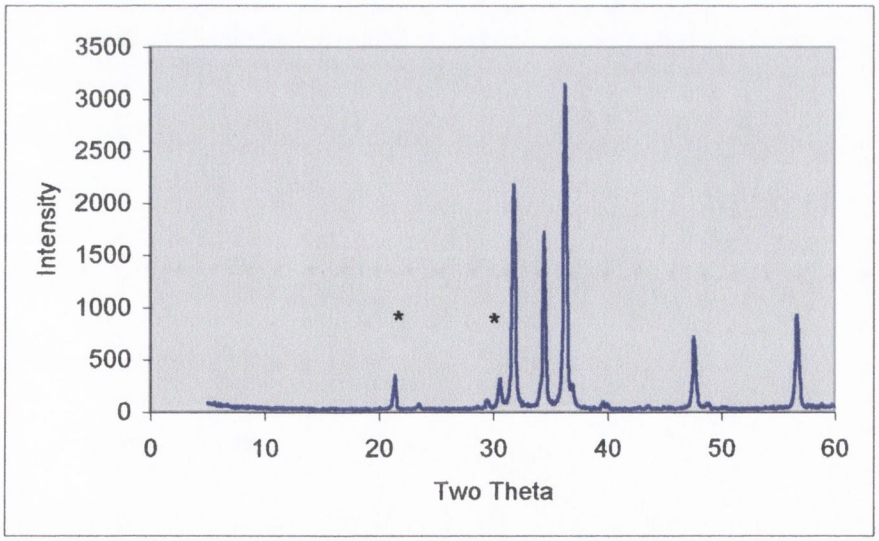

Fig. 3.18 X-ray powder diffraction pattern of the nano ZnO calcined at 500°C (Spanhel and Anderson route [7]) * = impurity peaks due to Li complexes

TEM images of the nano-size ZnO prepared through Spanhel and Anderson[7] route showed a needle like morphology with particles of 80-150 nm in length and 15 to 50 nm in width. X-ray powder diffraction studies of these material showed an average particle size of 74 ± 5 nm. The difference in particle size may be due to the morphological effect. In the Debye-Scherrer equation,[10] it is assumed that the particles are spherical and in the above case they are rod shaped.

Spherical particles of average diameter 128 ± 15 nm were obtained for ZnO particles prepared by Meulenkamp's method.[8] X-ray powder diffraction showed a wurtzite type ZnO with a particle size of 147 ± 10 nm. It is important to notice that the particles were grown much larger compared to the initial particle size before calcination.

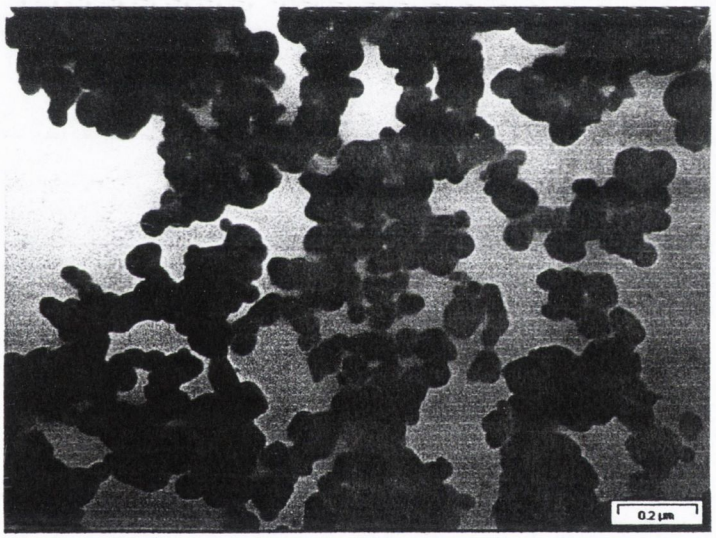

200 nm

Fig. 3.19 TEM image of the nano ZnO calcined at 500°C (prepared by Meulenkamp's route)

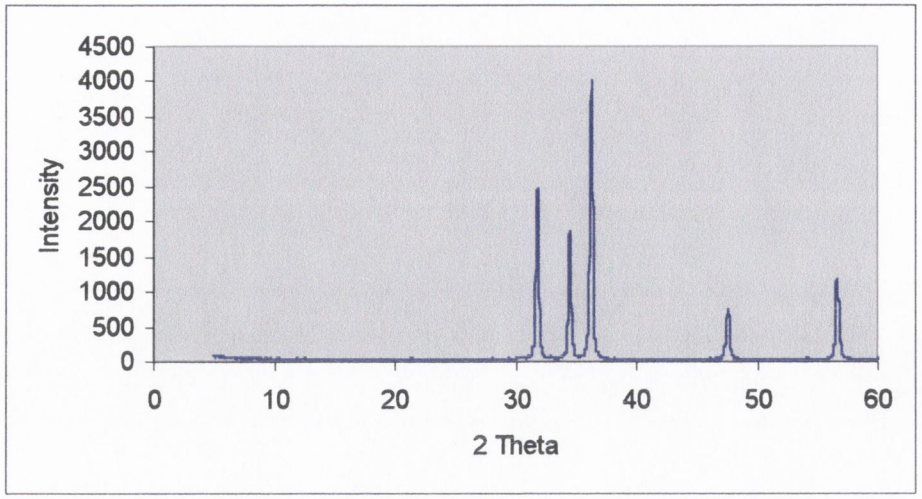

Fig. 3.20 X-ray powder diffraction pattern of the nano ZnO calcined at 500°C (prepared by Meulenkamp's route)

The particles prepared by the Weller method showed an average particle size of 15 ± 2 nm. X-ray powder diffraction studies of these material showed an average particle size of 16 ± 3 nm. Therefore the particles are only 3-4 times larger than the initially prepared (section 3.3).

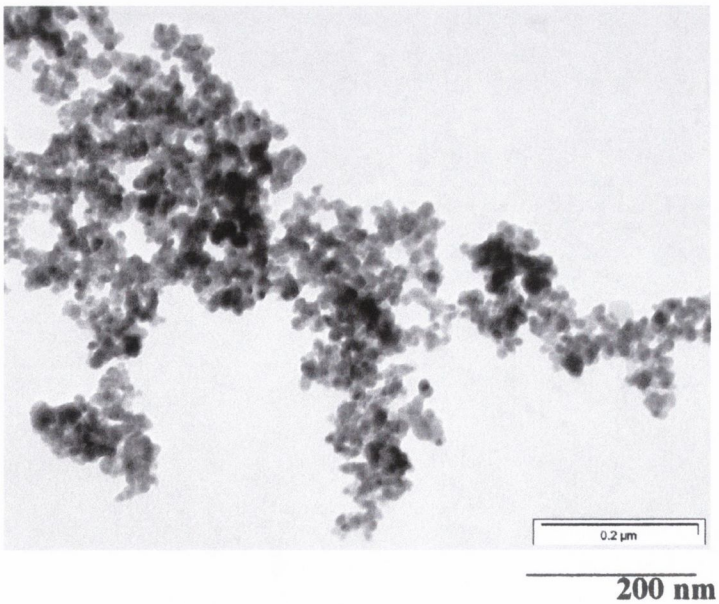

Fig. 3.21 TEM image of the nano ZnO calcined at 500°C (Weller route[9])

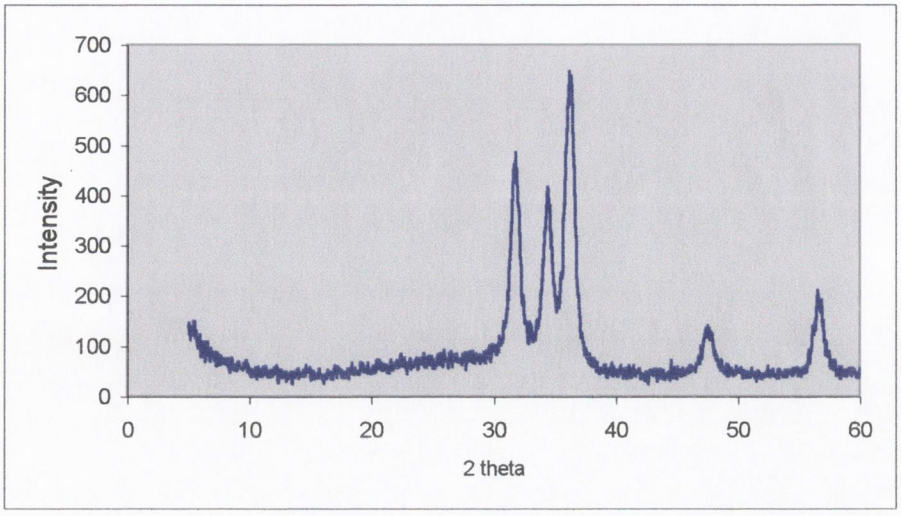

Fig. 3.22 X-ray powder diffraction pattern of the nano ZnO calcined at 500°C (prepared by Weller route[9])

Larger grain growth of 500°C calcined ZnO materials prepared from the Spanhel and Anderson[6] and the Meulenkamp[7] procedures may be due to the presence of Li ions. Meulenkamp[7] studied the effect of addition of 9.6 millimolar solution of lithium acetate to a 50 millimolar solution of ZnO at room temperature for 12 days. ZnO particles grew from 3.0 nm to 4.1 nm while the particles grew only 3.7 nm under similar experimental conditions without the use of lithium acetate. These results show that the Li ions have a great influence on the particle growth of ZnO. There are no reports available in the literature of the effect of Li ions on the ZnO particle growth at 500°C.

3.7 Sintering and electrical properties of varistors prepared by the above three methods

Varistor discs prepared from doped nano ZnO materials were sintered at 1050°C for 2 hours. The samples prepared by Spanhel and Anderson[7] route were melted fully and could not be removed from the ceramic tile (used as the sample holder). The average % densification values of the sintered samples are shown in table 3.3. It is important to notice that more than 90% densification has been achieved in the Meulenkamp[8] and the commercial samples. The varistors made from Weller[9] samples were found to have less densification (80%) than the other two samples.

Table 3.3 Densification of the varistor samples during sintering

Sample	Density (g/cm^3)	% Densification*
Meulenkamp	5.12	91.49
Weller	4.50	80.27
Commercial	5.24	93.50

* Theoretical density of ZnO is 5.60 (g/cm^3)

From I-V characteristics of the sintered nano varistors prepared by Meulenkamp and Weller methods it can be seen that there is conducting behaviour up to 10^{-4} A followed by a linear behaviour. This is very different from the commercial sample where there is a linear region first (10^{-6} A) and then a non-linear region. From the above studies it could be concluded that these materials would not be useful as a varistor material. This is probably due to the impurities (Li^+ and Na^+) present in the preparation step.[12]

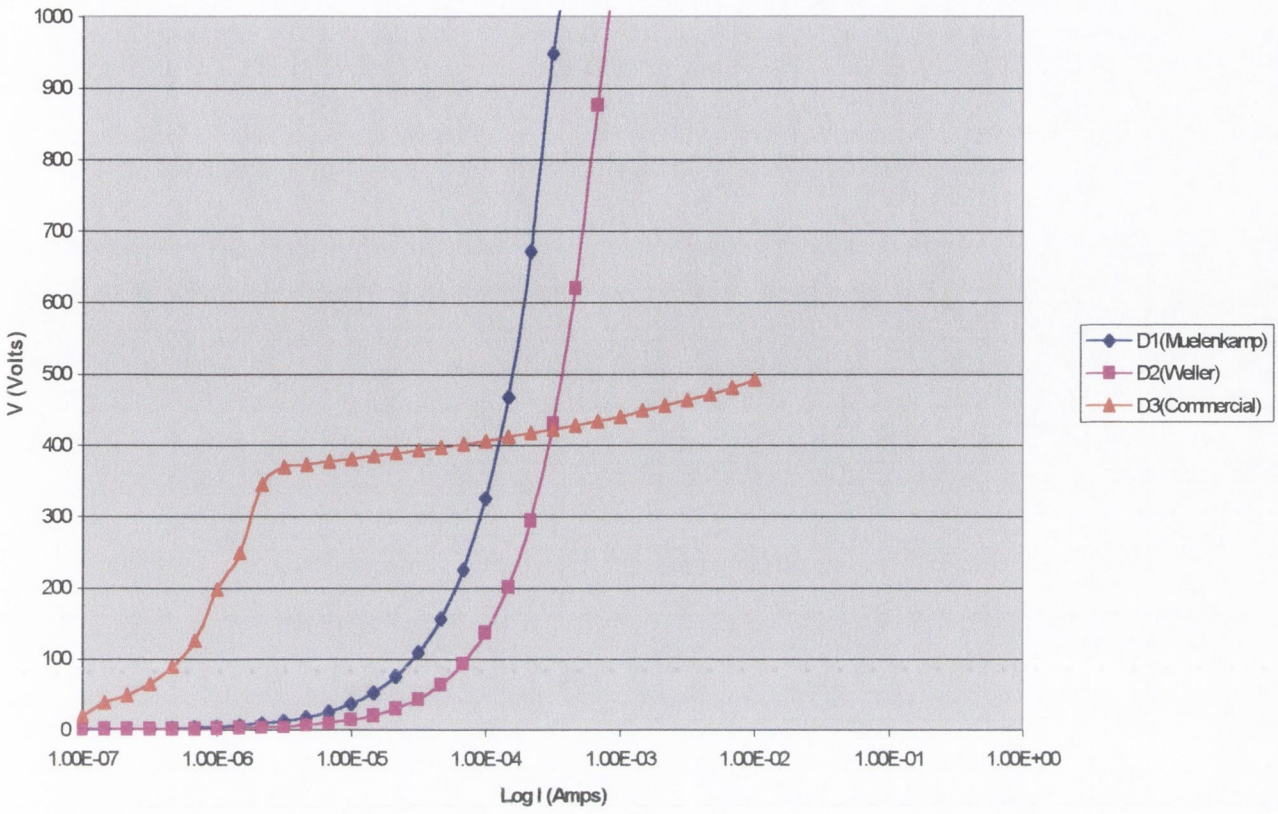

Fig 3.23 I-V characteristics of the samples sintered at 1050°C

3.8 Conclusions

1. Three methods have been used successfully to prepare nanocrystalline ZnO. The materials have been characterised by TEM, XRD and UV/Vis. Among the reported procedures tried, the Weller method is found to be most simple to reproduce. However this method requires very dilute solutions and is not suitable for the large-scale production of nano ZnO.
2. Aging studies show that ZnO nanoparticles are growing in alcoholic solutions and it is seen from the spectral plots that the particle growth is time dependent.
3. Calcination studies showed that ZnO nanomaterials synthesised from the Weller method grew to a smaller size compared to the other two routes. The reason for a larger grain growth of ZnO nanoparticles prepared by the Spanhel and Anderson and the Meulenkamp method was due to the presence of Li^+ ions.

4. Electrical studies show that these ZnO materials cannot be used as a varistor material.
5. In order to get better varistor materials studies were directed towards novel processing routes to get pure materials, which will be described in chapters 4 and 5.

3.9 References

1. H. D. Alamdari, S. Boily, M. Blouin, A. V. Neste and R. Schulz, *Mater. Sci. Forum,* 2000, **343**, 909.
2. Y. Lin, Z. Zhang, Z. Tang, F. Yuan and J. Li, *Adv. Mater. Opt. Electro.*, 2000, **9**, 205.
6. P. Duran, F. Capel, J. Tartaj and C. Moure, *J. Amer. Ceram. Soc.*, 2001, **84**, 1661.
7. A. Sinha and B. P. Sharma, *Mat. Res. Bull.,* 1997, **32**, 1571.
8. R. N. Viswanath, S. Ramasamy, R. Ramamoorthy, P. Jayavel and T. Nagarajan, *Nanostructured Materials.*, 1995, **6**, 993.
6. G. Hohenberger and G.Tomandl, *J.Mat.Res.*, 1992, **7**, 546.
7. L. Spanhel and M. A. Anderson, *J. Am. Chem. Soc.*, 1991, **113,** 2826.
8. a) E. A. Meulenkamp *J. Phys. Chem. B.,* 1998, **102**, 5566 b) E. A. Meulenkamp *J. Phys. Chem. B.*, 1998, **102**, 7764.
9. U. Koch, A. Fojtik, H. Weller and A. Henglein, *Chem. Phys. Lett.,* 1985, **122**, 507.
10. A. R. West, *Solid State Chemistry and Its Applications,* John Wiley & Sons London, 1984, p 174.
11. Private communication-a) D. D. Ebrel, U.S. Geological Survey 3215, Marine St.,Boulder, Co. 80303-1066 USA b) D. H. Doff, Department of Geology, Trinity College Dublin, Dublin 2, Ireland.
12. Private communication – Dr. Ramesh Raghavendra, Littelfuse Ireland Ltd, Dundalk, Co. Louth, Ireland.
13. E. M. Wong, J. E. Bonevich and P. C. Searson, *J. Phys. Chem. B,* 1998, **102**, 7770.
14. D. H. Everett *"Basic principles of colloid science"* The Royal Society of Chemistry, London, 1988.

Chapter 4

Synthesis of novel ZnO nanoparticles and self assembled nanowire arrays

4.1 Introduction

A number of preparative techniques, many based on the reaction of a zinc salt with alkali metal hydroxides or alkoxide based sol gel synthesis, have been shown to yield spherical well-defined particles in the range of 2 to 7 nm.[1-4] However only very recently have ZnO nanowires been reported. This has been achieved using anodic alumina membranes,[5,6] physical vapour deposition method,[7] and by a vapour-liquid-solid growth using gold as catalyst.[8] In this chapter we report a novel and simple procedure to fabricate ZnO nanoparticles and ZnO nanowire arrays using a non-hydrolytic sol gel condensation reaction and subsequent calcination. These methods, unlike most of the previous methods, allow the production of the template free ZnO nanowires and nanoparticles in large quantities without using any templates.

Since the discovery of carbon nanotubes,[9] numerous nanofabrication techniques have been reported for the production of nanowires,[10] nanorods,[11] and nanofibres.[12] Electrochemical synthesis using a template is one of the efficient methods for the fabrication of assembled nanomaterials in a desired shape because the growth occurs in the direction of the template.[13] Metal oxide nanostructures of TiO_2, MnO_2, Co_3O_4, ZnO, WO_3, and SiO_2 have been synthesised by the sol gel technique using porous alumina and polymeric filler as templates. Fibres and tubules of the oxide material are formed within each pore of the template membrane.[12] The fabrication of metal oxide nanofibres/nanorods of V_2O_5, MoO_2, RuO_2, IrO_2, and GeO_2 using the carbon nanotubes as removable templates have been reported.[5, 14-17] The formation of a palladium nanowire on a DNA template was reported recently.[18] CdSe nanowire arrays were also fabricated by direct current electrodeposition in porous anodic aluminium oxide templates from a dimethyl sulfoxide solution containing $CdCl_2$ and elemental Se.[19] $Mg(OH)_2$ nanorods were prepared from Mg powder and water with ethylenediamine at 180°C under pressure in an autoclave.[20] Fitzmaurice *et al*[21] achieved the synthesis of silver nanocrystals without a template into two dimensional nanowire arrays using dodecanethiol as a chelating (capping) ligand.

Varistors have been fabricated from these materials by doping with metal oxides and by a core shell type synthesis, using ZnO nanoparticles as core materials and Sb, Bi and Co metal as shells, has also been achieved.

Core shell materials: These are materials with solid spherical particles covered with an organic or inorganic layer by chemical technology.[22-27] This typically involves tailoring the surface properties of particles often accomplished by coating or encapsulating them within a shell of preferred material.[28,29] Preparation of TiO_2-$BaCO_3$ particles as precursor of $BaTiO_3$ has been achieved by a two step procedure by first coating the TiO_2 core by $Ba(OH)_2$ shell followed by conversion of the shell region with CO_2 gas by the formation of $BaCO_3$.[30] Recently the photoluminescence properties of ZnO particles with BN capsules (ZnO as core and BN as shell) have been reported.[31]

With improved chemical and physical properties over their single counterparts, core shell materials are potentially useful in a broader range of applications. The shell alters the charge, functionality and dispersibility of the colloidal core. Encasing colloids in a shell of different composition may also protect the core from extraneous chemical and physical changes. Core shell materials have been utilised in the areas of opto-electronics,[28,32] coatings,[24] and catalysis.[22] Hollow spheres of magnetic nanoparticles were prepared by a sequential layering approach for the application of diagnostics.[24]

By homogeneous coating of each spherical particle, more grain boundaries will be formed by dopants compared to the conventional techniques. Thereby it is possible to produce more varistor-active grain boundaries per unit area. Grain growth is expected to be much less, as each grain is homogeneously covered with dopants (grain growth inhibitors). Furthermore the sintering temperature could be decreased with the homogeneous addition of sintering aids.

4.2 Synthesis of ZnO nanoparticles

Reaction of an ethanolic solution of zinc acetate with an ethanolic solution of oxalic acid produced a thick semi-gel. Subsequent drying at 80°C and calcination of this gel at 500°C produced ZnO (Scheme 4.1) as identified by its powder X-ray diffraction pattern (Fig. 4.1).

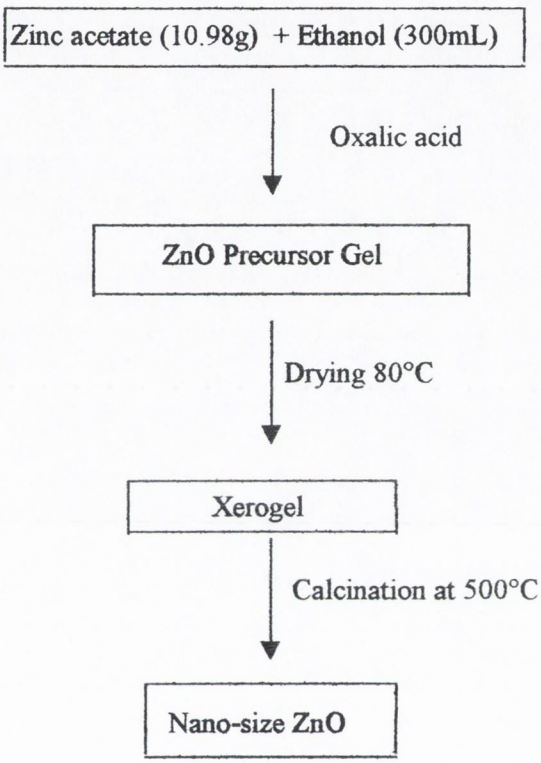

Scheme 4.1 Flowchart for the synthesis of ZnO nanoparticles through a non-hydrolytic condensation reaction.

The X-ray powder diffraction pattern shows 2θ values and relative intensities (except 002 plane) of the peaks coincident with JCPDS data of zincite (Table 4.1).

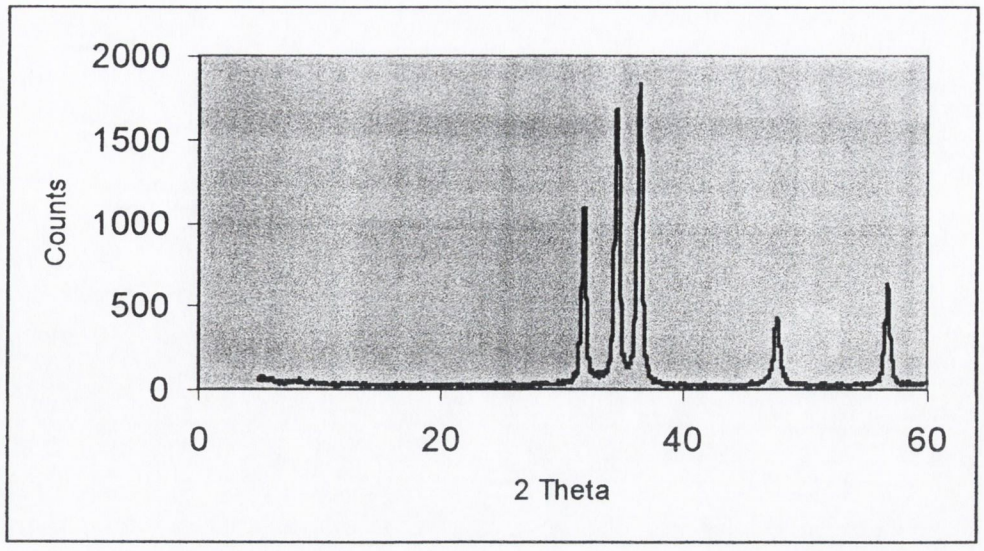

Fig. 4.1 X-ray powder diffraction plot of ZnO material calcined at 500°C

Table 4.1 X-ray powder diffraction data of ZnO material calcined at 500°C

Literature JCPDS (36-1451)				Experimental		
hkl	2θ	d (Å)	Intensity	2θ	d (Å)	Intensity
100	31.76	2.81	57	31.85	2.81	50
002	34.42	2.60	44	34.50	2.59	84
101	36.25	2.48	100	36.42	2.46	100
102	47.53	1.91	23	47.55	1.91	23
110	56.60	1.62	32	56.60	1.62	36

Broadening of the X-ray bands allowed an estimate of the average particle size as 27 ± 5 nm using the Debye-Scherrer equation[33] (refer section 2.5.4). This was confirmed using transmission electron microscopy (Fig. 4.2) which revealed that the material consisted of agglomerates of spherical particles with a diameter of

34 ± 5 nm. BET surface area for material calcined at 500°C was found to be 17 m^2/g.

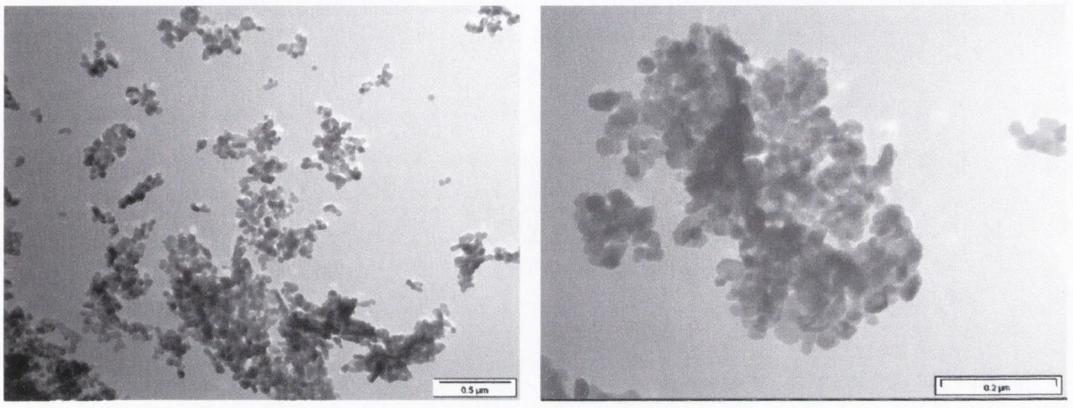

Fig. 4. 2 TEM image of ZnO powder calcined at 500°C

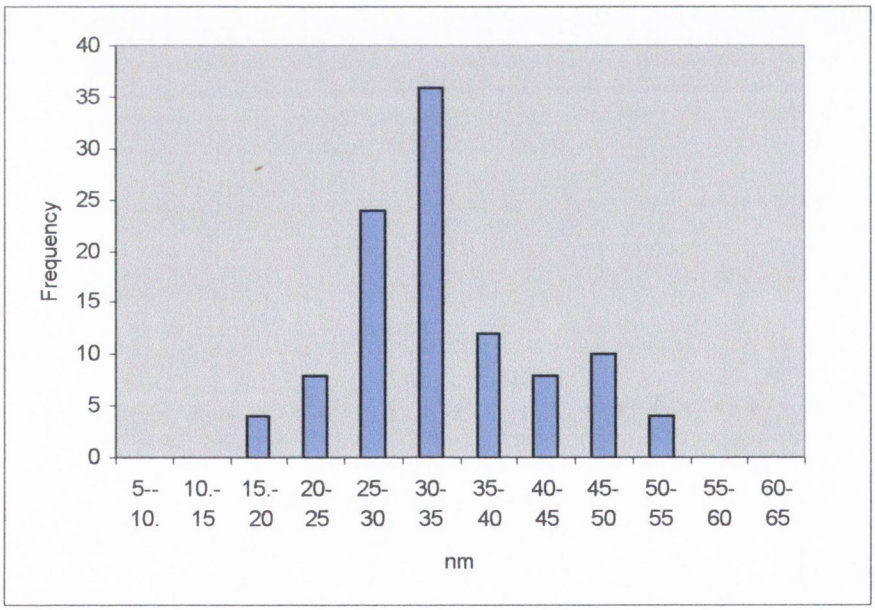

Fig. 4.3 Size histogram (TEM) of the ZnO nanoparticles

4.3. Synthesis of nanowire arrays of ZnO

In this experiment the procedure was similar to section 4.2, expect that chemical modifiers [diethanolamine (DEA) and ethyleneglycol (EG), Zn:EG:DEA molar ratio used was 1.0:2.0:0.1] were added to the ethanolic solution of zinc acetate ten minutes before the addition of the ethanolic solution of oxalic acid.

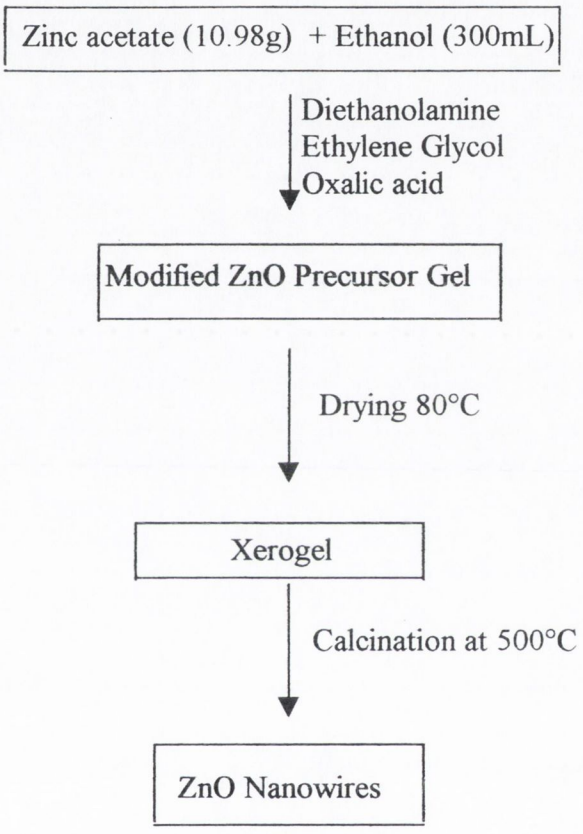

Scheme 4.2 Flowchart for the synthesis of ZnO nanowires

The thick white gel was dried at 80°C and subsequently calcined at 500°C. BET surface area for the powder calcined at 500° C was found to be 21 m^2/g.

The X-ray powder diffraction pattern shows 2θ values and relative intensities of the peaks coincident with JCPDS data of zincite (Table 4.2). Small difference in intensities may be due to the broadening of the lines. The broadening of these

lines in the XRD pattern (Fig 4.4) of zincite ZnO showed the presence of nanoparticles but this time with an average size of 19 ± 4 nm.

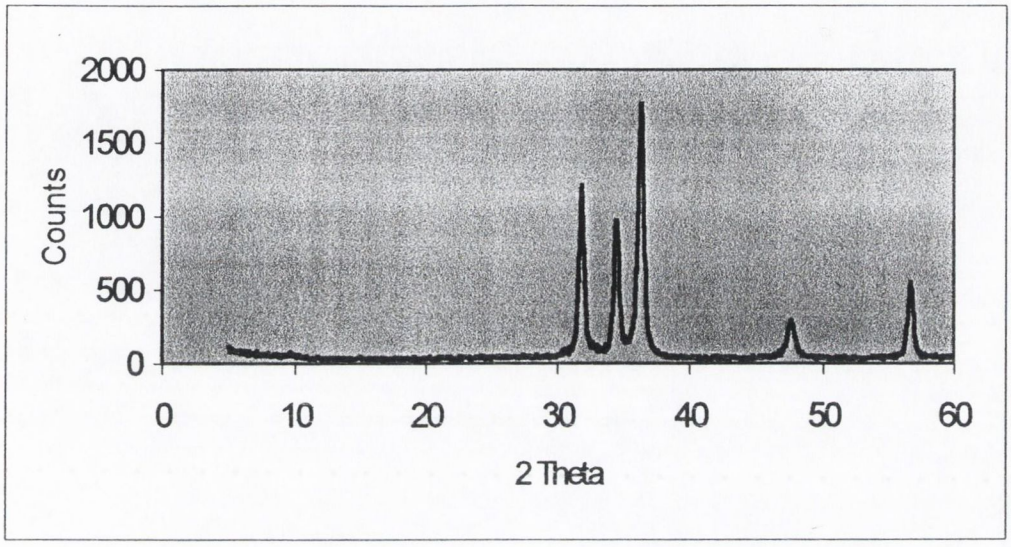

Fig. 4.4 X-ray powder diffraction plot of ZnO calcined at 500°C.

Table 4.2 X-ray powder diffraction data of ZnO calcined at 500°C

Literature JCPDS (36-1451)				Experimental		
hkl	2θ	d (Å)	Intensity	2θ	d (Å)	Intensity
100	31.76	2.81	57	31.80	2.81	65
002	34.42	2.60	44	34.45	2.63	50
101	36.25	2.48	100	36.36	2.48	100
102	47.53	1.91	23	47.52	1.91	14
110	56.60	1.62	32	56.57	1.62	30

However, as shown in Fig. 4.5, field emission scanning electron microscopy (FESEM) revealed a fibrous material containing elongated bundles of nanowires of 100 nm width and 2-4 μm in length.

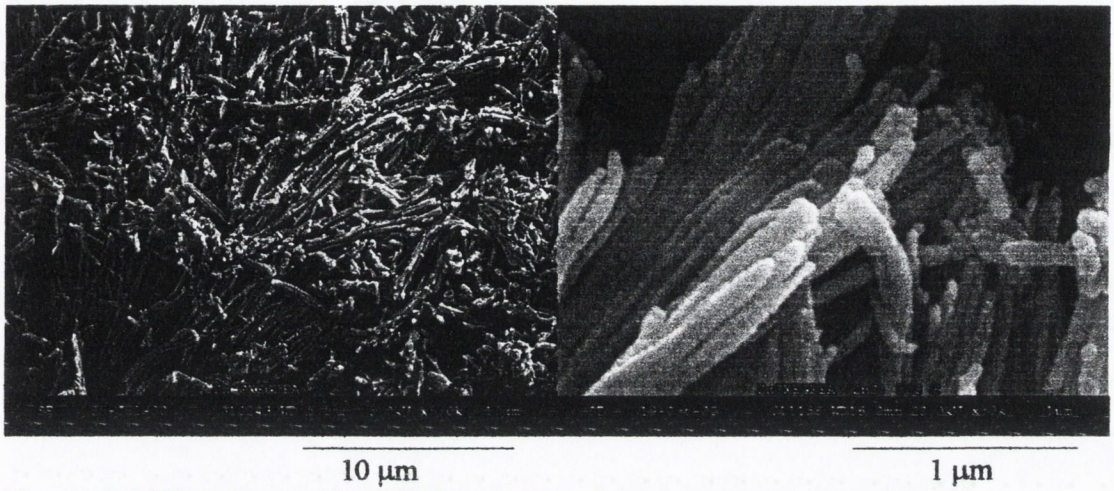

Fig. 4.5 FESEM picture of the ZnO material calcined at 500° C (40 minutes)

This material was subsequently suspended in ethanol and ultrasonicated for periods of up to 40 minutes. TEM studies showed that this treatment separates the individual wires from the bundle (*e.g.* Figure 4.6).

Fig.4.6 TEM picture of a single wire (calcined at 500 °C) separated by dispersing in ethanol and further ultrasonication (40 minutes)

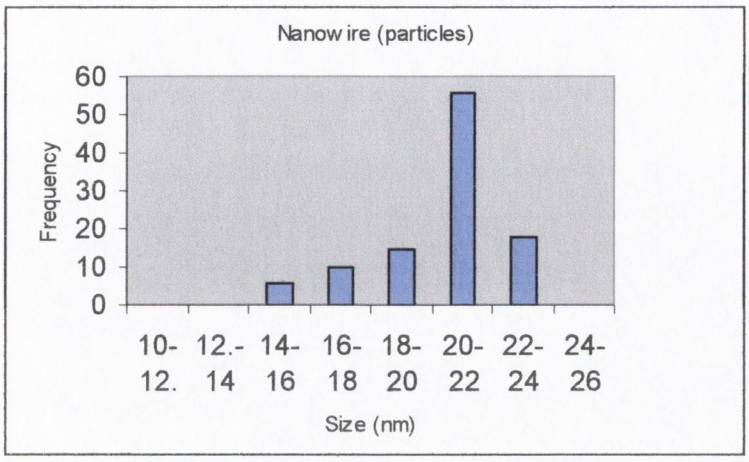

Fig.4.7 Size histogram (TEM) of the ZnO nanoparticles in the nanowires

These wires are composed of approximately spherical nanoparticles of average diameter 21 ± 3 nm (Fig. 4.7), self assembled to form one–dimensional arrays covering a length of 2-4 μm without a break (Fig. 4.6). The morphology is therefore similar to that previously reported for the gold,[34] silver,[21] palladium[18] and CdSe[19] nanoparticle arrays. There is not much appreciable effect of surfactants in separating the individual wires. However sodium dodecyl sulphate (SDS) an anionic surfactant was found to be better in separating the bundles compared to the cationic surfactant cetyl trimethyl ammonium bromide (CTAB).

The 500°C calcined nanowires were further annealed to 1000°C and the morphology was studied by FESEM (Fig. 4.8.). It is also interesting to notice that at this higher temperature the individual particles have sintered together to form continuous wires of width 0.3 to 0.4 μm and 10- 20 μm in length.

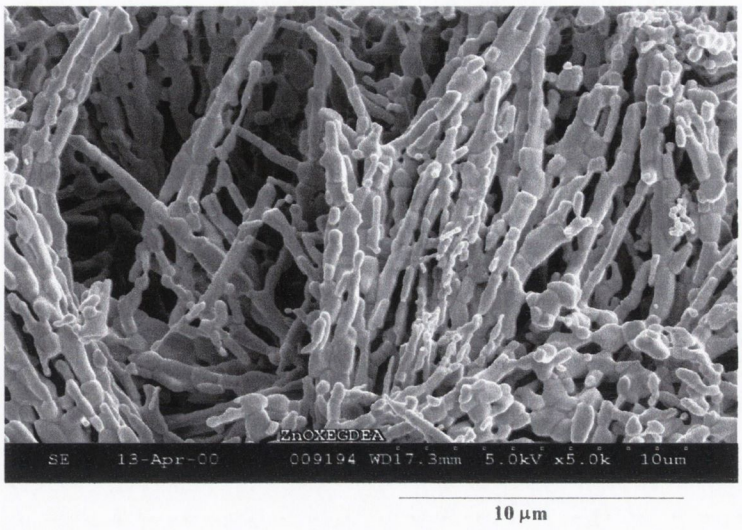

Fig. 4.8 FESEM picture of ZnO nanowires calcined at 1000°C

This is more obvious in the sample calcined at 1000°C (Fig 4.8). During sintering ions first diffuse along grain boundaries of the surface to the points of contact between particles,[35] providing bridging and connection of the grains results in the fusion of individual wires (Fig 4.9).

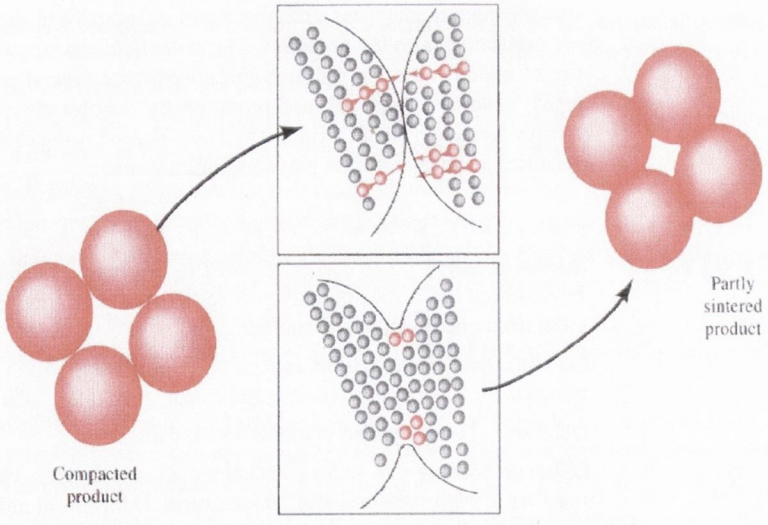

Fig. 4.9 Diagrammatic representation of a sintering process.[35]

4.4 A detailed microstructural studies of the two precursors

In order to understand the formation mechanism of nanowires the precursor morphology was studied by TEM at various stages of the preparation.

4.4.1 Gel Structure of the precursor of ZnO nanoparticles prepared without using modifiers

The thick white gel dried at room temperature, 80°C and calcined at 250°C resulted in elongated or spherical morphologies (Fig. 4.10 & 4.11).

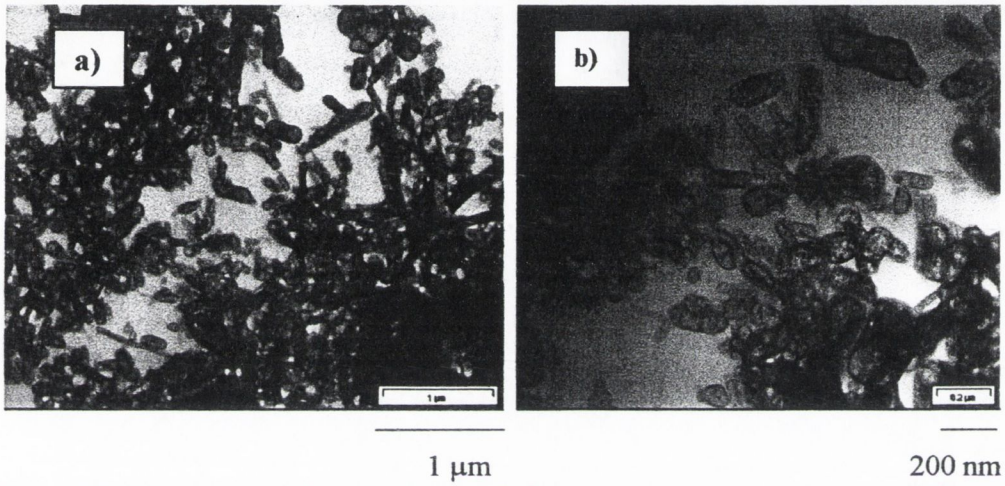

Fig. 4.10 TEM image of the fresh gel dried at room temperature in two different magnifications a) X 20000 b) X 50000

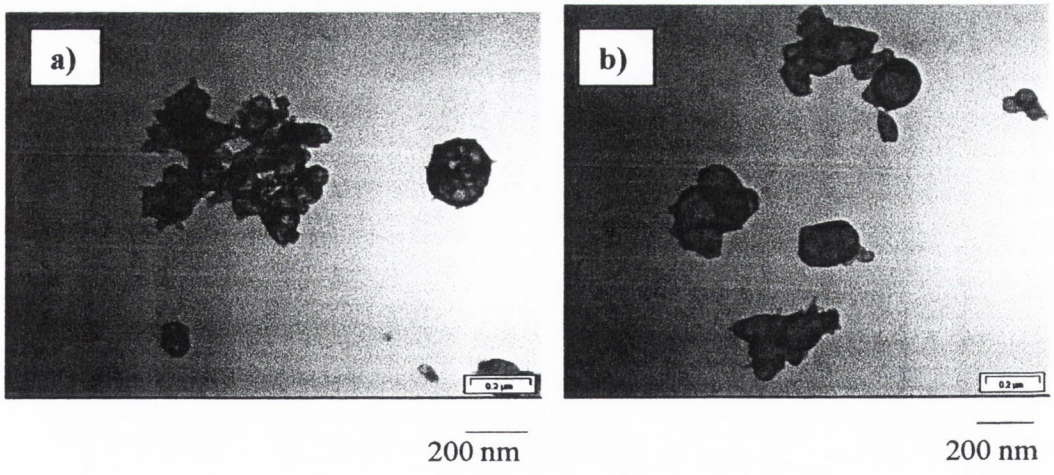

Fig. 4.11 TEM of the gel treated at different temperatures a) fresh gel dried at 80°C b) dried gel calcined at 250°C

4.4.2. FTIR analysis of the dried and calcined powder prepared without chemical modifiers

FTIR spectrum of the xerogel (80°C) is typical of an acetate salt.[36] Two principal peaks are observed at 1627 cm^{-1} and 1364 cm^{-1} corresponding to the asymmetric and symmetric stretching of the carboxyl group respectively (Fig 4.12). The bands at 3398 cm^{-1} and 2900 cm^{-1} are due to OH stretching and CH (acetate) stretching respectively (Table 4.3). The 250°C sample also showed a similar pattern but less intense peaks observed. The ZnO stretching mode at 495 cm^{-1} appears in this case. The 500°C calcined sample showed a very strong band at 450 cm^{-1} due to the Zn-O stretching (Fig. 4.12). The small signal at 3411 cm^{-1} is observed probably due to the contact of the ZnO sample with air resulting in adsorption of small amount of water vapour.[37]

Table 4.3 FTIR analysis of the ZnO precursor gel dried at 80°C (xerogel) and the xerogel calcined at 250 and 500°C

Assignment	(80°C)	250°C	500°C
ν_{asCOO-}	1627 vs	1621s	
ν_{sCOO-}	1364s	1364s	
δ_{COO-}	740s	750w	
ν_{OH} (H_2O)	3398s	3402w	3411vw
ν_{CH} (CH_3)	2900vw		
ν_{Zn-O} (ZnO)		495vw	450vs

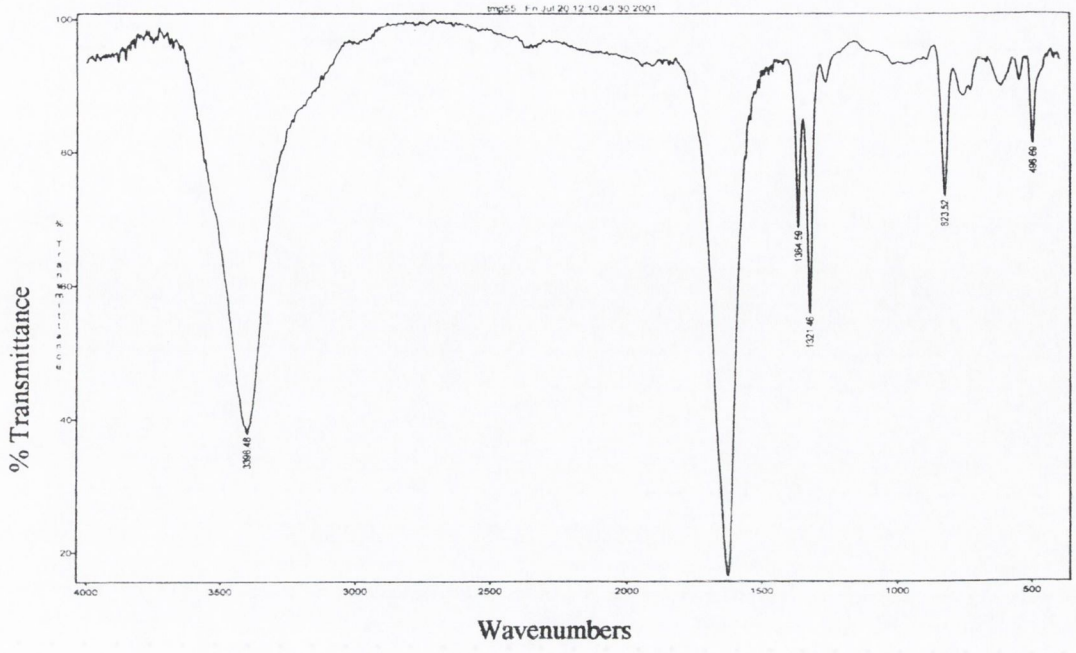

Fig. 4.12 FTIR spectra of the Xerogel (dried at 80°C)

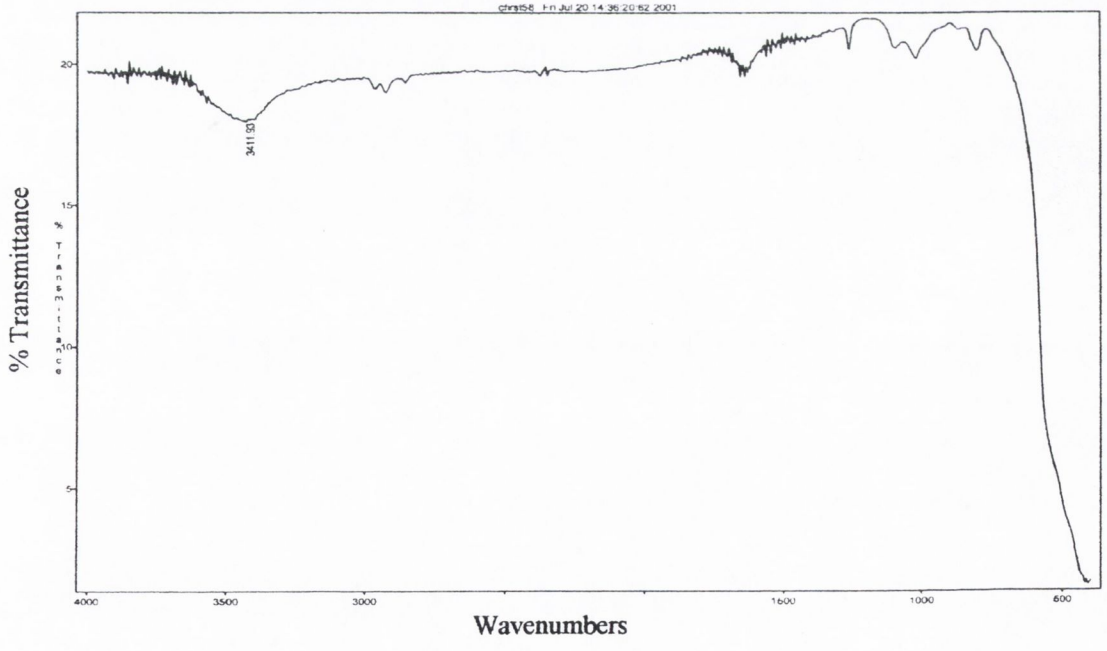

Fig. 4.13 FTIR spectra of the ZnO material (calcined at 500°C)

4.4.3 Thermal analysis of the xerogel

The thermo gravimetric analysis curve of the xerogel is shown in Fig. 4.14. A total weight loss of 59% is obtained which is lower than expected weight loss (calculated from the amount of zinc acetate dihydrate and oxalic acid) of 79%. This is probably due to the removal of water and small amounts of unbound organics during the oven drying at 80°C for 20 hours. Two stages of weight loss are observed at 176°C and 435°C. The first stage of the weight loss (80-176°C) is regarded as the removal of the water of dehydration (17%) and the second stage (176-435°C) of weight loss (42%) can be explained as the formation of ZnO from the decomposition of the precursors. (XRD results showed that the ZnO formation occurred after 250°C). DSC analysis (Fig. 4.15) also showed two well-defined endothermic peaks at 170 and 440°C.

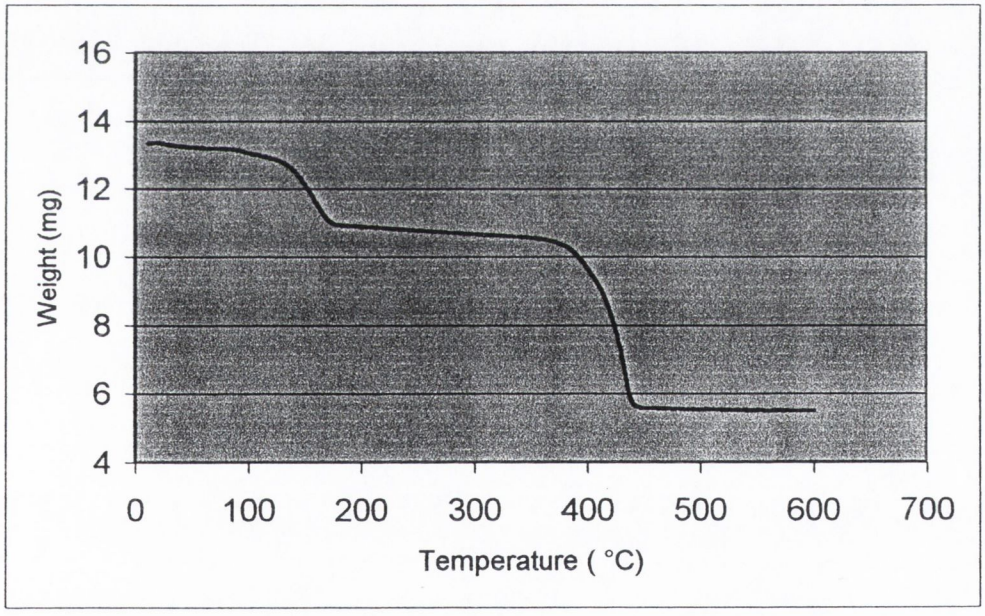

Fig. 4.14 TGA curve of ZnO xerogel (80°C)

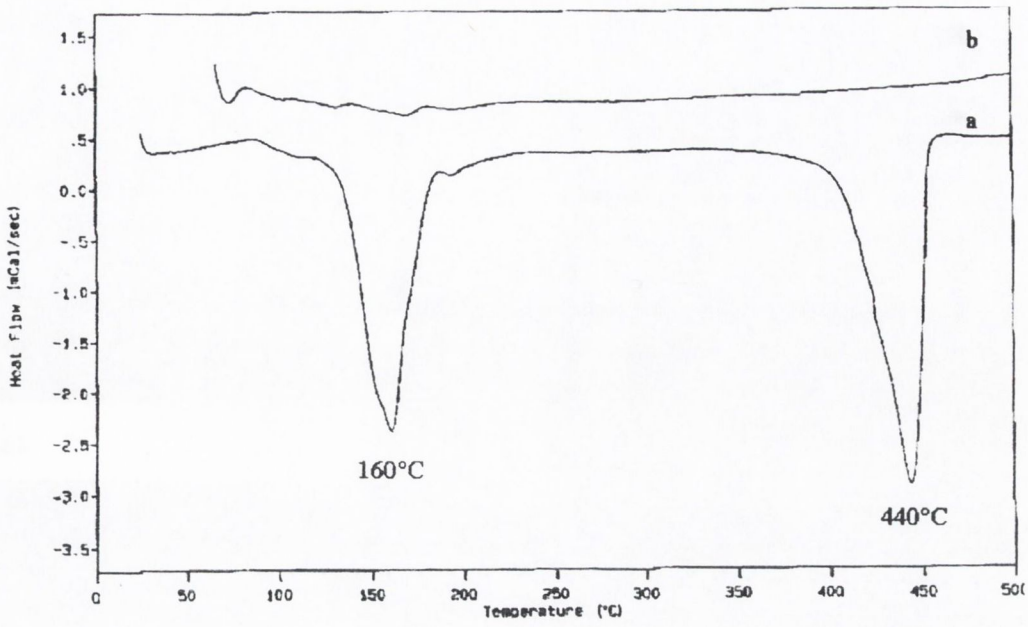

Fig. 4.15 DSC plot of the xerogel (80°C) a) First scan b) Second scan

4.4.4 Gel Structure of the precursor of ZnO nanowires

Electron microscopy studies were carried out at various stages in the synthetic process. Fig. 4.16 shows the FESEM images of the fresh gel dried at room temperature on alumina stubs. The gel dried as an elongated fibrous network of several millimetres (Fig. 4.16 a) and each fibre is made up of rods < 1 μm in length (Fig. 4.16 d)

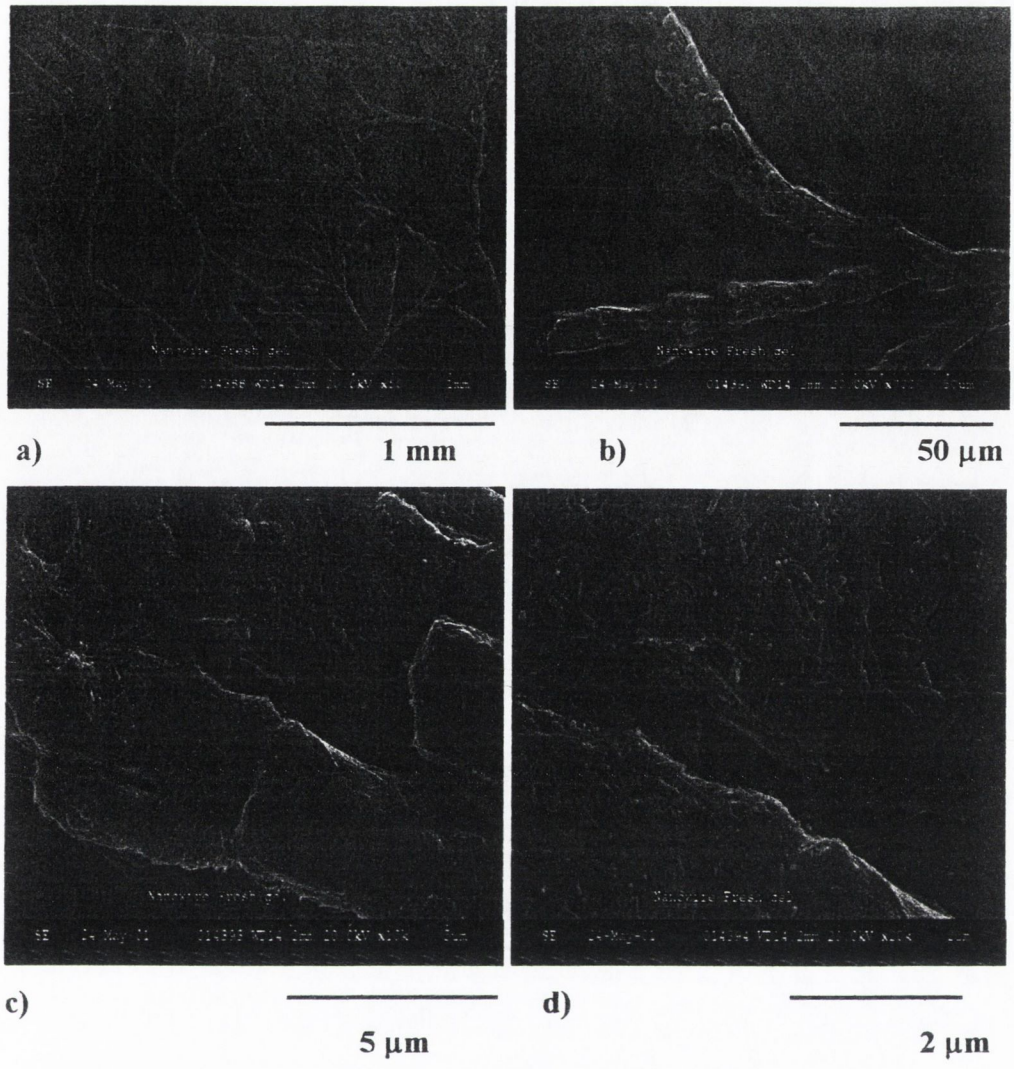

Fig. 4.16 FESEM of the fresh gel dried in air at different magnifications a) 50 b) 700 c) 10000 d) 20000

The morphology was further confirmed by TEM studies (Fig. 4.17). The fresh gel was dried in air on a formvar coated copper grids and the images were taken at different magnification.

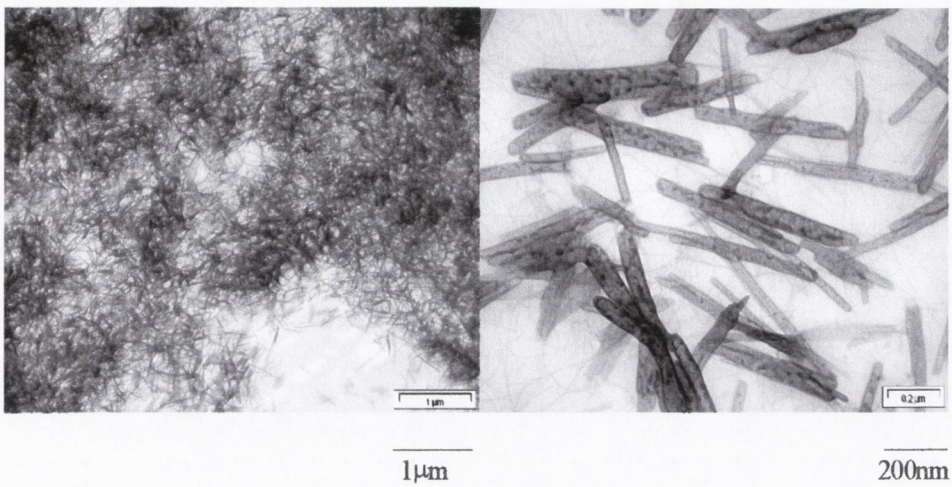

Fig. 4.17 TEM images of the nanowire precursor fresh gel dried in air at room temperature

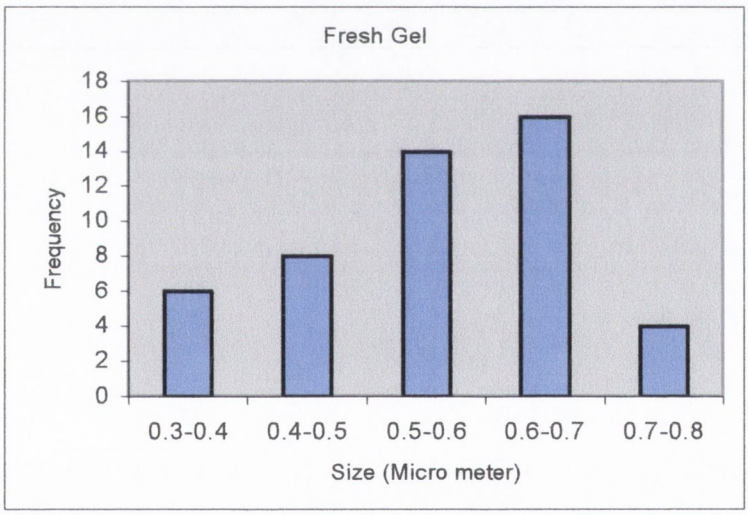

Fig. 4.18 TEM Histogram of the rods (fresh gel dried in air)

It may be observed that even in the fresh gel elongated crystals are formed (rods 0.6 μm in length, Fig. 4.17), while at 80°C longer particles are produced (Fig. 4.19), probably by aggregation.

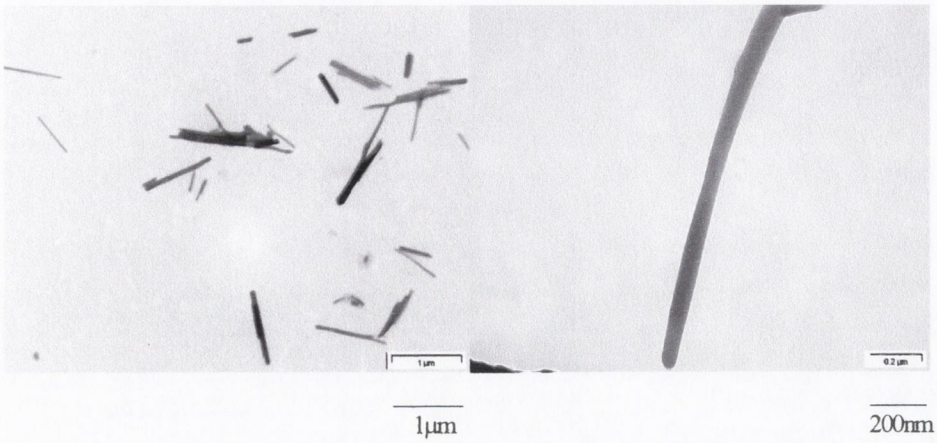

Fig. 4.19 TEM images of the nanowire precursor gel dried in an oven set at 80°C

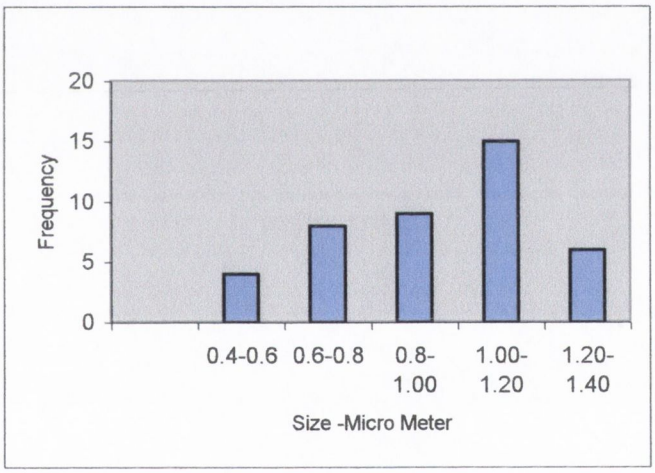

Fig. 4.20 TEM Histogram of the rods (fresh gel dried in air)

Heating the xerogel further to 250°C in a chamber furnace causes a change to the internal morphology of the rods. TEM images show (Fig. 4.21) that the rods grew further to 2 to 3 μm in length and 100 nm in width. The XRD of samples taken after heating to 80°C or 250°C showed no evidence for ZnO. X-ray diffraction pattern of the xerogel heat treated at 80°C (2θ of 10.5, 14.7, 17.8, 20.5, 23.9, 34.2, 45.0 and 49.4) and 250°C (2θ of 24.4, 33.2, 35.26 and 49.86) of

were showed crystalline peaks but these did not correlate with JCPDS data for Zn compounds.

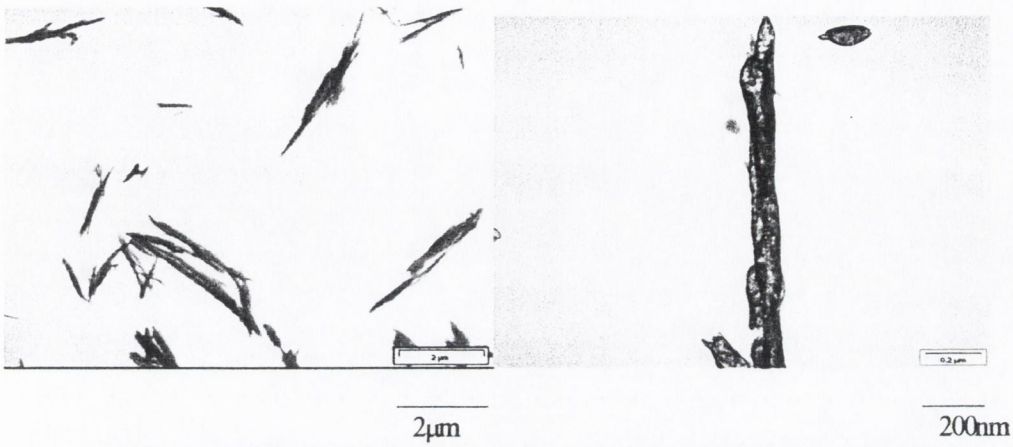

Fig. 4.21 TEM images of the nanowire xerogel calcined at 250°C

4.4.5 FTIR Analysis of the fresh gel, xerogel and nanowire

FTIR spectra of the xerogel (80°C) shows the presence of acetate groups as evident from the ν_{asCOO-} and ν_{sCOO-} stretching frequencies[38,39] at 1632 cm^{-1} and 1471 cm^{-1}. Bands at 2920 cm^{-1} and 817 cm^{-1} are assigned for the stretching vibrations of NH (Fig. 4.22). The band at 3264 cm^{-1} is a consequence of ν_{OH} vibration. There is no Zn-O vibration observed in this case.

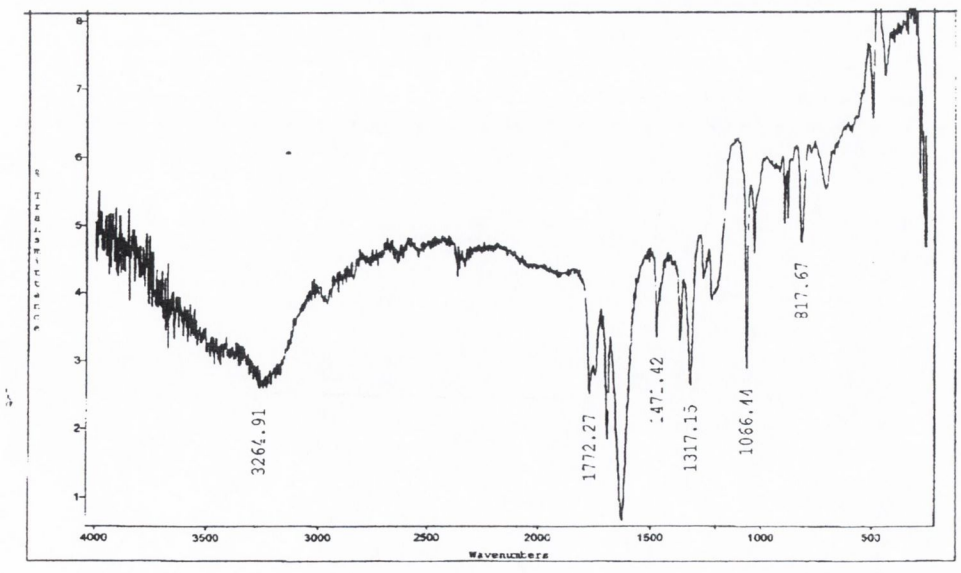

Fig. 4. 22 FTIR spectra of the xerogel (dried at 80°C)

A similar spectrum is obtained for 250°C calcined material a Zn-O vibration ($460cm^{-1}$) is observed in this case. The spectrum of 500°C (Fig. 4.23) calcined material has a strong band at $452cm^{-1}$ (Zn-O stretching) that is similar to the spectra of ZnO prepared without the modifiers. The additional peaks at $842cm^{-1}$ and $1143cm^{-1}$ are due to the presence of very small amount of diethylamine present in the sample. This result also implies the chelating ability of ethanolamines even at high temperatures.

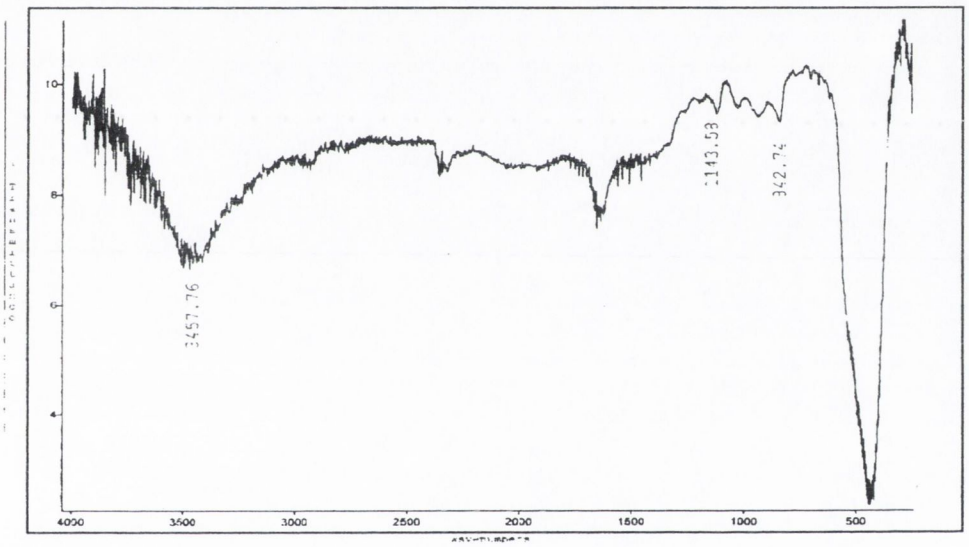

Fig. 4. 23 FTIR spectra of the ZnO material (calcined at 500°C)

Table 4.4 FTIR analysis of the ZnO precursor gel dried at 80°C (xerogel) and the xerogel calcined at 250 and 500°C

Assignment	80°C	250°C	500°C
ν_{asCOO-}	1632vs	1644s	
ν_{sCOO-}	1471s		
δ_{COO-}	750s		
ν_{OH} (H_2O)	3264s	3453w	3457w
ν_{NH} (NH_2)	2920w	2920w	
δ_{NH} (NH_2)	817s	817s	842vw
ν_{CH} (CH_3)	2900w	2864vw	
δ_{CH} (CH_3)	1192w	1328vw	1143vw
ν_{Zn-O} (ZnO)	-	460vw	452vs

4.4.6 Thermal analysis of the nanowire xerogel

The thermo-gravimetric analysis curve of the nanowire xerogel is shown in Fig. 4.24. Two well-defined stages of weight losses are observed at 270°C and 443°C respectively. A total weight loss of 67% is obtained (expected value is 84%; calculated from the amount of zinc acetate dihydrate, oxalic acid, diethanolamine and ethylene glycol). The weight loss (35%) between 100 and 270°C is due to the removal of water of hydration and ethylene glycol (expected weight loss for ethylene glycol and water of hydration are 23% and 20% respectively).

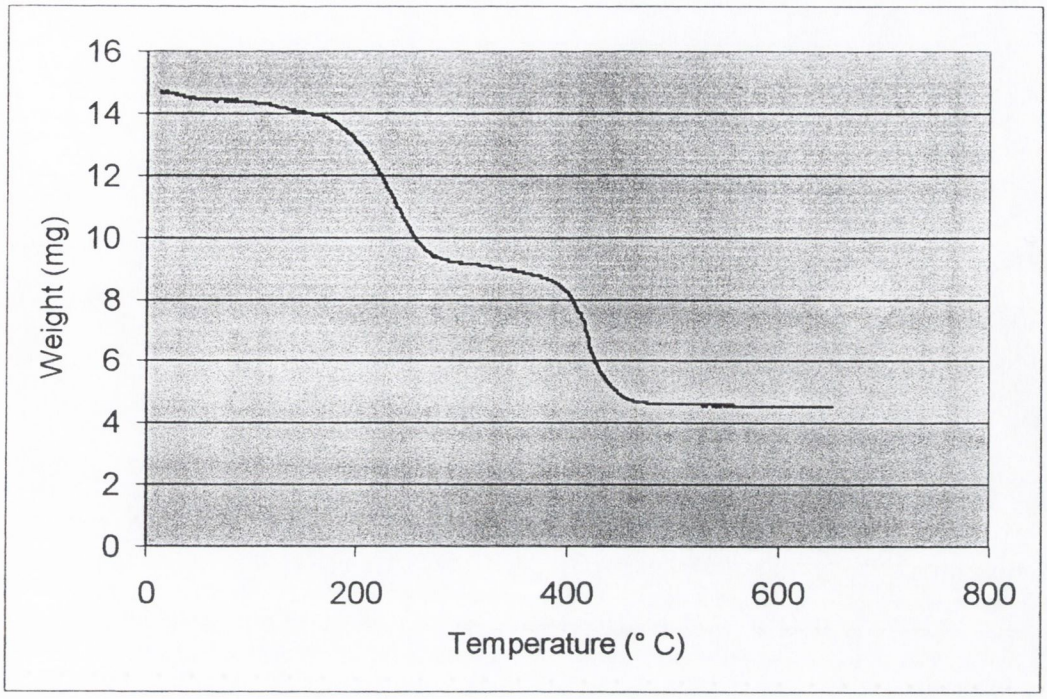

Fig. 4.24 TGA curve of ZnO xerogel (80°C)

More information on the bonding nature of the capping agents could be obtained from the DSC analysis of the dried gel (Fig. 4.25). In the DSC plot a broad endothermic peak seen at 120°C possibly due to the removal of solvated alcohol and small amount of water.[40-42] The broad endothermic below around 200°C is due to the removal of acetate and peaks at 210°C and 240°C are due to the removal of ethylene glycol and diethanolamine respectively.[38-43] This was confirmed by comparing the DSC of pure ethylene glycol and DEA sample. The main transition observed at 440°C suggested that the formation of ZnO from the precursors.[38-40] Calcination temperature used was 500°C since the decomposition finished at this temperature and XRD results showed that it was pure ZnO.

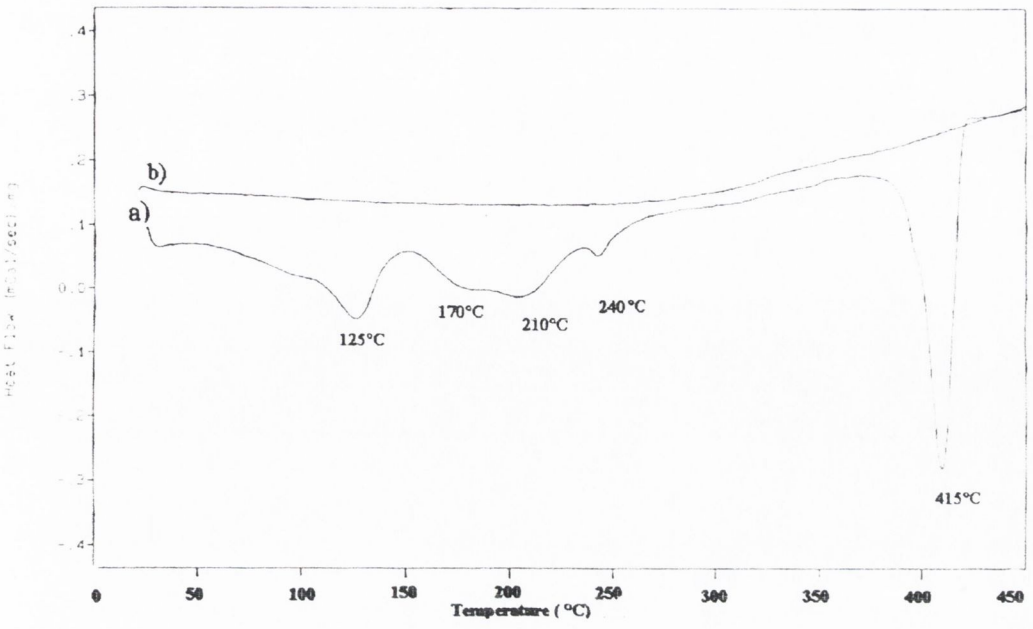

Fig. 4.25 DSC plot of the nanowire xerogel (80°C) a) First scan b) Second scan

Ethylene glycol and DEA were used to modify the condensation reaction in the precursor gel. It is clear that these species have a determining role in controlling the morphology of the ZnO, which is formed at temperature above 250°C. Several chemical modifiers like dodecanethiole,[21] and ethylenediamine[44,45] were also earlier reported in order to obtain well defined morphologies. These capping agents seem to be functioning like a small sheath and align the particle in a regular manner (Fig. 4.16 & 4.18). It is particularly noted that DEA has a major influence even though it is present in a lower molar ratio. During the drying process solvent trapped in the pores of the gel is removed and the morphology is retained even at higher temperatures (Fig. 4.5, 4.6 & 4.8). This study has shown the strong dependence of precursor morphology on the formation of nanowires. It may also be noted that decomposition of zinc oxalate in the range 330 - 650°C has previously been reported to yield spherical particles of ZnO, but not in the form of nano-wires.[46,47]

The effect of chelating ligands was further confirmed from the following reaction. The nanowire xerogel (80°C) was dispersed in ethanol by ultrasonication (10 min) and the microstructure studied by TEM. It was

interesting to notice that the rod like morphology was destroyed (Fig. 4.26) and the structure was similar to the precursor gel without the modifiers (Fig. 4.11). This is probably due to the removal of capping ligands during alcohol treatment and ultrasonication.

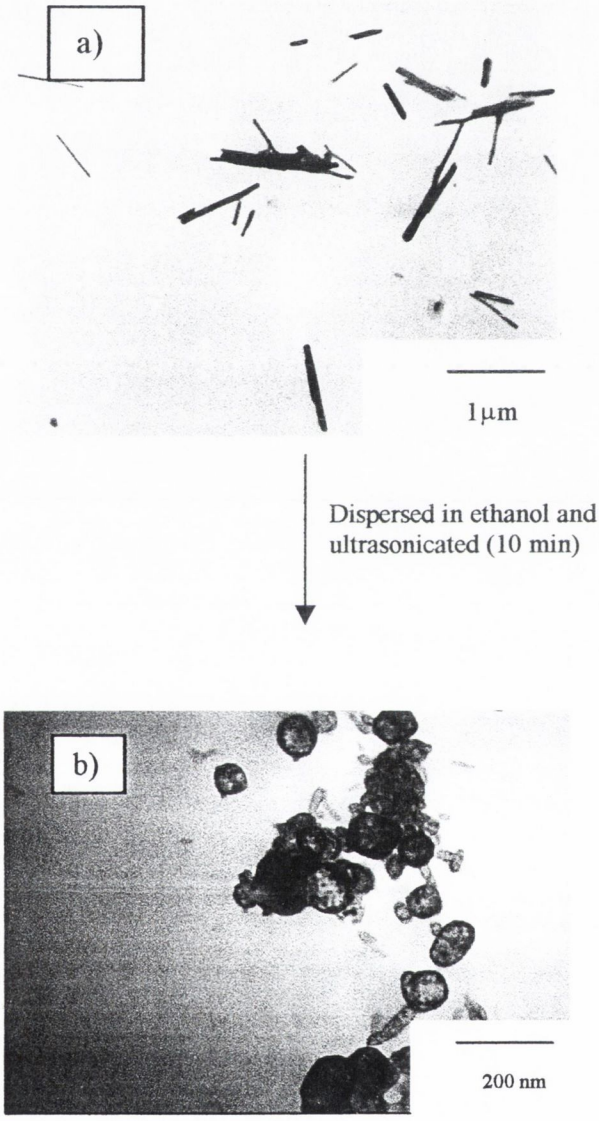

Fig. 4.26 Dispersion of the nanowire xerogel rods with ethanol a) TEM image before washing b) TEM image after washing. It can be seen from the figure that the rod like morphology is destroyed and spherical aggregates are formed.

4.5 Variation in modifier concentration

Oxalic acid in the presence of chemical modifiers (ethylene glycol and diethanolamine) is believed to align the particles together and facilitate condensation as a fibrous semi-gel form. The synthesis of nanowire was optimised as 0.1 molar ratio diethanolamine (DEA) and 2 molar ratio ethylene glycol (EG) with respect to zinc acetate (Section 2.3.2.2). To understand the effect of capping ligands on the wire formation the following synthetic procedure were tried exactly as earlier with different amounts of DEA and EG (Table 4.5). The morphology was studied by TEM (Fig. 4.27, 4.28, 4.29 and 4.30). The structure of the xerogel and the calcined materials are discussed in detail sections 4.2 and 4.4.1. Wires are not formed without the use of any of the chemical modifiers. There is an increase in size of the xerogel morphology as the amount of diethanolamine increases (Fig 4.31) and a sheet like morphology was formed when 0.4 molar ratio diethanolamine was used (Fig. 4.31c). The size of wire dimensions was also subsequently increased by calcination at higher temperature 500°C (Fig. 4.32).

Table 4. 5 Morphology of the material formed with different concentrations of chemical modifiers.

Chemical modifiers (Molar ratio with respect to Zn)		Morphology of the material	
Ethylene Glycol	Diethanolamine	80°C	500°C
0	0	Spherical balls (Fig. 4.11a)	Agglomerates of sheet like structure (Fig. 4.2)
0	0.1	Sheet like structure (Fig. 4.28b)	Agglomerates of sheet like structure (Fig. 4.30a)
1	0.1	Rods (1-2 μm) (Fig. 4.29b)	Nanowires (Fig. 30c)
2	0.05	Rods (1μm) (Fig. 4.31a)	Nanowires (Fig. 4.32a)
2	0.1	Rods (1 μm) (Fig. 4.18)	Nanowires (Fig. 4.6)
2	0.2	Rods (1-3μm) (Fig. 4.31b)	Nanowires (Fig. 4.32b)
2	0.4	Elongated sheet like morphology (Fig. 4.31c)	Spherical particles arranged to form a sheet like morphology (Fig. 4.32c)

Molar ratio of Zn to oxalic acid was remained same in all compositions and only EG and DEA concentrations were changed.

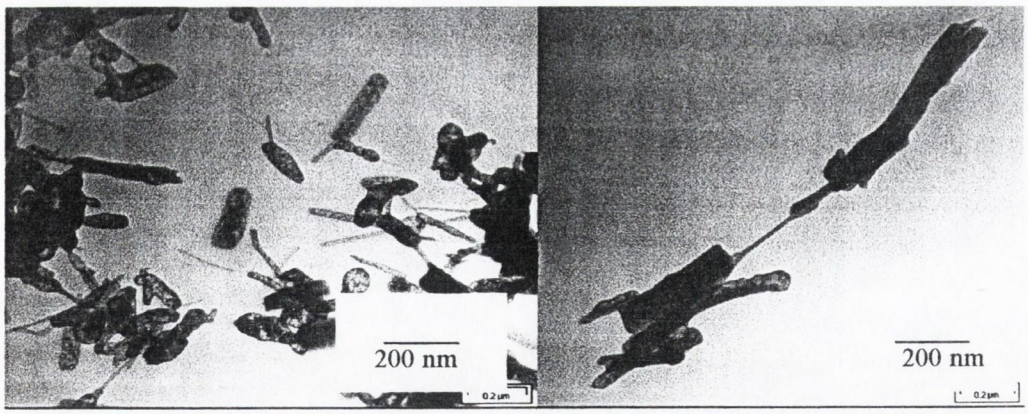

Fig.4. 27 Nanowire precursor with 2 molar ratio of EG and without DEA
a) Fresh gel b) Xerogel

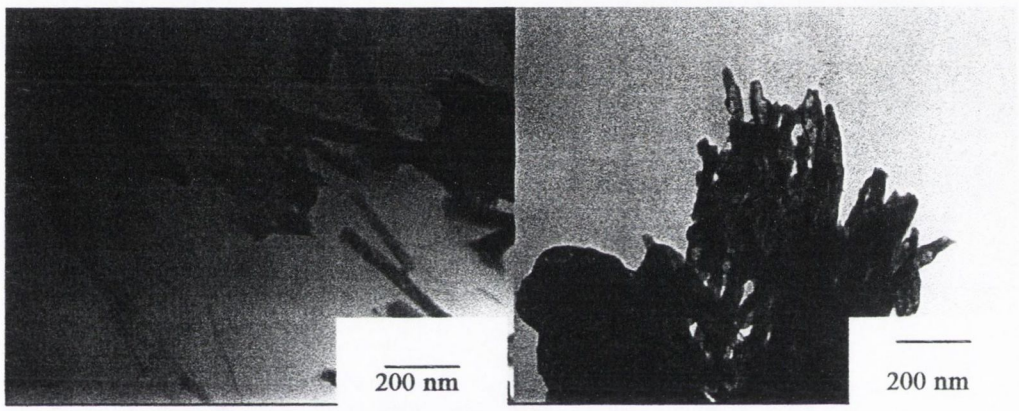

Fig. 4.28 Nanowire precursor with 0.1 molar ratio of DEA and without EG
a) Fresh gel b) Xerogel.

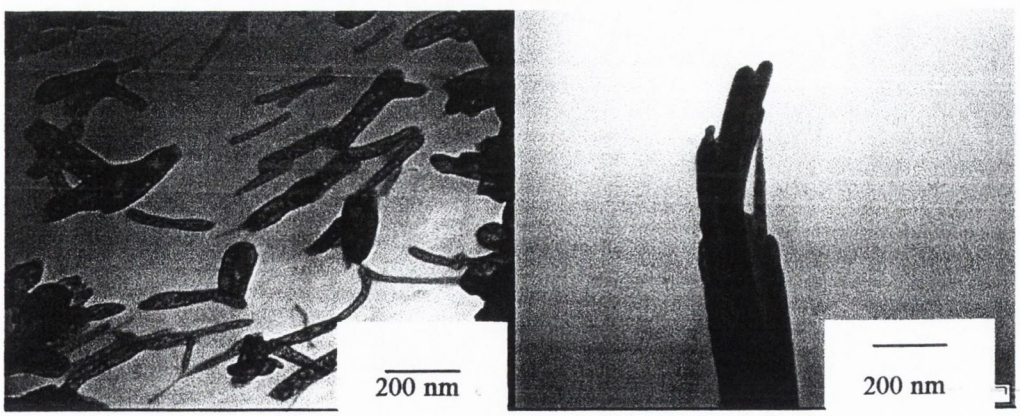

Fig. 4.29 Nanowire precursor with molar ratios of EG (1) and DEA (0.1)
a) Fresh gel b) Xerogel

(bar 200 nm)

Fig. 4.30 TEM of 500 °C calcined samples of nanowires prepared with different concentrations of EG and DEA a) No EG with 0.1 molar ratio DEA b) No DEA and 2 molar ratio of EG c) 1 molar ratio of EG and 0.1 molar ratio of DEA

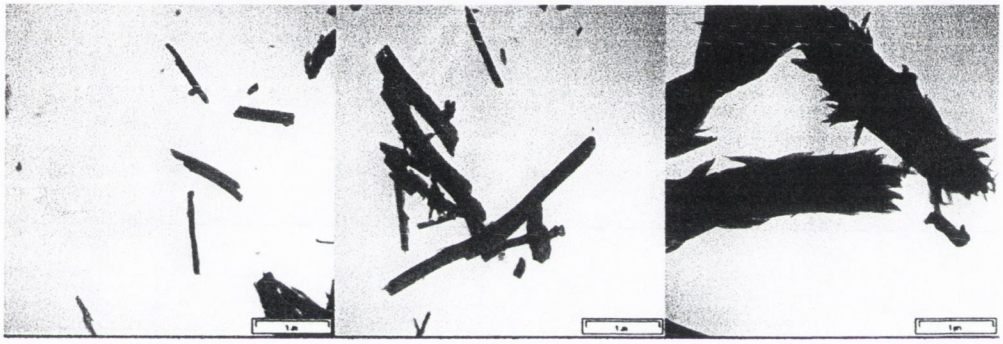

(bar 1μm)

Fig. 4.31 Nanowire precursor xerogel with 2 molar ratio of EG and different molar ratios of DEA a) 0.05 b) 0.2 c) 0.4

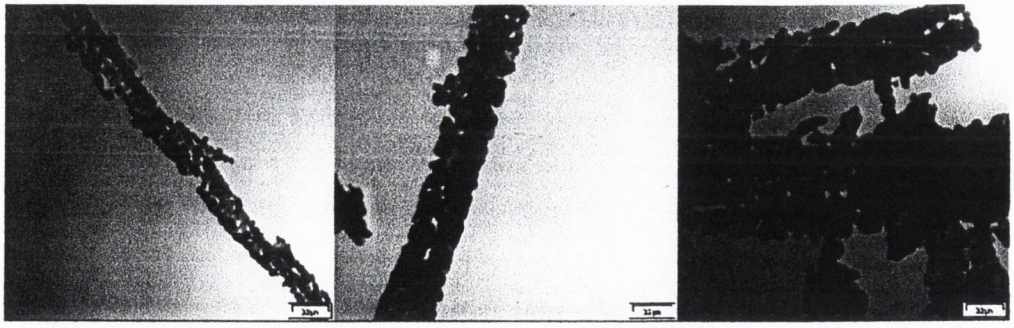

(bar 200 nm)

Fig. 4.32 TEM of 500° C calcined samples of nanowires prepared with with 2 molar ratio EG and different molar ratios of DEA a) 0.05 b) 0.2 c) 0.4.

4.6 Coating of dopants on ZnO materials

Scheme 4.6 illustrates the detailed procedure used to prepare varistor discs using the nano-size core shell type ZnO. The aim of this procedure was to get a homogeneous coating of (Sb, Bi, and Co) oxides around the ZnO particle. The ammonium carbonate precipitates the metal chlorides of Sb, Bi and Co on the spherical ZnO particles. The other dopants such as Ni, Cr, Mn, Mg, Al and Si were dispersed as a homogeneous solution among the ZnO particles.

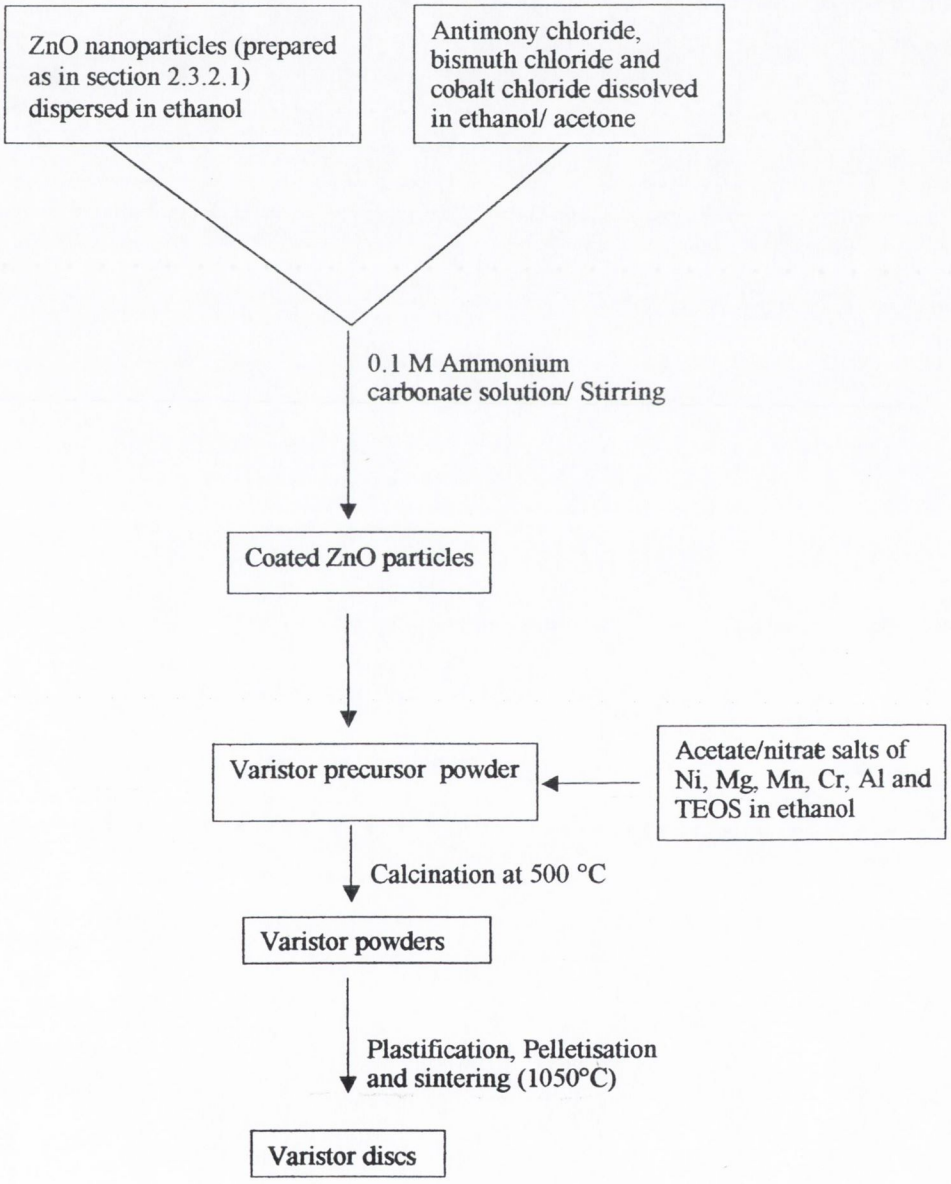

Scheme 4.6 Procedure of coating of dopant ions on ZnO nanoparticles

HRTEM studies were carried out at Manchester Materials Science Centre, UMIST, Manchester. HRTEM diagram shows that the precipitation of the dopants ions did occur on the ZnO particles (Fig. 4.33). 2 to 10 nm thick layer of dopants is formed. The presence of Sb, Bi and Co were further confirmed by EDX analysis (Fig.4.35).

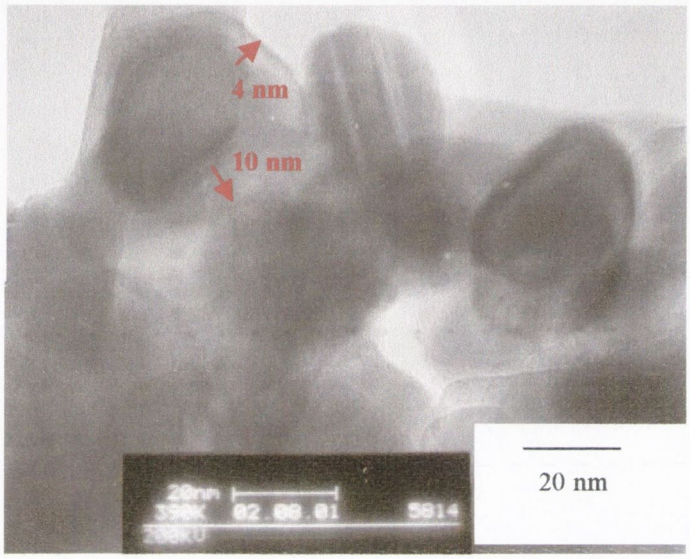

Fig. 4.33 HRTEM of ZnO nanoparticles coated with (Sb, Bi and Co) oxides

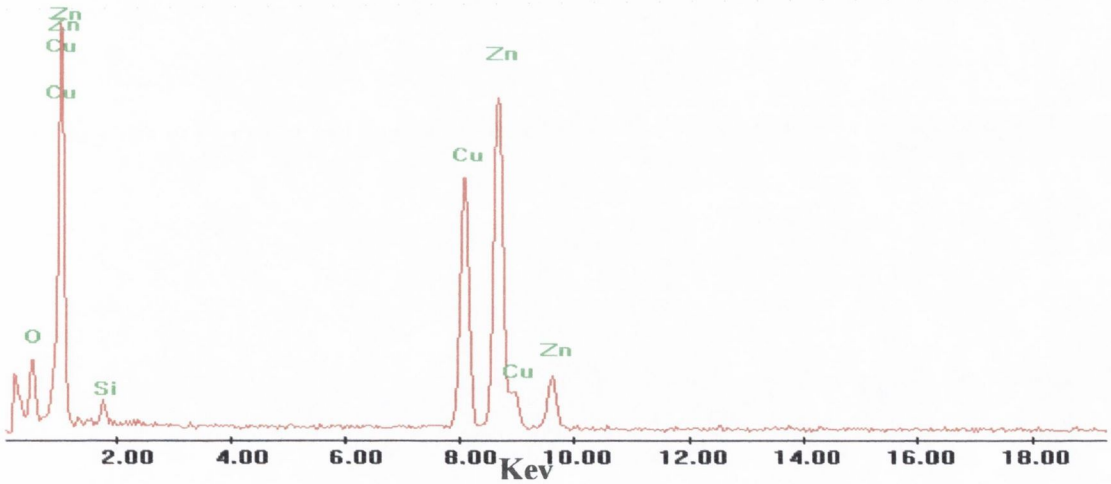

Fig. 4.34 EDX spectrum of ZnO nanoparticles before coating (Cu and Si signals are from the Cu grid)

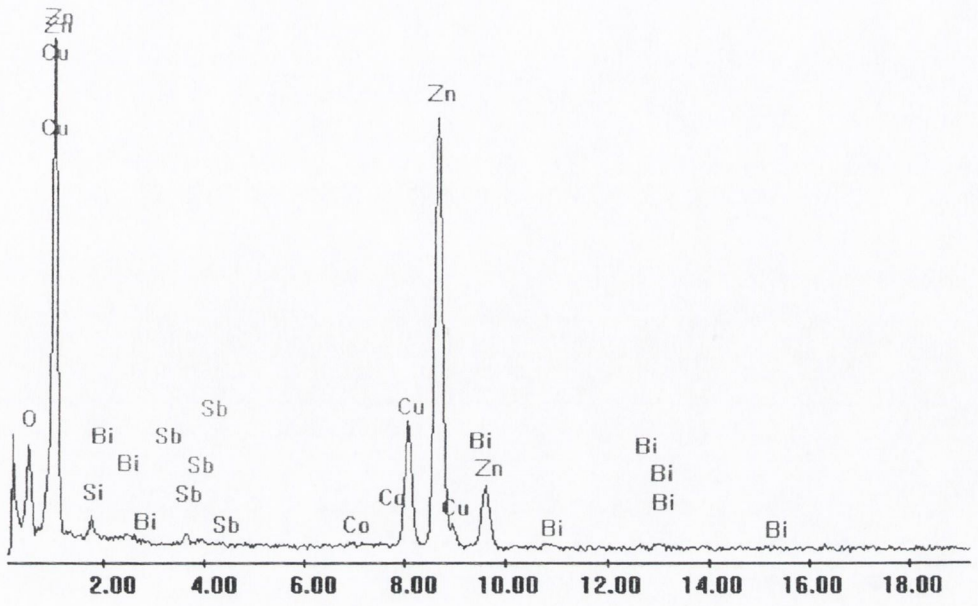

Fig. 4.35 EDX spectrum of ZnO nanoparticles coated with (Sb, Bi and Co) oxides

All other dopant ions (Ni, Cr, Mn, Mg, Al and Si) were dispersed as a homogeneous solution among the coated particles. Further drying of the solution produced a varistor powder. EDX analysis shows (Fig. 4.37) the presence of different dopant ions such as Bi, Sb, Co, Cr and Mn in the microstructure of the varistor powder.

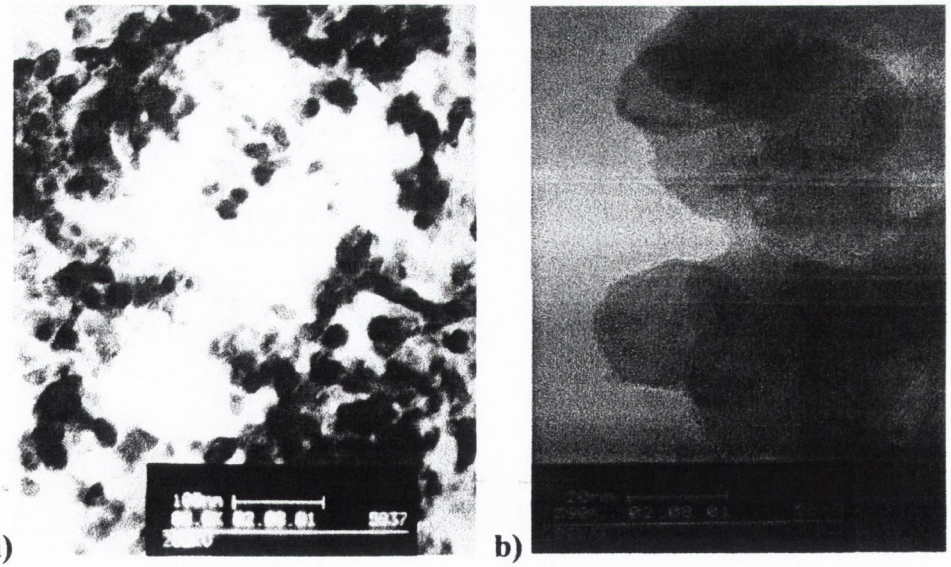

Fig. 4.36 HRTEM picture of core-shell varistor powder at different magnifications a) 88 K b) 390 K

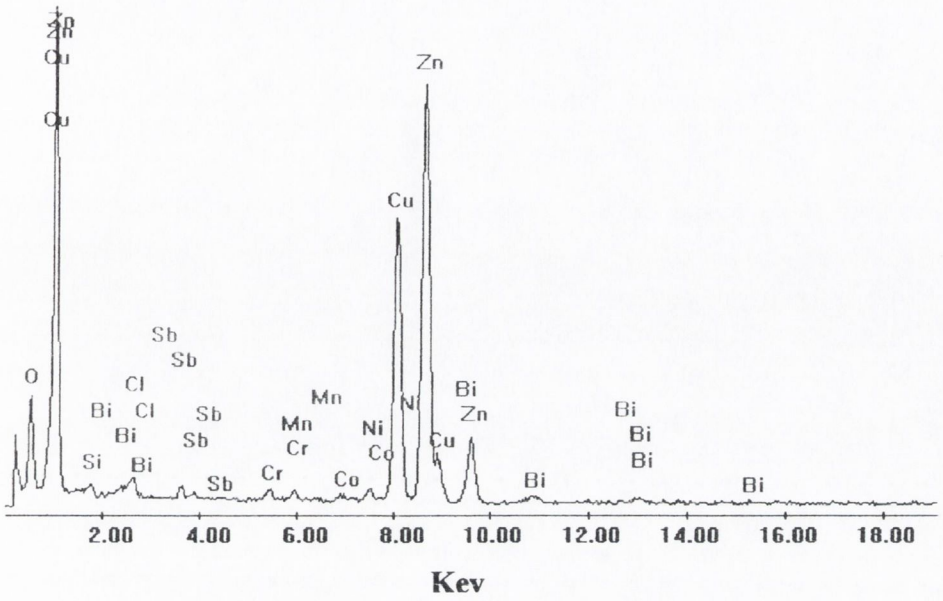

Fig. 4.37 EDX analysis of the dried varistor powder.

4.7 Varistor properties of the doped ZnO materials

Three types of varistors were prepared (*c.f.* section 2.4 for experimental details) and compared with the commercial varistor material: a) ZnO nanowire (500°C calcined) materials were mixed with metal oxide dopants; b) ZnO nanoparticles prepared without using chemical modifiers (500°C calcined) were mixed with metal oxide dopants and c) core shell type varistor materials (In core shell procedure all dopant metal ions were dissolved either in ethanol or ethylene glycol for varistor preparations, while all other procedures used commercial metal oxide dopants).

The above materials were plastified pelletised and sintered at 1050°C to study the varistor properties. Table 4.6 provides the average geometrical density values of the green (pre-sintered) samples prepared by the above routes.

Table 4.6 Geometrical density values of the green (pre-sintered) samples.

Sample	Geometrical density (g/cm^3)	% Green density*
Nanowire varistor	3.28	58.56
Nano ZnO Varistor	3.32	59.20
Core shell varistor	3.35	59.88
Commercial varistor	3.78	65.40

* Theoretical density of ZnO = 5.606 g/cm^3

Nano varistor samples were found to have lesser compaction than the micron size samples. This may be due to the fact that the commercial varistors were pre-calcined at 900°C during the industrial processing.

The 1050°C samples were subjected to density and electrical measurements. The percentage densification and electrical characteristics at 1050°C is given in Table 4.7. From the table it is clear that the varistors prepared from core shell samples have achieved a higher densification compared to the commercial samples and other nano samples. The better sinterability can be explained by the homogeneous addition of dopant ions among the grains.

I-V characteristics of the nano samples and commercial samples are given in Fig. 4.38. Voltage was plotted against log current. The average thickness of the pellets was 0.65 mm. Breakdown voltage (V/mm) and α values were calculated from 1 mA to 0.1 A (see section 2.8).

Table 4.7 Densification of samples sintered at 1050°C/ 2 h.

Sample	Sintered density (g/cm^3)	% Final Density	α (± 3)	Breakdown Voltage V/mm ± 30
Nanowire varistor	5.38	95.96	24	786
Nano ZnO Varistor	5.17	92.28	25	683
Core shell varistor	5.45	97.21	17	850
Commercial varistor	5.40	96.44	28	507

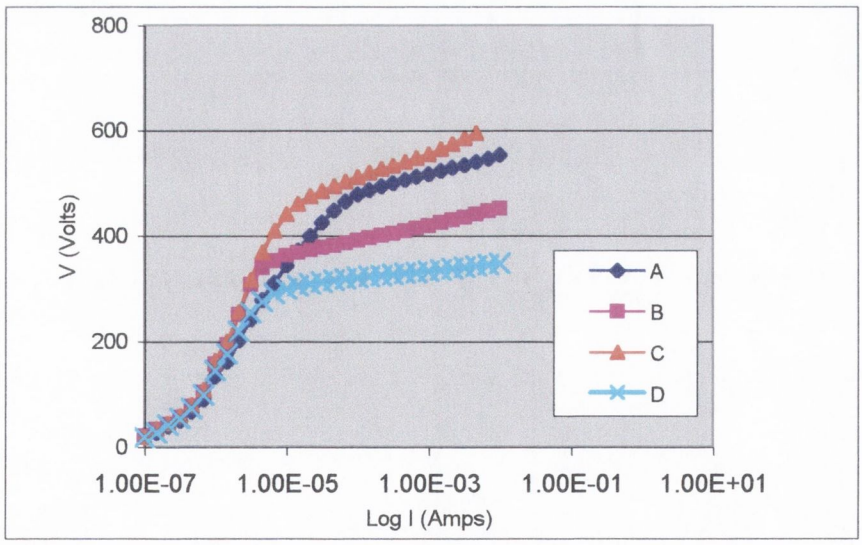

Fig. 4.38 I V curve of varistor samples sintered at 1050°C/2hr. A = Varistors prepared from nanowire samples B = Varistors prepared from nano ZnO samples C= Varistors prepared from core shell samples D = Varistors prepared from commercial mixed oxide powder.

Breakdown voltages (V_c) were calculated at 1 mA for all the samples. Higher breakdown voltage (850 ± 30 V/mm) with an α of 17 ± 3 is obtained for core shell samples compared to the commercial samples (V_c = 507 ± 30 V/mm ; α = 28 ± 3), nano ZnO samples (V_c = 683 ± 30 V/mm ; α = 25 ± 3) and nanowire samples (V_c = 786 ± 30 V/mm ; α = 24 ± 3). Electrical characterisations indicate that the varistors prepared from nano samples show considerably higher breakdown voltage than the commercial sample. These results point towards the formation of more grain boundaries per unit area by nano-structuring. Further core shell nano samples show higher breakdown voltage than that of other nano samples, which were prepared by mixing the nano ZnO with commercial oxide dopants. This is due to the fact that the core shell procedure may produce varistor powder with a greater homogeneity of the additives.

This study concentrated mainly on the grain size effect to get a high breakdown voltage and a reasonably high α. Note that breakdown voltage is the only varistor property controlled by grain size. α Values could be further increased by varying the dopant concentrations or by introducing new processing routes. Though the core shell varistor materials show superior electrical properties these coating methods are not industrially viable, as it requires a large volume of solvent, multi step processing and expensive chemicals. Also note that only 97.2% density could be achieved for 1050°C sintered varistors prepared from core shell materials.

4.8 Conclusions

Methods for creating template free nanowire arrays of ZnO, by a bulk sol gel method have been established. For the first time we report the use of a non-hydrolytic sol gel condensation and calcination methods for nanowire ZnO. Electron microscopy studies show that the ZnO nanowires are composed of nanoparticles of ~20 nm and the morphology is similar to the silver, palladium and CdSe nanowires produced by others. Heating the sample to 1000°C caused fusion of the nanowire arrays giving sintered wires. Spherical agglomerated ZnO nanoparticles were also synthesised in a similar way and the morphology of the

precursors were studied. Varistor powders were made from 500°C calcined nanowires and nanoparticles mixed with commercial additives. Novel core shell type varistor powders were prepared by coating ZnO nanoparticles by additive metal salts. Core shell type varistor materials show superior electrical characteristics ($V_c = 850 \pm 30$ V/mm) compared to the commercial varistors and nano samples doped with commercial additives.

Nearly full density could not be achieved even at 1050°C for any of these varistor samples. This sintering temperature (1050°C) may be lower to get a fully dense ZnO varistor ceramics for these materials (commercial varistors are usually sintered at 1200°C-1300°C). Thus there is a requirement for a new processing route, which could obtain a fully dense varistor at a lower sintering temperature with superior electrical properties. Chapter 5 discusses a novel mixed nano-size oxide precursor method for the fabrication of better varistor materials.

4.9 References

1. L. Spanhel and M. A. Anderson, *J. Am. Chem. Soc.*, 1991, **113**, 2826.
2. E. A. Meulenkamp, *J. Phys. Chem. B.*, 1998, **102**, 5566.
3. U. Koch, A. Fojtik, Weller and A. Henglein *Chem. Phys. Lett.*, 1985, **122,** 507.
4. C. L. Carnes and K. J. Klabunde, *Langmuir*, 2000, **16,** 3764.
5. Y. Li, G.W. Meng, L.D. Zhang and F. Phillipp, *App. Phys. Lett.*, 2000, **76,** 2011.
6. Y. Li, G.S. Cheng and L.D. Zhang, *J. Mater. Res.*, 2000, **15**, 2305.
7. Y. C. Kong, D.P. Yu, B. Zhang, W. Fang and S.Q. Feng, *App. Phys. Lett.*, 2001, **78,** 407.
8. M.H. Huang, Y. Wu, H. Feick, N. Tran, E. Weber and P. Yang, *Adv. Mater.*, 2001, **13**, 113. ; M.H. Huang, S. Mao, H. Feick, H. Yan, Y. Wu, H. Kind, E. Weber, R. Russo and P. Yang, *Science,* 2001, **292**, 1897.
9. S. Iijima, *Nature*, 1991, **354**, 56.
10. W-S Shi, H-Y Peng, Y-F Zheng, N. Wang, N-G Shang, Z-W Pan, C-S Lee and S-T Lee *Adv. Mater.*, 2000, **12**, 1343.
11. B. Nikoobakht, Z. L. Wang and M. A. El-Sayed, *J. Phys. Chem. B*, 2000, **104**, 8635.
12. B. B. Lakshmi, C.J. Patrissi and C. R. Martin, *Chem. Mat.*, 1997, **9**, 2544.
13. D. Xu, Y. Xu, D. Chen, G. Guo, L. Gui and Y. Tang, *Adv. Mater.*, 2000, **12**, 520.
14. P. M. Ajayan, O. Stephan, P. Redlich and C. Colliex, *Nature*, 1995, **375**, 564.
15. B. C. Satishkumar, A. Govindraj, M Nath and C. N. R. Rao *J. Mater. Chem.*, 2000, **10**, 2115.
16. Y. J. Zhang, J. Zhu, Q. Zhang, Y. J. Yan, N. L. Wang and X. Z. Zhang, *Chem. Phys. Lett.*, 2000, **317**, 504.
17. F. Krumeich, H.J. Muhr, M. Niederberger, F. Bieri, B. Schnyder and R. Nesper, *J. Am. Chem. Soc.*, 1999, **121**, 8324.
18. J. Richter, R. Seidel, R. Kirsch, M. Mertig, W. Pompe, J. Plaschke and H. K. Schackert, *Adv. Mater.*, 2000, **12**, 507.
19. D. Xu, X. Shi, G. Guo, L. Gui and Y. Tang, *J. Phys. Chem. B*, 2000, **104**,

5061.

20. Y. Li, M. Sui, Yi Ding, G. Zhang, J. Zhuang and C. Wang, *Adv. Mater.*,2000, **12**, 818.
21. B. A. Korgel and D. Fitzmaurice, *Adv. Mater.*, 1998, **10**, 661.
22. F. Caruso, *Adv. Mater.*, 2001, **13,** 11.
23. W. Schartl, *Adv. Mater.*, 2001, **12,** 1899.
24. F. Caruso, M. Spasova, A. Susha, M. Giersig and R. A. Caruso, *Chem. Mater.*, 2001, **13**, 109.
25. S-M Liu, H-Q Guo, Z-H Zhang, R. Li, W. Chen and Z-G. Wang, *Physica E*, 2000, **8,** 174.
26. K. K. Fung, B. Qin and X. X. Zhang, *Mater. Sci. Engg. A,* 2000, **286**, 135.
27. M. S. Fleming, T. K. Mandal and D. R. Walt, *Chem. Mater.*, 2001, **13**, 2210
28. A. Glozman and E. Lifshitz, *Mater. Sci. Engg. C,* 2001, **15**, 17.
29. G. Oldfield, T. Ung and P. Mulvaney, *Adv. Mater.*, 2001, **12,** 1519.
30. S. Gablenz, C. Damm, F. W. Muller, G. Israel, M. Rossel, A. Roder and H-P. Abicht, *Solid State Sci.,* 2001, **2**, 291.
31. F. Li, L. Z. Yao, C. H. Ye, C. M. Mo, W. L. Cai, Y. Zhang and L. D. Zhang, *J. Cryst. Growth,* 2001, **113,** 535.
32. Y. Xie, J. Huang, B. Li and Y. Qian, *Adv. Mater.*, 2000, **12,** 1523.
33. A. R. West, *Solid State Chemistry and Its Applications*; John Wiley & Sons London, 1984: pp 174.
34. S. Fullam, D. Cottel, H. Rensmo and D. Fitzmaurice, *Adv. Mater.,* 2000, **12**, 1430.
35. D. R. Askeland, *The Science and Engineering of Materials*, PWS Publishing Company, Boston, 1994, p 127
36. E. Reverchon, G. D. Porta, D. Sannino and P. Ciambelli, *Powder Technology,* 1999, **102**, 127.
37. A. E. Jimenez-Gonzalez, J.A. S. Urueta and R. Suarez-Parra *J. Cryst. Growth*, 1998, **192**, 430.
38. A. M. Donia, *Polyhedron*, 1997, **17,** 3013
39. A. K. Nikumbh, S. K. Pardeshi and M. N. Raste, *Thermochimica Acta,* 2001 **374**, 115.

40. X. Zhao, B. Zheng, C. Li and H. Gu *Powder Tech.* 1998, **100,** 20.

41. L-W. Tai and P. A. Lessing, *J. Mater. Res.*, 1992, **7,** 502.

42. C. Suresh, V. Biju, P. Mukundan and K. G. K. Warrier, *Polyhedron*, 1998, **17**, 3131.

43. V. T. Yilmaz and A. Karadag, *Thermochimica Acta*, 2000, **348**, 121.

44. T. Trinidade, J.D. Pedrosa de Jesus and P. O'Brien, *J. Mater. Chem.*, 1994, **4,** 611.

45. P. O'Brien, T. Saeed, J. Knowles, *J. Mater. Chem.*, 1996, **6,** 1135.

46. V. Bolis, B. Fubibi, E. Giamello, A. Reller, *J. Chem. Soc., Faraday Trans. I,* 1989, **85**, 855.

47. J-P. Auffredic, A. Boultif, J.I. Langford, D. Louer, *J. Am. Ceram. Soc.,* 1995, **78,** 323.

Chapter 5

Varistors prepared from nano-size precursors

5.1 Introduction

As discussed in chapter 1, varistors are electronic ceramic devices whose function is to limit voltage surges.[1-10] The method of preparation, crystalline size and the additive homogeneity are the critical parameters to produce a better varistor material.[11-17] Varistors with inhomogeneous microstructure can cause a large spread in current/voltage characteristics due to high local currents and this leads to the degradation of the varistor during electrical operation.[14,17,18] Electrical and electronic characteristics can be altered by varying the microstructure at the grain boundaries.[2,11-15] Thus careful control of the microstructure is required to get a perfect varistor. Commercial varistors are usually fabricated by solid state mixing of 1 to 3 μm ZnO particles with dopant oxides such as Bi_2O_3, Sb_2O_3, CoO, MnO, NiO and Cr_2O_3. [2,3,9,10] The mixed powder is then pressed and sintered at higher temperatures. The final grain size after sintering is of the order of 8-12 μm and the corresponding breakdown voltage is around 2–3 kV/cm which is equivalent to a voltage drop of 1.6 volts per inter granular barrier,[12] as the breakdown voltage of the sintered body is proportional to the number of grain boundaries. Nanocrystalline material contains large grain boundary volumes and more varistor active grain boundaries per unit volume can be produced in order to develop a better device with smaller dimensions. Nanoparticles yield a narrow grain size distribution and can be sintered at a lower temperature compared to the coarse grained ceramics.[11] It is reported that the basic building block of the ZnO varistor are the ZnO grains formed as result of sintering.[2,3,7,8] During sintering the additive atoms are arranged in such a way in the microstructure that the near grain boundary region becomes highly resistive (r_{gb}~10^{12} Ω cm) and the grain interior becomes highly conducting.[2]

Several attempts using chemical methods have been reported earlier for producing varistor discs [11-30] (See section 1.6.4). Most of these methods are conducted on a laboratory scale and need further advancement for commercial viability. The major problems with many of the chemical methods reported are expensive reactants, complex synthetic procedures and multiple step reactions.

In chapter 4, sol gel synthesis of ZnO nanowires and nanoparticles has been discussed. Varistors were made from these nanomaterials by adding commercial oxide additives. Core shell type varistor materials were also prepared by coating metal salts on ZnO nanoparticles. Varistor discs made from the core shell type materials showed better electrical properties and a better sinterability. This was due to the better homogeneity of additive ions among the ZnO grains. The additive homogeneity could be further improved if the additives were added in the initial stages of synthesis. Investigations were directed towards making a better material with improved properties. A similar synthetic approach, as discussed in chapter 4, was attempted to make nanometer size varistor powders. In this case the procedure was similar but all additive solutions were added to the zinc acetate solution to get a better molecular level homogeneity.

5.2 Synthesis of varistor nanopowder

5.2.1 Synthetic procedures

The detailed experimental procedure for the synthesis of varistor nanopowder is given in section 2.5 and a flowchart for the synthesis is given Scheme 5.1. Zinc acetate, cobalt acetate, manganese acetate and nickel acetate were added to ethanol. Diethanolamine was further added to the above solution and refluxed for 20 minutes. A homogeneous green solution was obtained and to this solution dopants (antimony acetate, bismuth nitrate and chromium nitrate) dissolved in ethylene glycol were added. Addition of an ethanolic solution of oxalic acid with vigorous stirring produced a thick semi-gel. Subsequent drying at 80°C produced a pale violet xerogel and calcination of this gel at 500°C produced a dark green free flowing powder.

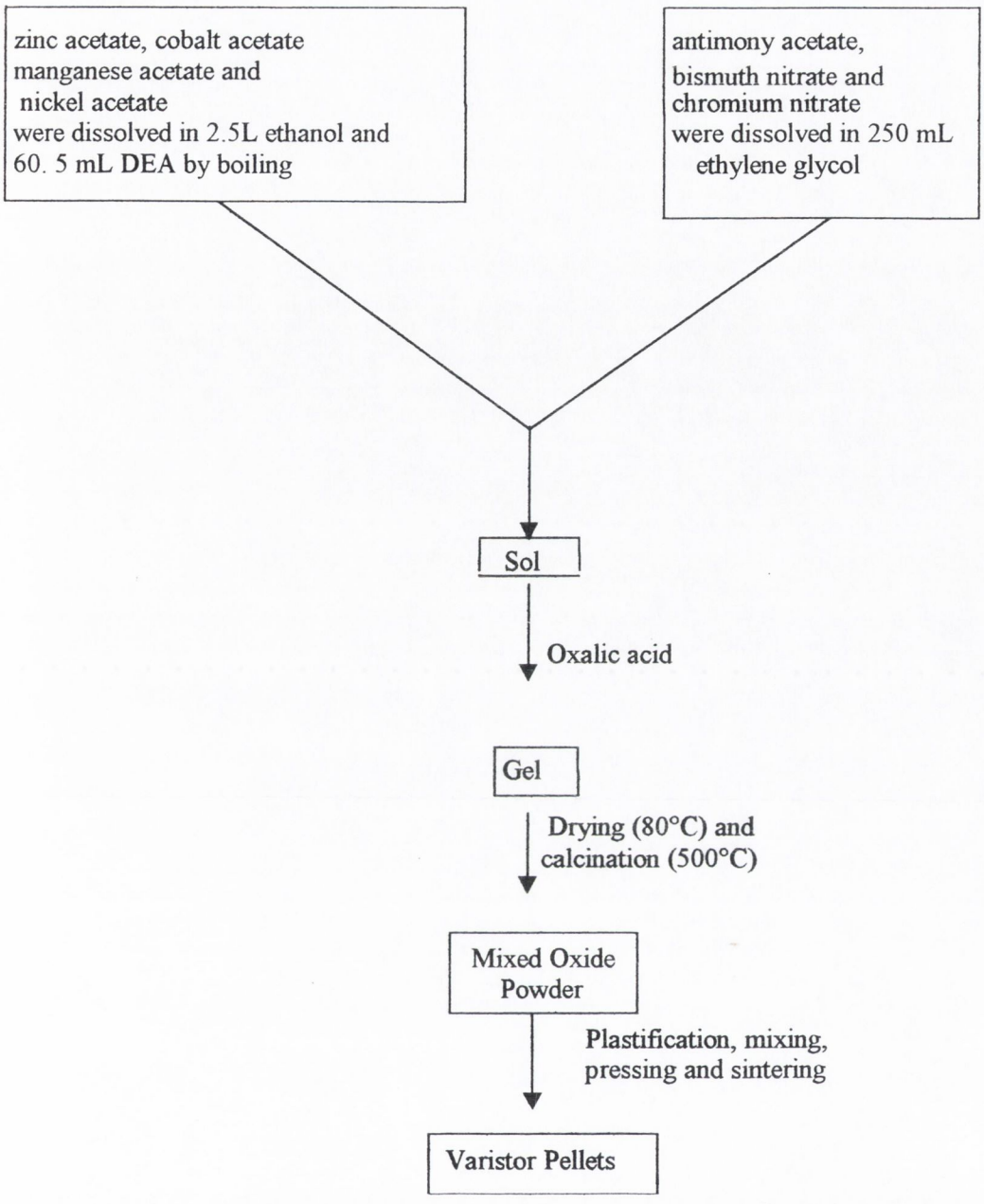

Scheme 5.1 Flowchart for the synthesis of ZnO varistor nano-materials through mixed precursor route.

Diethanolamine was used during the synthetic process for two reasons

a) To prevent the precipitation of metal salts in ethanol during boiling
b) To enhance the solubility of zinc acetate in ethanol.

The above observations were found during the small-scale synthesis of zinc oxide nanoparticles. A 500 mL ethanolic solution of zinc acetate (50 mmol; 10.9

g) was precipitated at room temperature after one hour of preparation. In a subsequent experiment 1 mL diethanolamine was added to the 500 mL ethanolic solution of zinc acetate (50 mmol; 10.9 g). The solution was observed for several hours at room temperature (~20°C) and no precipitate was formed up to 10 hours (precipitated only after 24 hours). The same experiment was repeated in an ice bath and the sol was stable for up to 30 minutes and slowly precipitated after that.

Dissolving 50 mmol (10.9 g) zinc acetate in 500 mL ethanol took around 15 to 30 minutes and the experiment was successful every time. In order to reduce the amount of solvents, the above experiment was repeated in 250 mL ethanol. It was observed that the dissolution was rather difficult and a precipitate occurred sometimes (one in three experiments). Also it takes 20 to 40 minutes to dissolve the zinc acetate fully. When 1 mL diethanolamine was added to the above solution before boiling, dissolution was much easier, the experiment was successful each and every time and took only 10 to 15 minutes. The experimental procedure was further repeated to dissolve 50 mmol (10.9 g) zinc acetate in 150 mL and 100 mL ethanol respectively and these experiments were also successful. Thus the amount of ethanol used for the dissolution of zinc acetate could be considerably reduced by the addition of a small amount of diethanolamine. Note that Spanhel and Anderson[31] dissolved 50 mmol (10.9 g) zinc acetate in 500 mL ethanol by just refluxing the solution without the use of any other chemicals. Meulenkamp[32] also adopted a similar procedure but in smaller amounts *i.e* (1.1 g) 5 mmol zinc acetate in 5 mL ethanol. No systematic studies are reported in the literature similar to the above presented one with the effect of diethanolamine. In the large-scale synthetic procedures for nano varistor powders (section 2.5) we used 274.5 g (1.25 mol) zinc acetate and a volume as high as 12.5 L ethanol would be required to dissolve the zinc acetate. The volume of ethanol required for dissolving the same amount of zinc acetate was reduced to 2.5 L by using 60.5 mL (625 mmol) diethanolamine. Ethylene glycol was used to dissolve antimony acetate, bismuth nitrate and chromium nitrate, which would not dissolve in ethanol. At this stage it is interesting to notice that in chapter 4, the use of ethylene glycol and diethanol amine produced rod-like morphologies for

the precursors and wire like morphologies for the calcined materials. A similar trend was observed here as well and will be discussed in the next section.

5.2.2 Characterisation of the precursor xerogel

The xerogel (80°C dried) before calcining at 500°C was pale violet in colour with a porous nature denoting a high content of organic materials. FESEM picture (Fig.5.1) shows rod/sheet like morphologies of 1-1.5 μm in length and 0.3 to 0.5 μm in thickness.

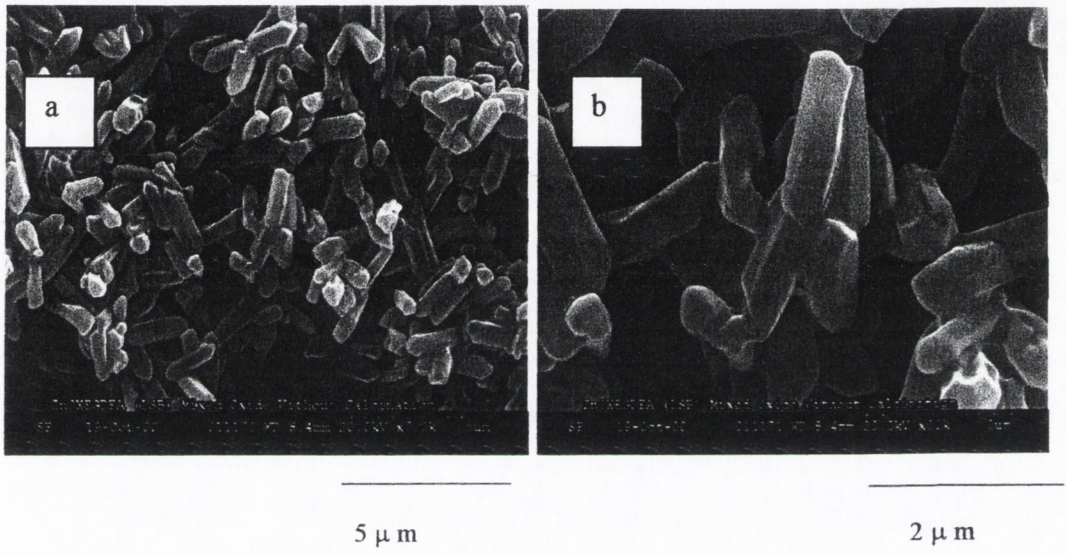

Fig. 5.1 FESEM images of the 80°C dried nano varistor precursor prepared by sol gel mixed precursor route

Rod like morphologies with 0.6 μm in length and 50 nm widths were earlier obtained for the nanowire precursor xerogel (section 4.4.4). In that case the zinc acetate to diethanolamine mole ratio was 1:0.1, but here we use a mole ratio of 1:0.5. The increase in dimension of the rods is apparently due to the increase in the amount of diethanolamine. Similar observation can also be found in section 4.5 (see Table 4.5 also), where size of the rods were increased with the amount of diethanolamine added.

The thermo gravimetric analysis curve of the xerogel is shown in Fig.5.2. A total weight loss of 72% is obtained. Three stages of weight loss are observed at (110-

200°C), (320-380°C) and (450-480°C). The first stage of the weight loss (110-200°C) is regarded as the removal of acetate groups[33,34] and the second stage of weight loss (320-380°C) can be explained as the removal of chelated diethanolamine[35] and (450-480°C) is explained as the formation of ZnO from the decomposition of the precursors.[34] (X-ray diffraction results showed that the ZnO formation occurred after 250°C). DSC analysis of the xerogel also showed four well-defined endothermic peaks at 175, 274, 365 and 454°C (Fig. 5.3).

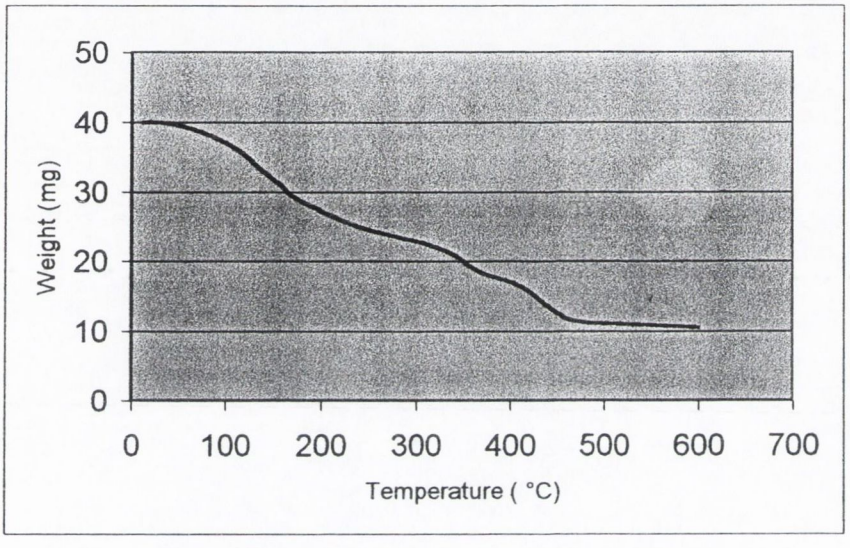

Fig. 5.2 TGA pattern of xerogel, dried at 80°C, prepared by sol gel mixed precursor route

In the DSC plot small and broad endothermic peaks seen below 150°C are due to the removal of solvated alcohol and a small amount of water.[34,35] The endotherm at around 175°C is due to the removal of acetate groups and peak at 274°C is due to the removal of diethanolamine.[35] A peak at 250°C was obtained when the DSC measurement was carried out for pure DEA sample. The peak at 365°C could be due to the removal of chelated diethanolamine. The transition observed at 454°C suggested the formation of ZnO from the precursors.[34,35] The second DSC scan of the same material did not show any peaks as expected. These results showed that 500°C was the suitable temperature to calcine the xerogel to get ZnO powders.

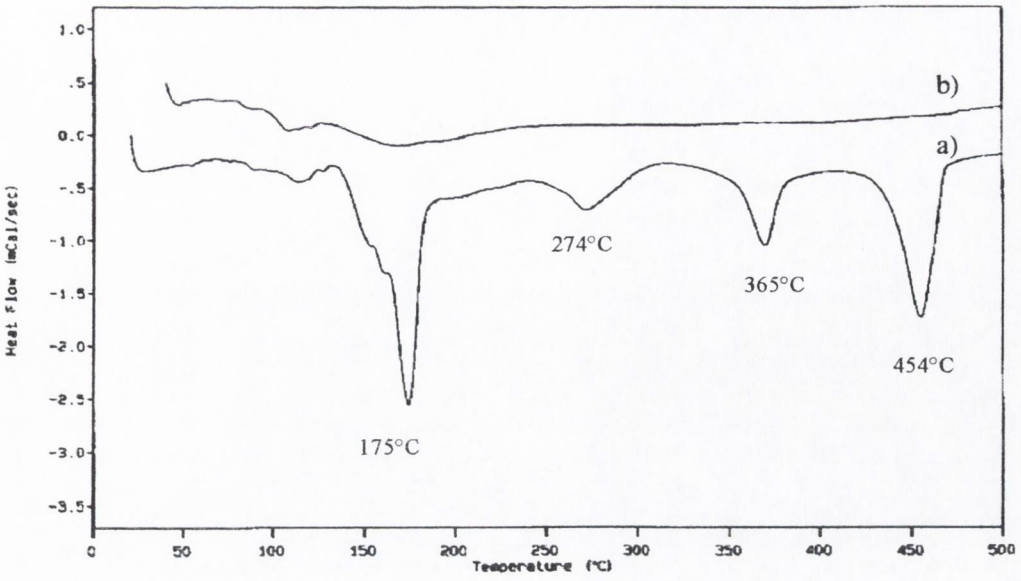

Fig. 5.3 DSC pattern of xerogel, dried at 80°C, prepared by sol gel mixed precursor route a) first scan b) second scan

5.2.3 Phase analysis of the nanopowder calcined at 500°C

The xerogel dried at 80°C was further calcined to 500°C for 2 hours (Scheme 5.1) and the powder thus obtained was analysed by X-ray powder diffraction (Fig 5.4)

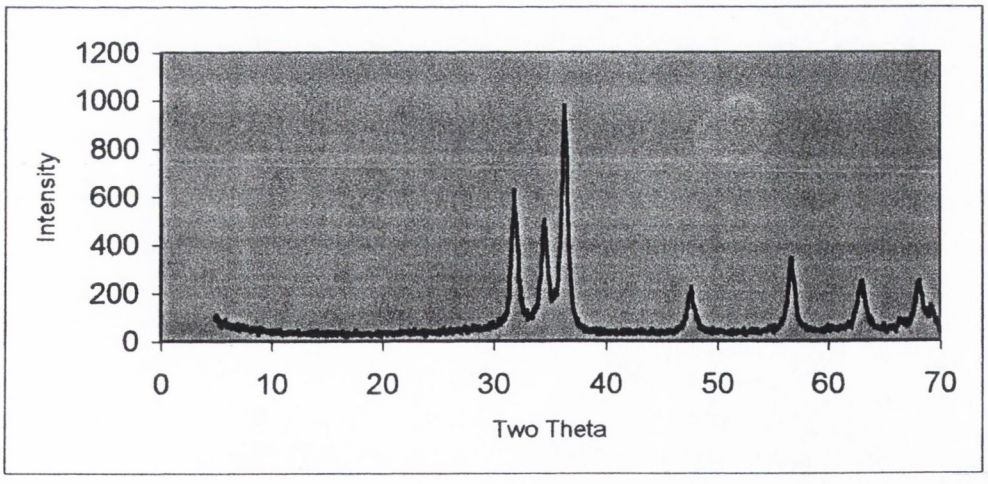

Fig. 5.4 XRD pattern of ZnO varistor nanoparticles prepared by 'sol gel mixed precursor' route calcined at 500°C

Broadening of the X-ray bands allowed an estimate of the average particle size as 15 ± 3 nm using the Debye-Scherrer equation[36] (refer section 2.5.4). This particle size is found to be smaller than the pure ZnO (19 ± 4 nm) prepared in a similar method (Section 4.3). This observed decrease in resultant particle size is possibly due to the effect of Sb_2O_3, which is added as a grain growth inhibitor in varistor ceramics or due to the effect of excess amount of diethanolamine.

X-ray analysis shows the presence of only ZnO (Table 5.1). This is either due to the fact that the dopant concentration is below the detection limit of the X-rays or that no crystalline phases formed.

Table 5.1 X-ray powder diffraction data of ZnO varistor nanoparticles calcined at 500°C

Literature JCPDS (36-1451)				Experimental		
hkl	2θ	d (A°)	Intensity	2θ	d (A°)	Intensity
100	31.76	2.81	57	31.84	2.81	62
002	34.42	2.60	44	34.45	2.59	47
101	36.25	2.48	100	36.26	2.47	100
102	47.53	1.91	23	46.70	1.94	20
110	56.60	1.62	32	56.70	1.62	32
103	62.86	1.47	29	62.82	1.47	22
200	66.37	1.40	4	66.45	1.40	5
112	67.96	1.38	23	68.13	1.37	22
201	69.09	1.34	11	69.18	1.35	11

5.2.4 Surface area and morphology of the nanopowder calcined at 500°C

A dark green coloured powder was obtained after calcination at 500°C (Scheme 5.1). These calcined powders were subjected to BET surface area analysis and a value of 45 m^2/g was obtained. This is a very high surface area compared to the commercial varistor sample, which has a surface area of 2.8 m^2/g. These powders contain an appreciable amount of agglomerates of stick like morphologies as evidenced from the FESEM images (Fig. 5.5). The length of these stick-like morphologies varies from 2 to 4 mm with a width of 0.3 to 0.5 μm.

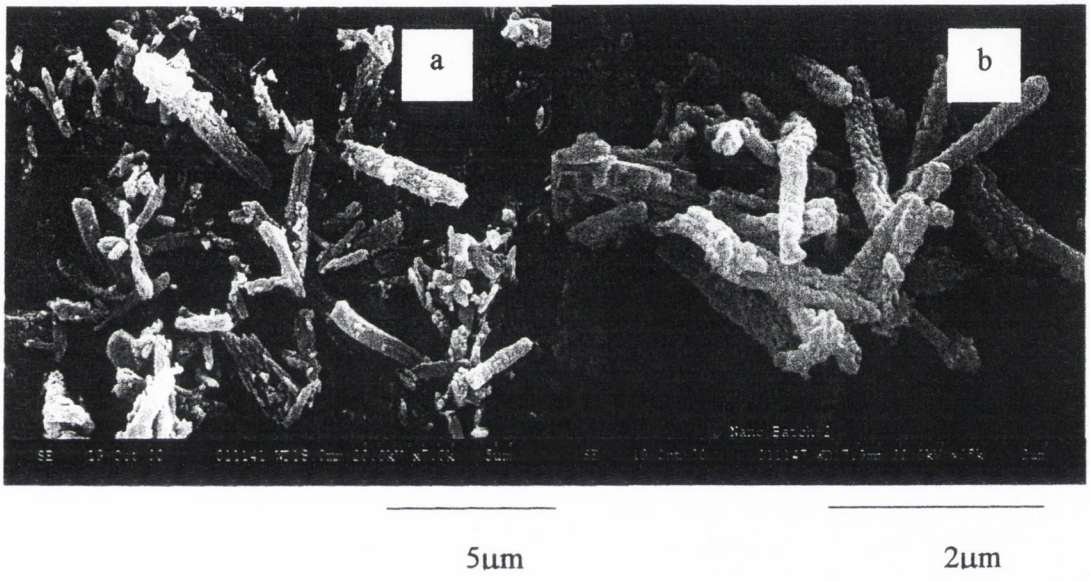

Fig. 5.5 FESEM images of the 500°C nano varistor powder prepared by 'sol gel mixed precursor' route without further treatment; Magnified at a) 7 k b) 25 k

A typical TEM micrograph, at low magnification (3.5 k), of the nanopowder is shown in Fig. 5.6 a, and stick like agglomerates can be observed. At a higher magnification (50 k) it could be seen that these sticks are made up of smaller particles (Fig. 5.6 b).

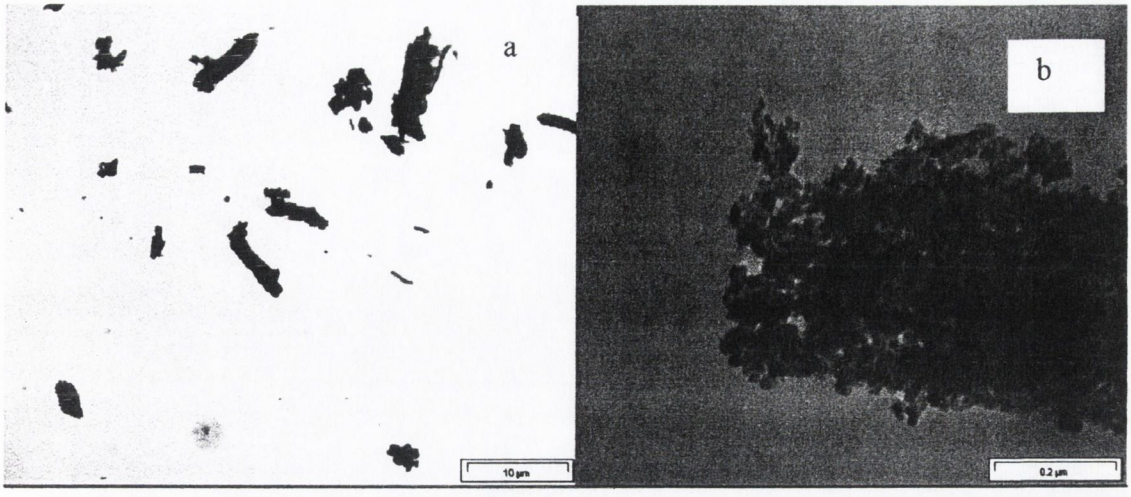

Fig. 5.6 TEM images of the 500°C nano varistor powder prepared by 'sol gel mixed precursor' route without further treatment; Magnified at a) 3.5 k b) 50 k

The particles are not aligned like a wire as seen in the case of nanowires (section 4.3). Also ultrasonication up to 40 minutes did not have any effect in separating these particles from the agglomerates.

More information could be obtained from a high resolution transmission electron micrographic images. HRTEM (Fig. 5.7) shows that these sticks contain spherical and non-spherical particles. Particles of 10 to 20 nm are seen. From the TEM images it is difficult to distinguish particles of ZnO and other metal oxides formed after calcinations at 500°C.

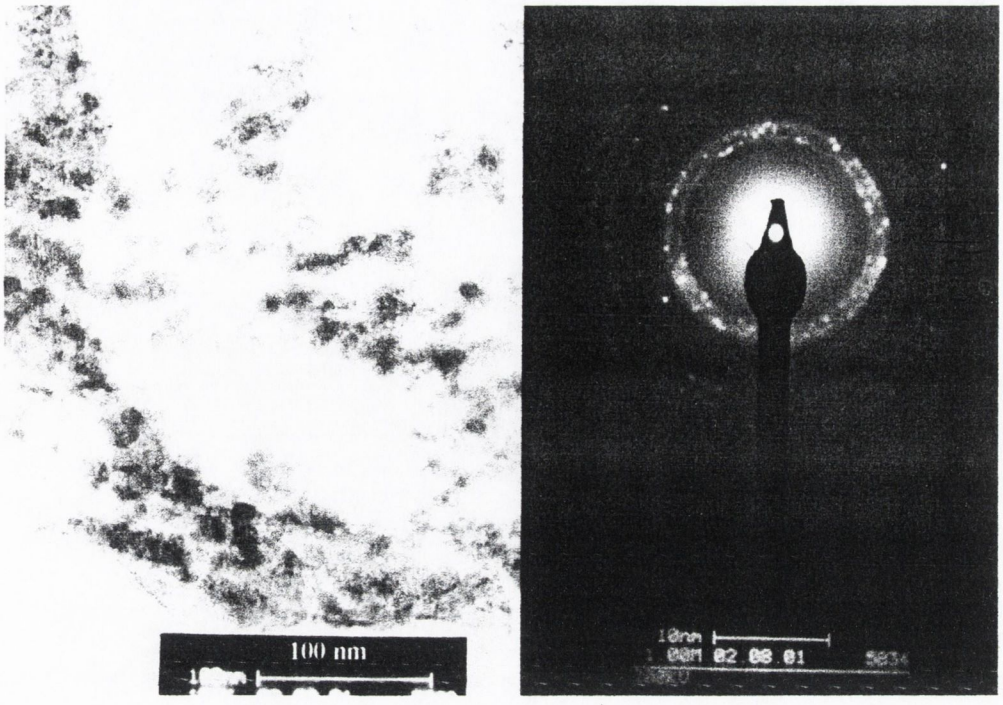

Fig. 5.7 HRTEM and SAED pattern of ZnO varistor nanoparticles prepared by sol gel mixed precursor route

The presence of crystalline phases of ZnO were further observed from the selected area diffraction pattern (SAED pattern). Crystalline planes and d values were calculated [37] from the diffraction pattern (Table 5.2). This is in reasonably good agreement with powder diffraction pattern (Table 5.1)

Table 5.2 Electron diffraction data for ZnO varistor nanoparticles prepared by sol gel mixed precursor route

R (mm) Error ± 5%	$d = \frac{\lambda L}{R}$ (Å)	*hkl*
9.5	2.52	002
11.5	2.08	102
14.5	1.65	110
17.0	1.44	103

Presence of additives (Sb, Bi, Cr and Ni) in the microstructure could be observed from TEM/EDX analysis of the nanopowder (Fig 5.8).

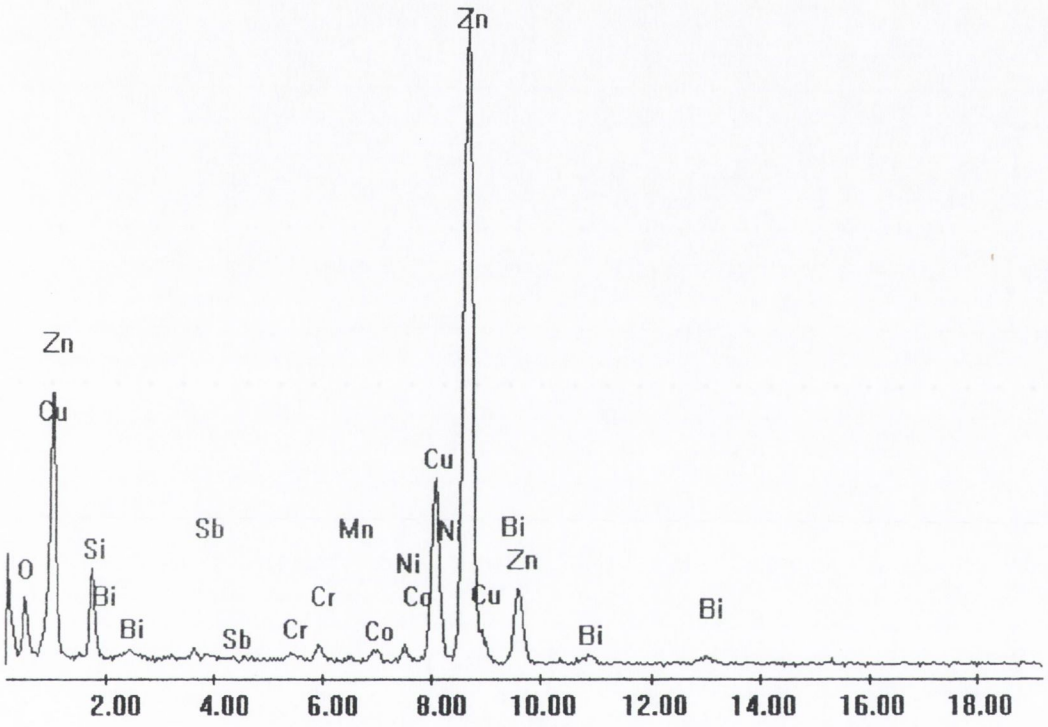

Fig. 5.8 EDX pattern of ZnO varistor nanoparticles calcined at 500°C

(Cu and Si peaks are from the polymer coated Cu grids)

5.2.5 Nanopowder de-agglomeration

It is obvious from the TEM and FESEM images (Fig 5.5& 5.6) that the as prepared nano powders are agglomerated into stick like morphologies. As strong agglomerates may lead to larger grains after sintering,[38] ball milling was used to crack these and hence lead to nanopowder de-agglomeration.[38] The ball milling was carried out at three different conditions for 30 minutes i) aqueous milling ii) aqueous milling in poly-acrylic acid medium and iii) dry milling. TEM results (Fig. 5.9) demonstrated that the dry milling at 30 minutes significantly helps to decrease strong agglomerates. The milling in aqueous medium and poly-acrylic acid media did not have much effect on de-agglomerating the particles.

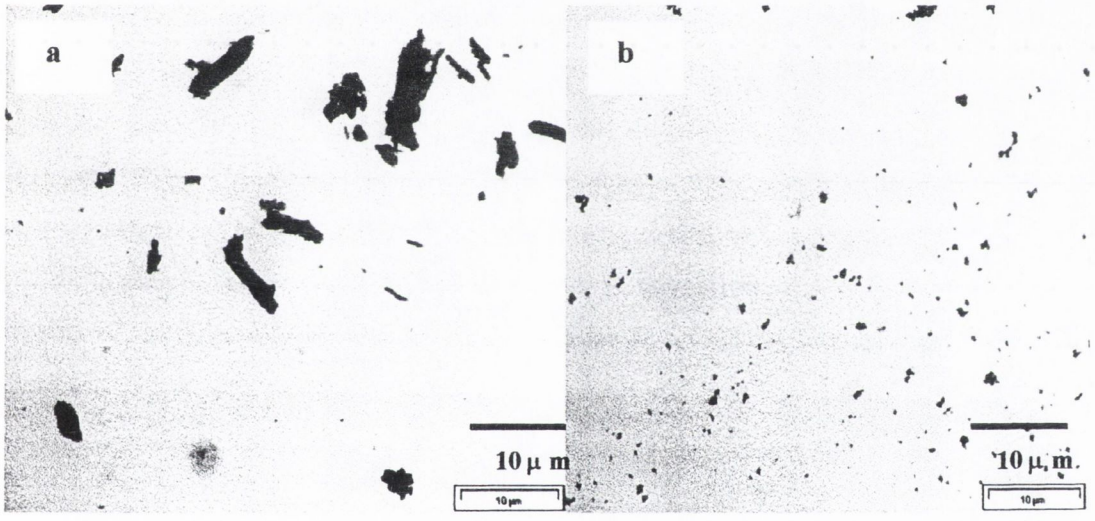

Fig. 5.9 TEM images showing the effect of milling on agglomerated nano powder prepared by sol gel mixed precursor route a) before milling b) after dry ball milling for 30 minute

5.3 Sintering, grain growth and electrical studies of varistors from nano-size precursors

Controlling grain growth during sintering is one of the challenges in ZnO nanomaterials research. Ya *et al*[25-26] prepared 20 nm ZnO particles using zinc nitrate, citric acid and ethylene glycol. However further dopant addition and sintering at 950°C/ 2h (densification = 98%) produced 2μm grains. In a similar approach Shah *et al* [14-16]synthesised 14 nm size doped ZnO varistor materials using micro-emulsion technology and found that sintering at 1200°C produced 2-3 μm grains. In a very recent work Duran *et al*[40] showed varistors, prepared from 20 nm by a citrate gel route, could be sintered at 850°C/5h with a limited grain growth of <1 μm.

Our sintering experiments have been performed at various temperatures from 700°C to 1050°C for 2 hours in a chamber furnace at a rate of 1.5°C/ min up to 300°C for one hour (for binder burn off) and 3°C/ min to the final temperature. Varistor discs prepared from nano-size precursors (*c.f.* section 2.5) were calcined and then dry ball milled (30 min), these materials were used for all sintering experiments. The colour of the pre-sintered pellets were dark green and changed to light green after sintering at 700°C and 800°C. The colour of the pellets changed to black at 900°C and further higher temperatures. The pellet dimension was also reduced considerably at 900°C compared to the 700 and 800°C sintered samples. Densities were measured and plotted against temperatures (Fig. 5.10). It is seen from the figures that the sintered density is considerably increased at 900°C and at 1050°C 100% sintered density is obtained (compared to the theoretical density of fully sintered ZnO). The dimensions of the pellets were also considerably decreased at 900°C compared to lower temperature sintered samples and linear and volume shrinkages were calculated. There is no shrinkage observed up to 800°C and at 900°C a linear shrinkage of 23% and a volume shrinkage of 52% were observed compared to the pre sintered sample. There is no appreciable change in linear or volume shrinkages up to 1050°C compared to 900°C sintered samples.

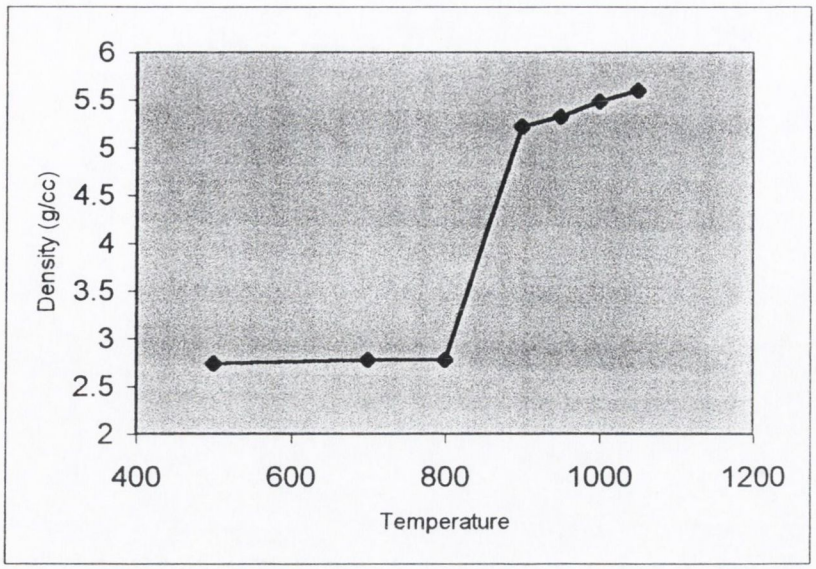

Fig. 5.10 Change in density with temperature of varistors prepared by sol gel mixed precursor route

The sintering behaviour was further confirmed by dilatometric studies (Fig 5.11). The dilatometer curve obtained at a rate of 5°C /min revealed that the onset of sintering occurred in the range 875-925°C and is finished in the range 1025 – 1050°C.

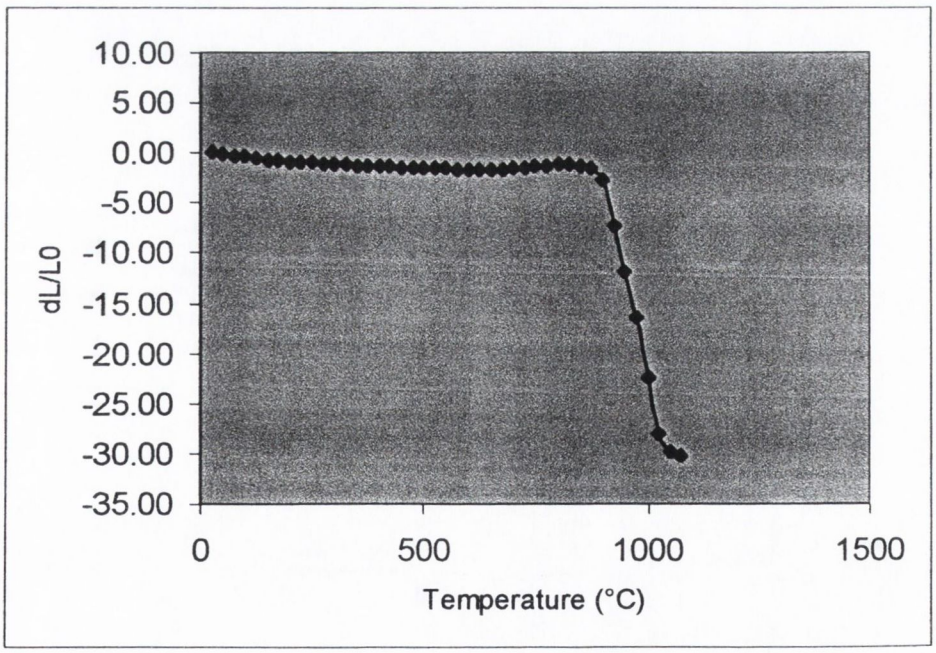

Fig. 5.11 Dilatometer curve of green sample prepared from nano-size precursors calcined at 500°C

The dilatometer curve obtained for the commercial sample at a rate of 5°C/min revealed that the onset of sintering occurred in the range 900-925°C and was not finished even at 1050°C. Thus a better sinterability at lower temperature is obtained for nano varistor precursor samples.

5.3.1 Grain growth studies

Grain growth is associated with the final stages of sintering and usually grain growth and sintering occur simultaneously. [39,41] Grain growth studies were carried out with FESEM (Fig.5.12-5.14). At 700°C the particle size was found to be 36 ± 5 nm and at 800°C it was estimated as 45 ± 5 nm .

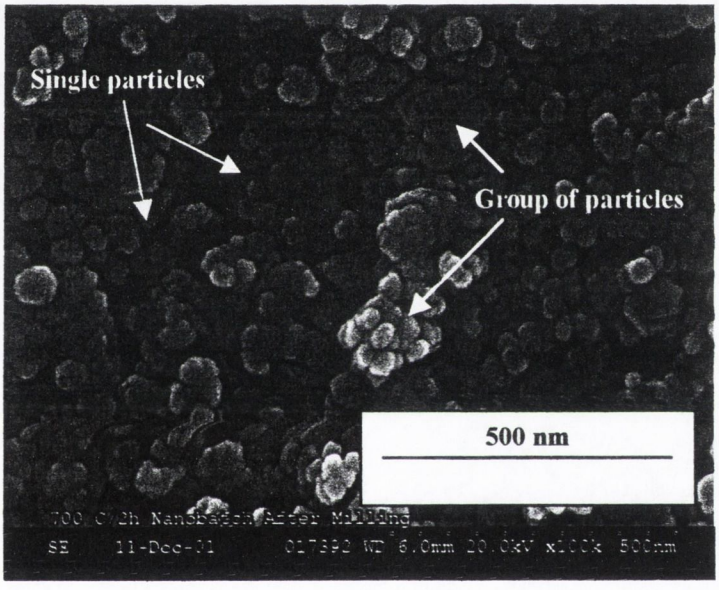

Fig. 5.12 Varistor discs prepared by sol gel mixed precursor route sintered at 700°C

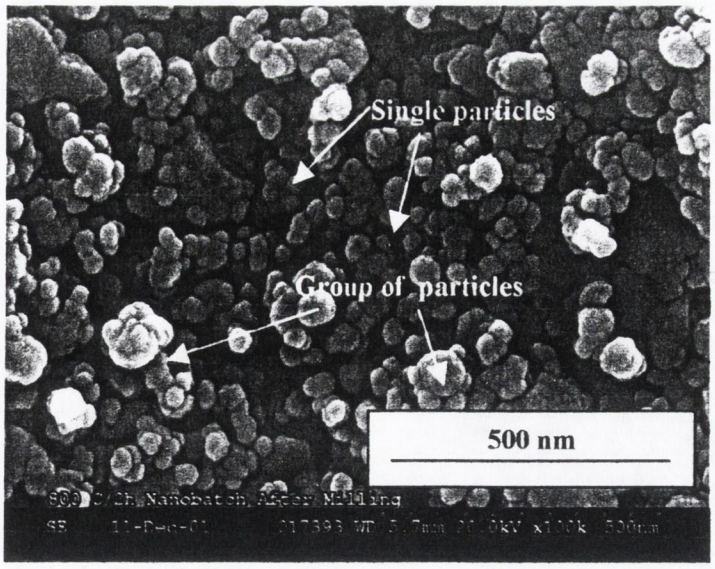

Fig. 5.13 Varistor discs prepared by sol gel mixed precursor route sintered at 800°C

It is seen from the FESEM images (Fig. 5.14) that the particles have grown considerably at 900°C compared to 800°C. A grain size of 1.60 ± 0.05 μm was obtained at 900°C (Fig 5.14) and the grains were further grown up to 2.02 ± 0.5 μm at 1050°C/ 2h. A plot of temperature vs grain size is given in Fig. 5.15.

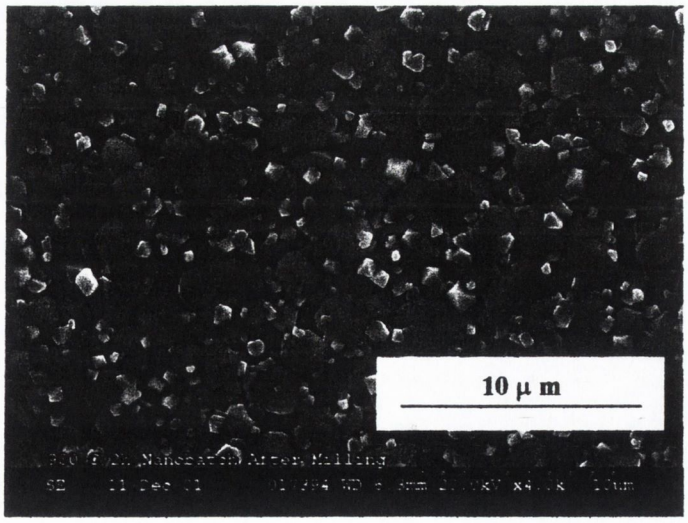

Fig. 5.14 Varistor discs prepared by sol gel mixed precursor route sintered at 900°C

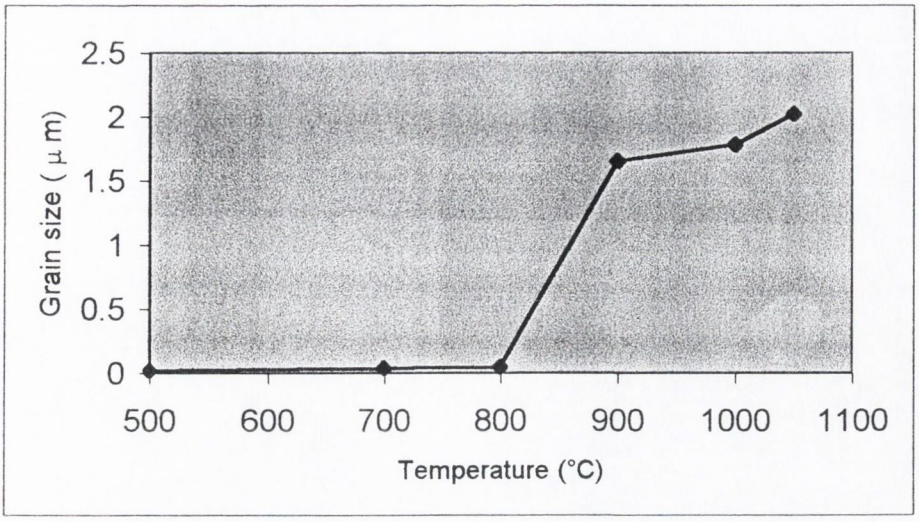

Fig. 5.15 Grain growth vs temperature of the varistor samples prepared by sol gel mixed precursor route sintered at different temperatures

Three different phases, which are responsible for varistor action, could be well identified in a sintered ZnO microstructure and which will be discussed in section 5.4.

5.3.2 Electrical studies of varistors prepared from nano-size precursors

Varistor powders prepared from nano-size precursors then calcined (500°C) and dry ball milled (30 min) were used for all electrical studies. The powders were pressed attaining a green density (pre-sintered density) of 49 ± 2 % for nano sample and 65 ± 2 % for the commercial samples. The difference in green density values between the nano and commercial samples was due to the fact that the commercial samples were pre-calcined at 950°C for 2 hours. Sintering was carried out in a chamber furnace at a rate of 1.5°C/min up to 300°C and held for one hour and then 3°C/min to the final temperature.

5.3.2.1 Electrical characteristics of samples sintered at 950°C/ 2h

The current voltage characteristics of the nano samples and commercial samples are given in Fig. 5.6. Voltage was plotted against log current. The average thickness of the sintered pellets was 0.65 mm. V/mm values and α values were calculated (Table 5.3).

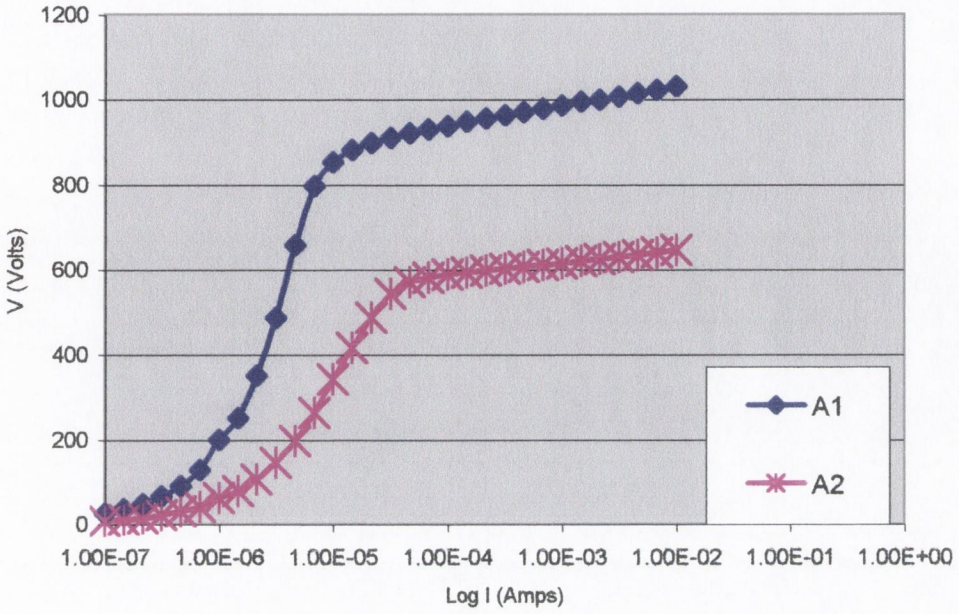

Fig. 5.16 I-V curve of varistor samples prepared by sol gel mixed precursor route intered at 950°C/2hr. A1 = Varistors prepared from nanometer size precursors and A2 = Varistors prepared from commercial mixed oxide powder.

Table 5.3 Electrical characteristics and densification of varistor samples prepared by sol gel mixed precursor route sintered at 950°C/2hr

Sample	Break down voltage (V/mm) ± 30	α ± 3	Density (g/cm^3)	% Density
Commercial varistor	946	24	4.77	85.1
Nano varistor	1450	31	5.32	94.9

Both the curves follow similar pattern except the lower current region (below 0.1 μA). A steeper change in voltage with current is observed for varistors prepared from nano-size precursors compared to the commercial varistors.

A considerably higher breakdown voltage of 1450 ± 30 V/mm with a reasonably good α of 31± 3 [V_2=1134 volts; V_1= 979 volts] is obtained for samples prepared from nano samples compared to the commercial samples (Vc = 946 ± 30 V/mm and α= 21 ± 3 [V_2=733 volts; V_1= 607 volts]). But the density measurements show that the sintering is not complete and further higher temperature sintering is required to achieve better density (>98%).

5.3.2.2 Electrical characteristics of samples sintered at 1000°C/ 2h

The I V characteristics of the nano samples and commercial samples sintered at 1000°C for 2 hours are given in Fig. 5.17.

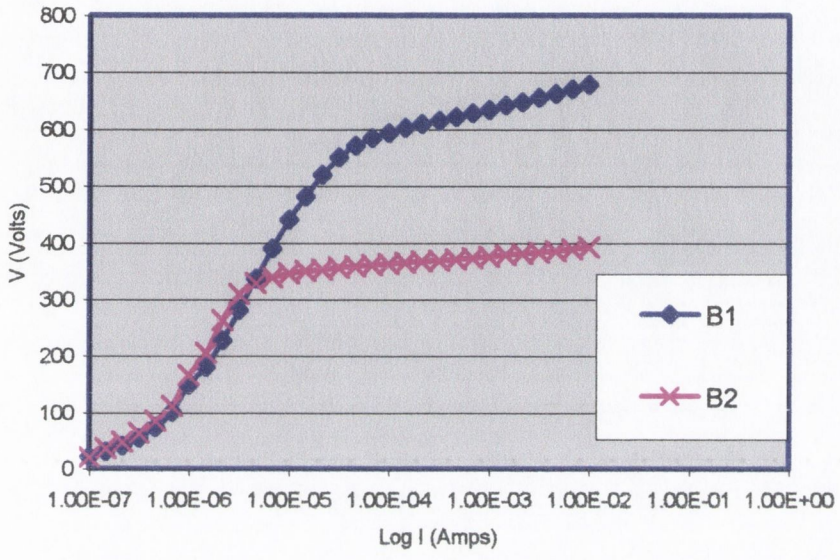

Fig. 5.17 I-V curve of varistor samples prepared by sol gel mixed precursor route sintered at 1000°C/2hr. B1 = Varistors prepared from nanometer size precursors and B2 = Varistors prepared from commercial mixed oxide powder

Table 5.4 Electrical characteristics and densification of varistor samples prepared by sol gel mixed precursor route sintered at 1000°C/ 2 h.

Sample	Break down voltage (V/mm) ± 30	α (± 3)	Density (g/cm^3)	% Density
Commercial varistor	584	22	5.31	94.7
Nano varistor	951	30	5.48	97.8

At 1000°C the breakdown voltage of varistors made from nano samples is found to be 951 ± 30 V/mm where as that of commercial varistors are 584 ± 30 V/mm (Fig 5.11). α values do not change for either of the samples compared to 950°C. (The nano varistor has an α value of 30 ± 3 [V_2 = 755 volts; V_1 = 647 volts] and the commercial varistor has an α value of 22 ± 3 [V_2 = 456 volts; V_1 = 371 volts]). There is a big difference in the breakdown voltages between 950 and 1000°C (Table 5.4). This is due to the increase in grain size at higher temperature (Grain growth studies were discussed in section 5.3.1). The sintered density of the nano samples was only 97.8% and further higher temperature is required to obtain better densification (>98%).

5.3.2.3 Electrical characteristics of samples sintered at 1050°C/ 2h

The current voltage characteristics of the nano samples and commercial samples are given in Fig. 5.18. Breakdown voltage of the nano samples and commercial samples were measure as 941 ± 30 V/mm and 507 ± 30 V/mm respectively.

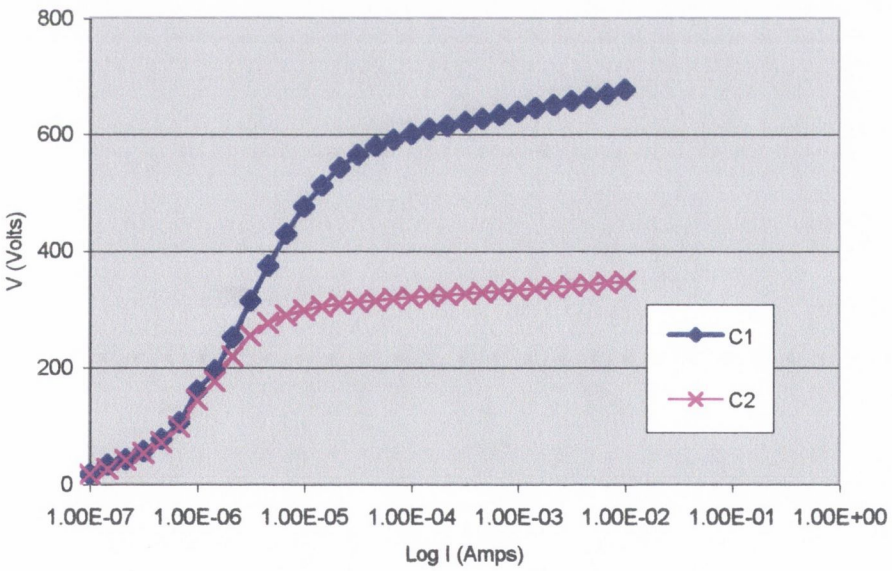

Fig. 5.18 I-V curve of varistor samples prepared by sol gel mixed precursor route sintered at 1050°C/2hr. C1 = Varistors prepared from nanometer size precursors and C2 = Varistors prepared from commercial mixed oxide powder.

The α value remains same for the nano varistor samples compared to the same at 1000°C. The nano varistor showed an α value of 33 ± 3 [V_2 = 735 volts; V_1 = 640 volts] and the commercial varistors showed an α value of 28 ± 3 [V_2 = 390 volts; V_1 = 330 volts]

Table 5.5 Electrical characteristics and densification of varistor samples prepared by sol gel mixed precursor route sintered at 1050°C/ 2 h.

Sample	Break down voltage V/mm ± 30	α (± 3)	Density (g/cm^3)	% Density
Commercial varistor	507	28	5.40	96.4
Nano varistor	941	33	5.60	100

100% density was obtained for the nano samples sintered at 1050°C/2h while a densification of 96.4% was obtained for the commercial sample at this temperature (Table 5.5). α values increased and the breakdown voltage decreased (941 ± 30 V/mm) for both nano samples and commercial samples sintered for 1050°C/ 2h compared to 1000°C/ 2h.

5.3.2.4 Step sintering

A novel sintering procedure has been reported recently for the sintering of nanocrystalline Y_2O_3.[39] This method uses two steps in the heating schedule. The pellet was first heated to a higher temperature to achieve an intermediate density, then rapidly cooled down and held at a slightly lower temperature for several hours. In our case two sintering experiments were carried out using this technique. In a typical experiment the samples were heated to 1100°C for 0 hours and the temperature was lowered to 950°C for 6 hours (1100/0h;950/6h). Similar procedures were repeated for 1000°C for 0 hours and 900°C for 6 hours

(1000/0h;900/6h). Table 5.6 shows the electrical properties and densification values of the sintered discs by these two sintering schedules.

Table 5.6 Electrical characteristics and densification of varistor samples prepared by sol gel mixed precursor route produced by step sintering process

Sample	Break down voltage V/mm ± 30	α (± 3)	Density (g/cm^3)	% Density
Commercial varistor (1000/0h;900/6h)	723	25	5.17	92.2
Nano varistor (1000/0h;900/6h)	1192	31	5.48	97.5
Commercial varistor (1100/0h;950/6h)	473	30	5.38	95.9
Nano varistor (1100/0h;950/6h)	906	36	5.52	98.5

Considerably higher breakdown voltages with a reasonably higher α values were obtained for the nano varistor precursor samples sintered by these methods compared to the commercial sample made under same experimental conditions. Higher densification >98% could also be achieved by 1100/0h;950/6h sintering methods. A densification of >98% is required for industrial applications. A detailed analysis of sintering temperatures and electrical properties are given in Table 5.7.

Table 5.7 Electrical properties and densities of varistor samples sintered at different temperatures

Sample	Properties	Temperature (°C)				
		950	1000	1050	1000/900	1100/950
Commercial	Vc	946	584	507	723	473
	α	24	22	28	25	30
	% density	85.1	94.7	96.4	92.2	95.9
Nano	Vc	1450	951	941	1192	906
	α	31	30	33	31	36
	% density	94.9	97.8	100	97.5	98.5

5.4 Discussion on varistor action and phase analysis of sintered samples

Metal oxide varistors contain ZnO grains as the major component (more than 90%) with several other metal oxides as additives. Each of the additives control one or more of the properties like electrical characteristics (breakdown voltage, non-linearity and leakage current), grain growth and sintering temperature.[2,40,42,43] Bi_2O_3 is the most essential component for forming the non-ohmic behaviour and addition of CoO and MnO enhances the non-linear properties.[2-6] A very low concentration of Al_2O_3[43] increases the ZnO grain conductivity and Sb_2O_3 controls the ZnO grain growth. It is also noted that there are other multiple dopants such as a combination of Bi_2O_3, Cr_2O_3, MnO and CoO, which have produced greater non-linearity than a single dopant. During sintering different phases are formed and the microstructure of a ZnO varistor comprises conductive ZnO grains surrounded by electrically insulating grain boundary regions. As discussed earlier, in section 1.6, the ZnO-Bi_2O_3-Sb_2O_3 system forms a pyrochlore phase $Zn_2Bi_3Sb_3O_{14}$ above 650°C.[7] Together with ZnO, pyrochlore ($Zn_2Bi_3Sb_3O_{14}$) further reacts to form spinel ($Zn_7Sb_2O_{12}$)

$$2\ Zn_2Bi_3Sb_3O_{14} + 17\ ZnO \xrightarrow{950\text{-}1050\ ^\circ C} 3\ Zn_7Sb_2O_{12} + 3\ Bi_2O_3\ [L]\ [\ 5.1]$$

Thus the following three major components should be detected in a typical varistor microstructure.[2,7,9]

1) ZnO grains,
2) $Zn_7Sb_2O_{12}$, spinel crystal structure,
3) Bismuth rich phases

Varistors, prepared from nano size precursors after milling, sintered at 1050°C/2h were studied in detail by XRD and microstructural analysis. Fig 5.19 represents the XRD pattern of the 1050°C/2h sample. Zinc Oxide, Spinel and bismuth rich phases could be identified from the XRD pattern [2,9,42] (Fig. 5.19).

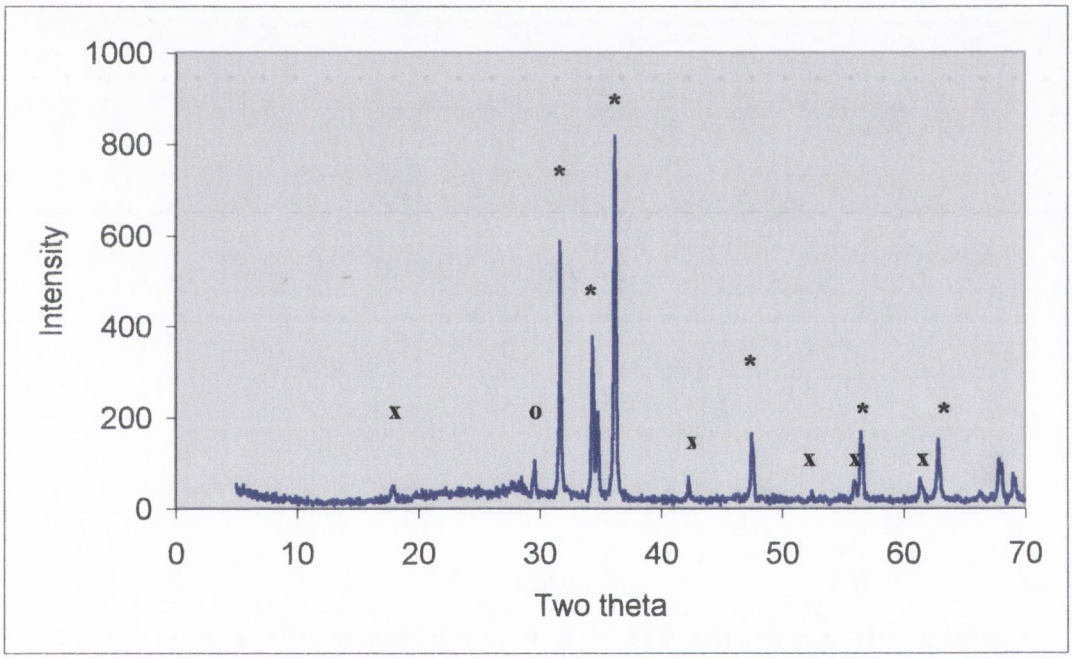

Fig. 5.19 XRD of the varistor sample prepared by sol gel mixed precursor route sintered at 1050°C/2h (* = ZnO; x = $Zn_7Sb_2O_{12}$; o = Bi_2O_3)

Similar patterns (Fig. 5.20) were identified for commercial samples sintered at 1050°C/2h

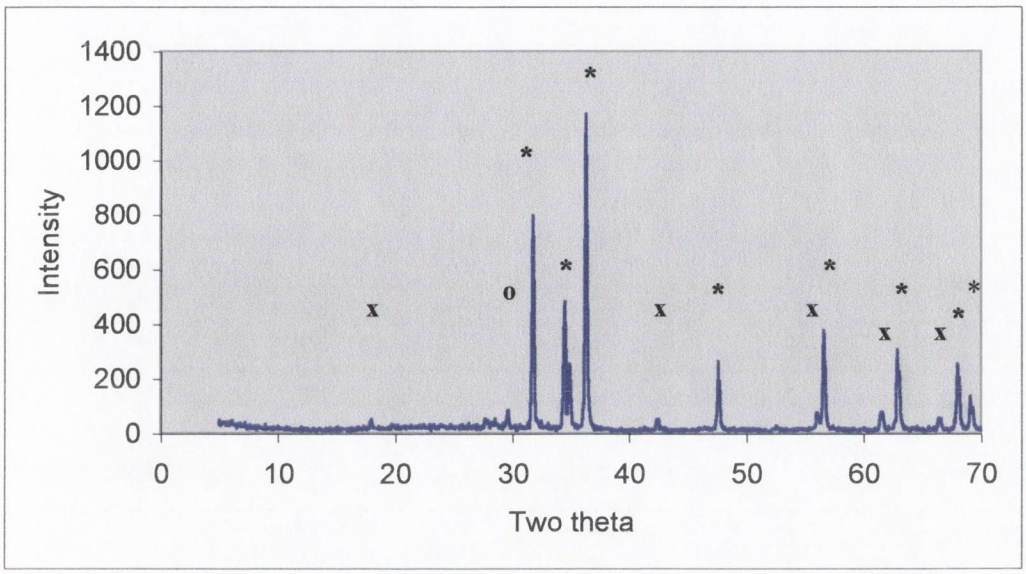

Fig 5.20 XRD of the standard (commercial sample) sintered at 1050°C/2h

(* = ZnO; **x** = $Zn_7Sb_2O_{12}$; **o** = Bi_2O_3)

The FESEM micrographs of the nano-samples and commercial samples sintered at 1050°C/2h are shown in Fig. 5.21 and 5.22 respectively. Microstructures obtained were similar to earlier reports[9,42,44] and different phases were identified with EDX analysis.

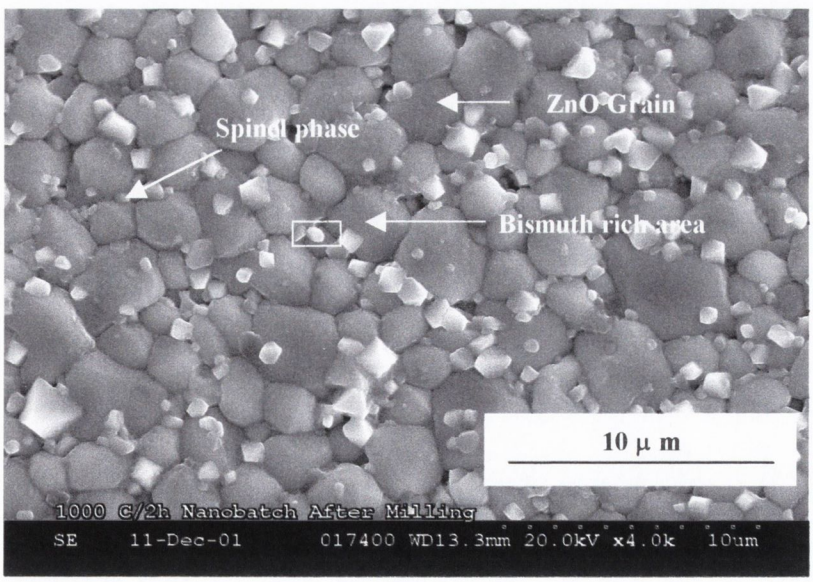

Fig. 5.21 FESEM image varistor sample, prepared by sol gel mixed precursor route, sintered at 1050°C/2h

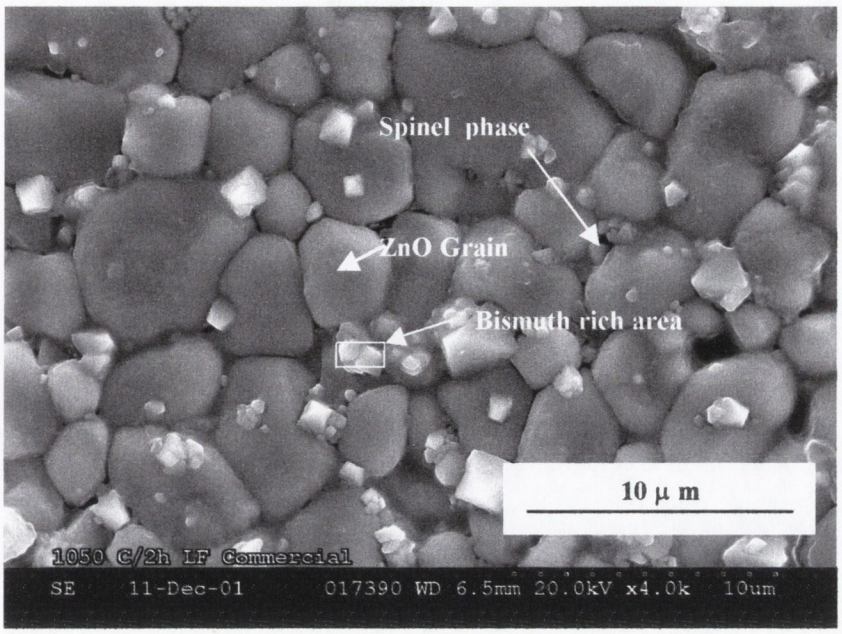

Fig. 5.22 FESEM image of varistor sample, prepared from micron size powders, sintered at 1050°C/ 2h

In order to identify different phases EDX analysis were carried out for the nano-samples sintered 1050°C/2h. Three phases could be well identified by EDX a) ZnO phase (Fig. 5.23) b) Spinel, $Zn_7Sb_2O_{12}$, phases found at the triple points and also on the grains (Fig. 5.24) c) Bismuth rich phase found in inter-granular grains and at triple points (Fig. 5.25).

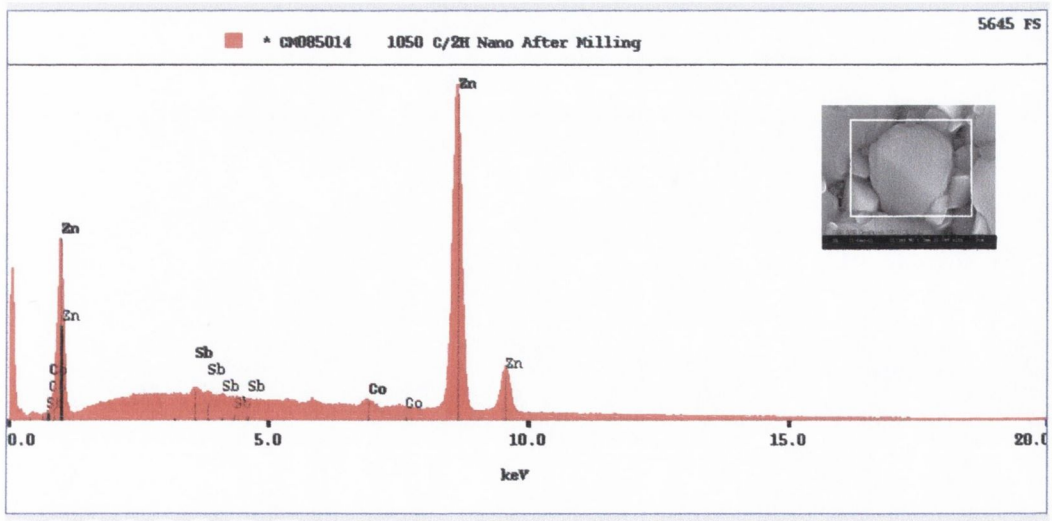

Fig. 5.23 EDX pattern of a typical ZnO grain found in a varistor microstructure

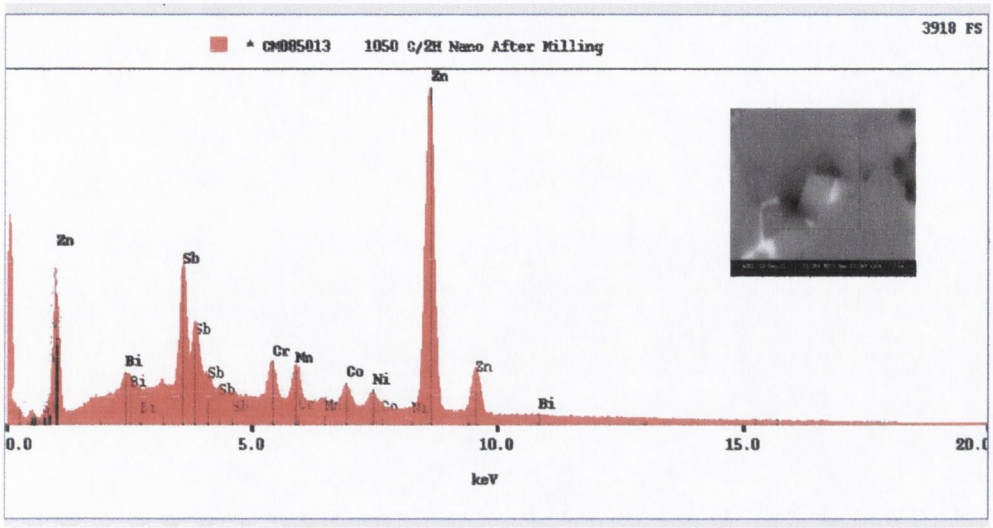

Fig. 5.24 EDX image of the Spinel ($Zn_7Sb_2O_{12}$) phase

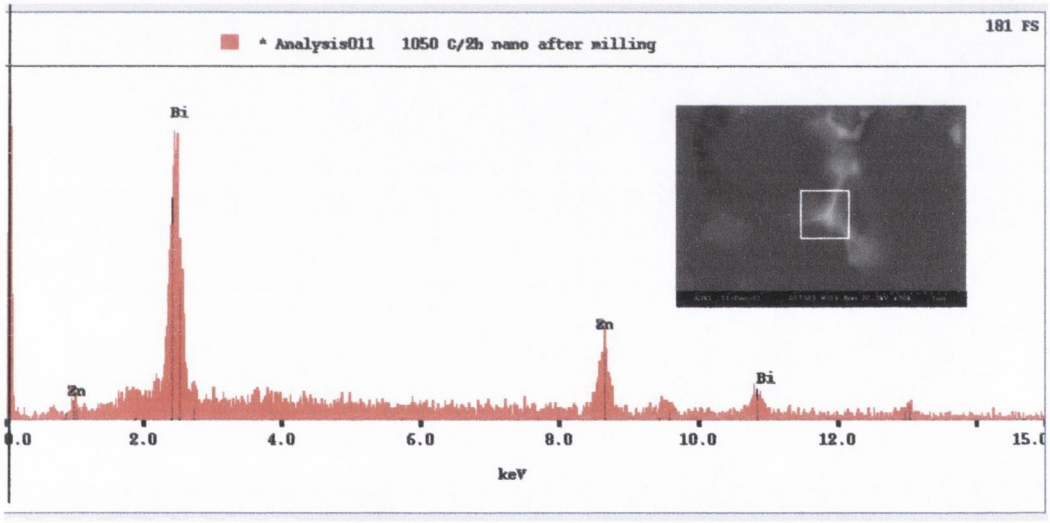

Fig. 5.25 EDX pattern of the bismuth rich phase (white areas in the microstructure). It is usually found at triple points and grain boundaries.

The better electrical properties of the varistors prepared from the nanometer size precursors compared to the commercial one can be explained on the basis of smaller grain size of the sintered material and greater homogeneity in the starting nano size powder. Considerably higher breakdown voltages were observed for varistors prepared from nanometer size precursors, which indicates a greater

number of varistor active grain boundaries per unit area. Hence compared to the conventional routes this novel procedure can be used as a better way of preparing homogeneous nano varistor precursor powder. Synthesis of these materials in different batches has been successfully carried out more than 10 times in our laboratory. Because of the simplicity of the experiment, inexpensive sources of starting materials and better electrical characteristics, these materials have been successfully produced in a kilogram batch in an industrial scale pilot plant operation. More studies on the industrial production of devices using these materials are underway at Littelfuse Ireland Ltd.

5.5 Conclusions

A novel mixed precursor method was successfully performed to synthesise bulk quantities of commercially viable nanometer size (~20 nm) doped ZnO varistor powders. TEM results showed that these particles were agglomerated and dry ball milling for 30 minutes de-agglomerated it considerably. Varistors were fabricated from these materials by sintering at various temperatures ranging from 700 to 1050°C. 100% densification, high breakdown voltage (941 ± 30 V/mm) and a reasonably good α (33 ± 3) were observed for samples sintered at 1050°C/2h. A novel step sintering procedure was also performed and 98.5% densification was achieved for samples sintered at 1100/0:950°C/6h. A breakdown voltage of 906 ± 30 V/mm and an α value of 36 ± 3 were obtained. Thus superior electrical properties, with a breakdown voltage of 1.5 times higher than the commercial varistor and reasonably good α value were obtained with varistors prepared from nano materials. Industrial pilot plant operations were successfully performed to produce large quantities of nano varistor powder.

5.6 References

1. D. R. Clarke, *J. Am. Ceram. Soc.*, 1999, **82,** 485.
2. T. K. Gupta, *J. Am. Ceram. Soc*, 1990, **73**, 1817.
3. M. Matsuoka, *Jpn. J. Appl. Phys.*, 1971, **10**, 736.
4. C. Leach Z. Ling and R. Freer, *J. Euro. Ceram. Soc*, 2000, **20**, 2759
5. K. Eda, *IEE Electrical Institution Magazine, 1989,* **5**, 28.
6. B. C. H. Steele, *Electronics ceramics*, Elsevier Applied Science London and New York, 1991, Page 17.
7. R. Einzinger, *Ann. Rev. Mater. Sci.*, 1987, **17**, 299.
8. M. Inada, *Jpn. J. Appl. Phys.*, 1980, **19**, 409.
9. E. Olsson, L. K. L. Falk and G. L. Dunlop, *J. Mater. Res.*, 1985, **20**, 4091.
10. L. M. Levinson and H. R. Philip, *Ceramic Bulletin.*, 1986, **65**, 639.
11. R. N. Viswanath, S. Ramasamy, R. Ramamoorthy, P. Jayavel and T. Nagarajan, *Nanostruct. Mater.*, 1995, **6**, 993.
12. G. Hohenberger and G. Tomandl, *J. Mat. Res.*, 1992, **7,** 546.
13. M. Singhal, V. Chhabra, P. Kang and D. O. Shah, *Mater. Res. Bull.*, 1997, **32**, 239.
14. S. Hingorani, V. Pillai, P. Kumar, M. S. Multani and D. O. Shah *Mat. Res. Bull.*, 1993, **28**, 1303.
15. S. Hingorani, D. O. Shah and M. S. Multani, *J. Mat. Res.*, 1995, **10,** 461.
16. S. Hishita, Y. Yao and S-I. Shirasaki, *J. Am. Ceram. Soc.*, 1989, **72**, 338.
17. S. M. Haile, D.W. Johnson, Jr. G. H. Wiseman and H. K. Bowen, *J. Am. Ceram. Soc.*, 1989, **72,** 2004.
18. A. Sinha and B. P. Sharma, *Mat. Res. Bull.*, 1997, **32**, 1571.
19. V. C. Sousa, A. M. Segadaes, M. R. Morelli, R. H. G. A. Kiminami, *Int. J. Inorg. Mater.*, 1999, **1**, 235.
20. Y. Li Z. Zhang, Z. Tang, F. Yuan and J. Li, *Adv. Mater. Opt. Electro.*, 1999, **9**, 205.
21. M. Takehana, T. Nishino, K. Sugawara and T. Sugawara, *Mater. Sci. Eng. B,* 1996, **41,** 186 : M. Takehana, T. Nishino, K. Sugawara and T. Sugawara, *Korean J. Chem. Eng.*, 1996, **13,** 538.
22. G. Westin and M. Nagren, *J. Mater. Chem.*, 1993, **3**, 367.

23. G. Westin, A. Ekstrand, M. Nagren, R. Osterlund and P. Merkelbach, *J. Mater. Chem.*, 1994, **4,** 615.

24. A. Ekstrand, M. Nagren and G. Westin, *J. Sol Gel Sci. Tech.*, 1997, **8**, 697.

25. K. X. Ya, H. Yin, T. M. De and T. M. Jing, *Mater. Res. Bull.*, 1998, **33,** 1703.

26. K. X. Ya, W. T. Diao, H. Yin, T. M. De and T. M. Jing, *Mater. Res. Bull.*, 1998, **32,** 1165.

27. R. Puyane, F.Toal and S. Hampshire, *J. Sol gel Sci. Tech.*, 1996, **6**, 219.

28. R. Puyane, I. Guy and R. Metz, *J. Sol gel Sci. Tech.*, 1998, **13**, 575.

29. L. Kong, F. Li, L. Zhang and X. Yao, *J. Mater. Sci. Lett.*, 1998, **17**, 769.

30. R. T. Lauf and W. D. Bond, *Ceramic Bulletin*,1984, **2**, 278.

31. L. Spanhel and M. A. Anderson, *J. Am. Chem. Soc.*, 1991, **113,** 2826.

32. E. A. Meulenkamp, *J. Phys. Chem. B.*, 1998, **102**, 5566.

33. A. M. Donia, *Polyhedron*, 1997, **17,** 3013.

34. A. K. Nikumbh, S. K. Prdeshi and M. N. Raste, *Thermochimica Acta,* 2001, **374**, 115

35. L-W. Tai and P. A. Lessing, *J. Mater. Res.*, 1992, **7,** 502.

36. A. R. West, *Solid State Chemistry and Its Applications*; John Wiley & Sons London, 1999, p 174.

37. D. E. McCormack, PhD. (1990), The University of Dublin, p 86.

38. H. Ferkel and R.J. Hellmig, *Nanostruct. Mater*,1999, **11**, 617.

39. I. -Wei and X.-H. Wang, *Nature*, 2000, **404**, 168.

40. P. Duran, F. Capel, J. Tartaj, and C. Moure *J. Am. Ceram., Soc*, 2001, **84**, 1661.

41. T. Sakuma, *Mater. Sci. Forum,* 1996, **20**, 109.

42. A. Banarjee, T.R. Rammohan and M. J. Ptani, *Mater. Res. Bull.*, 2001, **36**, 1259.

43. J. Fan and R. Freer, *British Ceramic Transactions,* 1993, **96**, 221.

44. T. Asokan and R. Freer, *J. Mater. Sci.*,1990, **25**, 2447.

Chapter 6

Conclusions and summary for the present work and suggestions for future work

6.1 Conclusions and summary

At the beginning of this project we had the following aims (section 1.8):

i) To synthesise ZnO nanoparticles based on well established procedures and compare the electrical properties

ii) To develop novel sol gel based nano ZnO materials suitable for varistor applications

iii) To develop industrially viable new mixed oxide nano varistor precursor materials

In chapter 3, the use of well-established synthetic procedures for varistor preparations was discussed. Three synthetic procedures (Spanhel and Anderson, Meulenkamp and Weller methods) were selected to make nanocrystalline ZnO of particle sizes less than 10 nm. Among the three procedures tried, the Weller method was found to be the simplest to reproduce. All three materials were calcined at 500°C for two hours and varistors were prepared via a conventional solid state mixing technique. Sintering was performed at 1050°C for two hours and electrically characterised. Varistor pellets made from the Spanhel and Anderson procedure fully melted during sintering and electrical studies showed that none of the procedure produced a material that could be used as a varistor. The poor electrical characteristics of these materials were due to the presence of impurity ions such as lithium and sodium. It was decided to develop novel methods for the synthesis of nano size ZnO and varistor materials to acheive better electrical properties.

Chapter 4 described the preparation of nanoparticles and nanowires using novel sol gel synthetic procedures. ZnO precursor gels were prepared by the reaction of an ethanolic solution of zinc acetate and ethanolic solution of oxalic acid (with and without the use of modifiers). The gel prepared without the use of modifiers was dried at 80°C and further calcination produced ZnO nanoparticles of size ~30± 5 nm. BET surface area for this material was found to be 17 m^2/g. In a similar experiment the two chemical modifiers (ethylene glycol and diethanolamine) were added to the ethanolic solution of zinc acetate before the addition of the ethanolic solution of oxalic acid. The gel formed was subsequently dried (80°C) and calcined (500°C for two hours) using similar conditions to above and was characterised by XRD, FESEM and TEM.

FESEM revealed a fibrous structure containing elongated bundles of 100 nm widths and 2-4 μm lengths. Further ultrasonication for 40 minutes separated the individual wires from the bundle. TEM studies showed that these wires were composed of spherical nanoparticles of 21 ± 3 nm. The 500°C calcined wire were calcined further to 1000°C and FESEM studies showed that the individual particles was sintered together to form continuous wires of width 0.3 to 0.4 μm and 10 to 20 μm length. The precursor morphologies and formation mechanisms were studied in detail by TEM, FTIR and thermal analysis. Two of the above materials were doped with commercial metal oxides using conventional solid state mixing technique and a core shell type doped varistor was also made using spherical ZnO nanoparticles and metal salts as additives. Sintering (1050°C for two hours) and electrical studies were carried out for each of these samples and compared with commercial varistor samples pelletised and sintered under the same conditions. Core shell type varistor material showed considerably higher breakdown voltage compared to the other nanosamples mixed with commercial additives and commercial varistors discs made under same conditions. Even though the electrical properties were superior, only 97% densification was achieved at 1050°C for two hours. Thus there was a need for a better procedure for the synthesis of a material, which can sinter at a lower temperature with superior electrical properties. Investigations were directed towards making a new material with superior electrical properties and lower sintering temperature.

Synthesis, characterisation and varistor preparations, based on a novel sol gel based mixed precursor route, were discussed in chapter 5. Drying (80°C) and calcination (500°C for two hours) of a gel containing zinc acetate and additive metal salts produced nano varistor precursor powders with average particle size of 15 ± 3nm. These powders were characterised by TEM, BET surface area, FESEM, XRD and EDX. The synthesised nano powder after calcinations at 500°C has a surface area of 45 m^2/g. FESEM analysis showed that these powders contain an appreciable amount of agglomerates. It was reported earlier that strong agglomerates might lead to larger grains after sintering. Dry ball milling for 30 minutes tried successfully removed these agglomerates. The milled powder was further plastified, pelletised and sintered at various temperatures from 700°C to 1050°C for two hours. A novel step sintering

procedure was also tried for the first time for sintering varistor materials. Electrical measurements were carried out for materials sintered at 950°C, 1000°C and 1050°C and also for step sintered samples. Nearly full dense varistor discs with 1.5 times higher breakdown voltage (906 ± 30V/mm) and reasonably good non-linear characteristics ($\alpha = 36 \pm 3$) compared to the commercial material have been obtained for varistor material prepared from nano-size precursors sintered by a novel step sintering procedure. Full densification (100%) with a breakdown voltage of 941 ± 30 V/mm and α of 33 ± 3 were obtained for these materials conventionally sintered at 1050°C. Sintering behaviour of the varistor discs prepared from nano samples was studied by densification studies and dilatometric studies. Density measurements indicated that the sintered density value was increased considerably at 900°C. The dilatometric results showed that the onset of sintering occurred in the range 875-925°C and is finished in the range 1025-1050°C. Grain growth studies showed that the particles have grown considerably at 900°C compared to 800°C. It confirmed that the sintering process and grain growth occurred simultaneously. Phase analyses of the samples sintered at 1050°C were carried out using FESEM, EDX and XRD. ZnO grains, spinel phases ($Zn_7Sb_2O_{12}$) and bismuth rich areas, which are the essential phases found in an ideal varistor were well identified in the microstructure. Thus a novel mixed precursor method was tried successfully to prepare commercially viable varistor precursor powders in the nanometer range. Industrial pilot plant operations were also successfully carried out to produce a kilogram batch of these materials.

Therefore, during the period of research we have achieved the following targets:

i) Three well established synthetic routes have been followed to make nano-size ZnO and the electrical characteristics of such materials were studied and compared with commercial varistor materials (chapter 3)

ii) Novel sol gel methods to create template free nano wire arrays of ZnO have been established (chapter 4)

iii) Spherical agglomerated ZnO nano particles were prepared and characterised (chapter 4)

iv) A novel core shell based synthesis of nano varistor precursor materials was established (chapter 4)

v) Varistors were prepared from ZnO nanowire materials, ZnO nano particles and core shell type varistor materials and the core shell materials showed better electrical properties compared to the other materials (chapter 4)

vi) A mixed precursor route has been established for the synthesis of varistor materials (chapter 5)

vii) Varistors were fabricated from these materials and showed superior electrical properties compared to the commercial varistors (chapter 5)

viii) A step sintering technique have been successfully tried for first time for sintering varistors (chapter 5)

ix) An industrial pilot plant synthesis has been successfully achieved and a kilogram of the nano varistor precursor material has been produced

6.2 Suggestions for future work

In chapter 5 it was reported how closely the grain growth and sintering temperature were related. Controlling the grain growth at higher temperature is a real challenge for varistor ceramics. Breakdown voltage could be further increased several times, if one could sinter the material to full density with sub-micrometer grain size. Novel sintering procedures like step sintering, as discussed in chapter 5, could be further modified to get a fully sintered varistor disc at a lower temperature. Microwave sintering methods have received much attention in recent years.[1,2] Nanometer size ferrite powders have been sintered using microwave energy without suffering major grain growth.[2] An investigation on sintering of varistors prepared from nano samples using microwave energy is in progress at Institute of Polymer Technology and Materials Engineering, Loughborough University, UK and preliminary results are encouraging.

This study was investigating how nano-size precursors and sol gel procedures could improve the breakdown voltage, which is controlled by grain size and additive homogeneity. Other electrical properties like non-linearity and leakage currents are dependent on the additives and its concentration. In this research, varistors were fabricated without changing any additive proportions currently used in Littelfuse Ltd. for making varistors from micron size samples. A long-term investigation is required for the dopant additions for nano samples as it contains a large number of grain

boundaries. By this way α, leakage current and sintering properties could be further improved.

6.3 References

1. R. Roy, D. Agrawal, J. Cheng and S. Gedevanishvili, *Nature*, 1999, **399**, 668.
2. J. G. P. Binner, I. Caro and J. Firkins, *J. Microwave Power EE,* 1999, **34**, 131.

Appendix I

Brus equation for particle size from absorption spectra

The particle size can be determined from the absorption spectra using the effective mass model derived by Brus[1]

$E^* = E^{bulk} + h^2\pi^2/2\, r^2\, [1/m_e m_o + 1/m_h m_o] - 1.8e^2/4\pi\varepsilon_o \varepsilon_r r$

E^{bulk} = Bulk bandgap (ZnO= 3.4 eV)

h = Plank's constant (6. 62 x 10^{-34} J. s)

m_e = Effective mass of electron (0. 24)

m_h = Effective mass of hole (0. 45)

m_o = Free electron mass (9. 11 x 10^{-31} kg)

ε_o= Permitivity of free space (8. 85x 10^{-12} $C^2/N. m^2$)

ε_r= Relative permitivity (3.7)

r= Crystalline radius (in nm)

The particle size can be obtained from the band gap inferred from the optical absorption spectra.

References

1. L. E. Brus, *J. Phys. Chem. B.*, 1986, **90**, 2555.
2. E. A. Meulenkamp *J. Phys. Chem. B.*, 1998, **102**, 5566.

Appendix II

List of author's publications

1. Preparation of self assembled nanowire arrays of ZnO,
   Suresh C. Pillai, John M. Kelly, Declan E. McCormack, Ramesh Raghavendra
   (*Manuscript under revision,* January, 2002)
2. ZnO varistors from nanocrystalline precursors by sol-gel route,
   Suresh C. Pillai, John M. Kelly, Declan E. McCormack, Ramesh Raghavendra
   (*Manuscript under preparation*, January, 2002)
3. Preparation of magnetic nanoparticles and their assemblies using a
   new Fe(II) alkoxide precursor, Grainne B. Biddlecombe, Yurii K. Gun'ko,
   John M. Kelly, Suresh C. Pillai, J.M.D. Coey, M. Venkatesan, A.P. Douvalis
   J. Mater. Chem. 2001, **11**, 2937
4. Magnetic nanoparticles and nanoparticle assemblies from metallorganic
   precursors, Yurii Gun'ko, Suresh C. Pillai, David McInerney,
   J. Mater. Sci. Mater. Electro. 2001, **12**, 299
5. Synthesis of thermally stable high surface area anatase-alumina mixed oxides,
   S.R. Kumar, Suresh C. Pillai, U.S. Hareesh, P. Mukundan and K. G. K. Warrier,
   Materials Letters, 2000, **43,** 286
6. Effect of Addition of silica to sol-gel titania in presence of different
   Solvents, S. Rajesh Kumar, C.Suresh, Asha.K.Vasudevan, N.R.Suja,
   P.Mukundan and K.G.K. Warrier, *Materials Letters,* 1999, **38**, 161
7. Anatase to rutile transformation in sol-gel titania by modification of precursor,
   C. Suresh, V.Biju, P. Mukundan and K.G.K. Warrier, *Polyhedron* 1998, **17**, 3131